4-28-2018

Investigating Uranium incorporation in modern carbonates by sequential extraction: Applied to the Permian - Triassic boundary in Lung Cam, Vietnam

Christopher Michael Wray
Louisiana State University and Agricultural and Mechanical College

INVESTIGATING URANIUM INCORPORATION INTO MODERN CARBONATES BY SEQUENTIAL EXTRACTION: APPLIED TOWARD PERMIAN–TRIASSIC BOUNDARY IN LUNG CAM, VIETNAM

A Thesis

Submitted to the Graduate Faculty of the
Louisiana State University and
Agricultural and Mechanical College
in partial fulfillment of the
requirements for the degree of
Master of Science

in

The Department of Geology and Geophysics

by
Christopher Michael Wray
B.S., Texas A&M University, 2011
August 2018

Acknowledgements

I would like to thank Dr. Achim Herrmann for his guidance, direction and funding throughout the duration of this project. I would also like to thank Dr. Brooks B. Ellwood for providing the Permian–Triassic samples from Lung Cam that were used in conjugation with the Bahamian samples provided by Dr. Herrmann. Special thanks to Adam Turner for assistance and a helpful hand during laboratory work. I am grateful to the American Chemical Society Petroleum Research Fund (ACS PRF#55392-DN12). Finally, I would like to thank Louisiana State University for providing research facilities.

Table of Contents

List of Tables

List of Figures

Abstract

The Uranium (U) isotopic system can be used to model the extent of global-scale ocean anoxia by utilizing the $^{238}U/^{235}U$ ratios as a paleo-redox indicator ($\delta^{238}U$). While recent studies have shown promise with the use of this novel proxy, variability is seen in modern carbonate sediment samples suggesting that more work is needed in order to understand elemental U uptake during early marine diagenesis. This thesis utilizes a sequential extraction methodology in order to understand the distribution of authigenic U within carbonate sediments.

This thesis consists of four parts, (1) an evaluation and modification of a sequential extraction methodology for U uptake in modern carbonate sediments, (2) application of the modified sequential extraction method to the study U distribution within chemical fractions within Bahamian bulk sediments, (3) the application of the modified methodology to study the U distribution across the Permian–Triassic boundary from the Lung Cam section in Northern Vietnam, and (4) the implications of authigenic U toward the $\delta^{238}U$ paleo-redox marker.

Results show that a sequential extraction can be successful within carbonate sediments. The results of this sequential extraction shows that the majority of authigenic U is found within the exchangeable and carbonate fraction. This thesis hypothesizes that this U component is a non-crystalline U(IV) species. Furthermore, this authigenic U component was also found within the Permian–Triassic section located in Lung Cam, Vietnam, thus illustrating preservation of heavy authigenic U within the rock record.

1. Introduction

In recent years, ^{238}U ratios ($\delta^{238}U$, defined below) in marine sediments have been used to reconstruct changes in the oxygenation of the global ocean (e.g. Brennecka et al., 2011; Montoya-Pino et al., 2010; Anderson et al., 2014; Asael et al., 2013; Dahl et al., 2014; Romaniello et al., 2013; Azmy et al., 2015; Elrick et al., 2017). The use of the $\delta^{238}U$ as a paleo-redox proxy is based on the equilibrium isotopic fractionation of U isotopes during redox conditions (Andersen et al., 2015, Romaniello et al., 2013; Brennecka et al., 2011; Weyer et al., 2008; Murphy et al., 2014; Stylo et al., 2015; Stirling et al., 2015). Equilibrium isotopic fractionation is the enrichment or partial separation of one isotope relative to another isotope of the same element, which in Uranium is related to nuclear volume fractionation rather than traditional mass-dependent fractionation (Schauble, 2007; Weyer et al., 2008). Many of these studies have utilized bulk sediment $\delta^{238}U$ values, despite the fact that Romaniello et al. (2013) have shown that early marine diagenesis can have a significant impact on bulk chemistry. Thus, more work is needed in fully understanding the fractionation dynamics of the $^{238}U/^{235}U$ system in order to rely on this proxy in future paleo-redox studies.

Under anoxic conditions, U is reduced from a soluble state (U^{VI}) to a particle reactive state (U^{IV}) (Klinkhammer & Palmer, 1991; Weyer et al., 2008; Swarzenki et al., 1999). This results in U accumulation and significant $^{238}U/^{235}U$ fractionation into sediment (Anderson et al., 2014; Weyer et al., 2008; Barnes & Cochran, 1990; Basu et al., 2014; McManus et al., 2006). Several mechanisms have been shown to be involved in the fractionation process such as bacterial reduction (Stirling et al., 2015; Basu et al., 2014; Yi et al., 2007; Lovely et al., 1991; Gu & Chen, 2003), oxygen penetration depth (Anderson et al., 2014; McManus et al., 2005), remobilization of U (Zheng et al., 2002), and authigenic U (McManus et al., 2005; Romaniello et

al., 2013). One challenge involved with using the $\delta^{238}U$ proxy regards the complicated fractionation seen in authigenic U processes, which have been found to fractionate in different direction pathways (Weyer et al., 2008; Stylo et al., 2015; Andersen et al., 2015; Romaniello et al., 2013). Despite previous studies to constrain authigenic U enrichment in carbonates, authigenic U continues to be poorly understood. The goal of this thesis is delineate which chemical phase authigenic U incorporates into, by using a sequential extraction technique. Sequential extraction methods have been used in various studies to determine the distribution of heavy metals within sediment phases (e.g. Rao et al., 2007; Surija & Branica, 1995; Rutten, 2001; Mseddi et al., 2010; Ruttenberg, 1992; Jensen et al., 1998; Yuan et al., 2004; Zimmerman & Weindorf 2010).

1.1 Uranium Geochemistry

The geochemical nature of U has been studied extensively in marine sediments (e.g. Klinkhammer & Palmer, 1991; Swarzenski et al., 1999; Anderson, 1987; Gvirtzman et al., 1973; Anderson et al., 2016; Ku et al., 1997). Uranium has two commonly identified redox states, U^{IV} and U^{VI}, which occur naturally due to low-temperature redox processes (Klinkhammer & Palmer, 1991) and have a high solubility in oxygen rich ocean waters (Weyer et al., 2008; Swarzenski et al., 1999). U^{VI} is commonly found as a uranyl ion, $U^{VI}O_2^{2-}$, that is stabilized by various carbonate complexes (Klinkhammer & Palmer, 1991).

In modern seawater U has a residence time of ~400 k yr. (Tribovillard et al., 2006; Weyer et al., 2008; Anderson et al., 2015; Ku et al., 1997; Dunk & Jenkins, 2002), as well as a relatively stable U concentration (Klinkhammer & Palmer, 1991). These conditions allow uranium ratios ($\delta^{238}U$) to be used as a potential global paleo-redox proxy (Brennecka et al., 2011; Stirling et al., 2007; Andersen et al. 2014).

δ^{238}U is defined as:

$$\delta^{238}U = \left(\frac{\left(\frac{^{238}U}{^{235}U}\right) sample}{\left(\frac{^{238}U}{^{235}U}\right) standard} - 1 \right) x1000$$

The standard that is used in defining δ^{238}U is CRM 145 which has taken the place of SRM 950a standard which is no longer being produced.

There are three naturally occurring U isotopes, ^{238}U, ^{235}U and ^{234}U. Two isotopes, ^{238}U and ^{235}U, have long half-lives at 4.458 x 10^9 yr., and 0.7038 x 10^9 yr., respectively (Jaffey et al., 1971; Bowen, 1988). These two isotopes also contribute the most toward the natural abundance of Uranium with ^{238}U being the most common isotope at 99.28% and 0.72% for ^{235}U (Faure 1977, Bowen 1988).

Natural fractionation of U isotopes during anoxic conditions causes the reduction of U^{VI} to U^{IV}, pushing δ^{238}U seawater values to a lighter isotopic composition as ^{238}U is preferentially enriched in anoxic facies (Montoya-Pino et al., 2010; Brennecka et al., 2011). Enrichment of the heavier isotope (^{238}U) is a function of the "nuclear volume effect" rather than mass-dependent fractionation (Schauble, 2007). This enrichment of ^{238}U into anoxic facies facilitates the application of δ^{238}U to indicate changes of redox states in sediments.

The U isotopic composition is constrained by primary flux of U into ocean water through riverine input (δ^{238}U = -0.3 ‰) and its ultimate output in sinks within oxic, suboxic, and anoxic/euxinic sediments (Brennecka et al., 2011; Dunk et al., 2002; Andersen et al., 2015). In the modern ocean, suboxic and oxic sinks account for the primary removal of U (~90%) with minor removal into anoxic/euxinic sinks (~10%) (Montoya-Pino et al., 2010; Brennecka et al., 2011; Andersen et al., 2014). However the relative size of these sinks have likely varied through geologic time. Various box models show that an increase in the amount of anoxic sinks

correlates with a decrease in U concentration through U removal into anoxic facies, which produces a isotopically lighter signal in marine deposits (Brennecka et al., 2011; Elrick et al., 2017; Lau et al. 2016).

U accumulation can occur in a variety of settings such as an anoxic water column or in anoxic pore waters below an oxygen penetration zone (Dunk et al. 2002, Andersen et al. 2016). Sediments in The Bahamas can have reducing conditions from oxygen-deprived sediments caused by high primary productivity and organic matter fluxes (Andersen et al., 2002; Andersen et al., 2015; Romaniello et al., 2013). U incorporation in authigenic phases has been found to be associated with biogenic carbonate (Gvirtzman et al., 1973; Weyer et al., 2008; Romaniello et al., 2013; Amiel et al., 1973), organics (Montoya-Pino et al., 2010; Weyer et al., 2008), authigenic precipitation (Klinkhammer & Palmer, 1991; McManus et al., 2005), and apatite production (Abed & Sadagah, 2013; Tuovinen et al., 1983; Altschuler et al., 1957; Fujino et al., 2000; Banning & Rude, 2015; Starinksy et al., 1982).

Several modern studies have shown that primary carbonates (e.g., corals, calcareous algae, and ooids) retain similar $\delta^{238}U$ values as seawater, $\delta^{238}U$= -0.37‰ – -0.41‰ (Weyer et al. 2008; Romaniello et al., 2013), suggesting that ancient carbonates deposited during anoxic conditions could provide estimates of seawater conditions based on past $\delta^{238}U$ values. Romaniello et al. (2013) found that U concentration ranged from 0.014 ppm U to 3.5 ppm U in primary precipitates (Figure 1) showing variability in U concentration in modern Bahamian sediments. However, all primary precipitates averaged values close to the $\delta^{238}U$ value of seawater regardless of U concentration (Romaniello et al., 2013)

Bulk sediment carbonate cores from The Bahamas (Fig. 1) show that U concentration increased with depth (Romaniello et al., 2013). Four bulk–sediment shallow water cores (water

depth <5m) were taken from various biotic communities (e.g., dense turtle grass flats, tidal flat, tidal pond) to determine U concentration and $\delta^{238}U$ variances from primary precipitates (Romaniello et al., 2013). Bulk sediment carbonate cores ranged from 4.2 to 4.7 ppm U, which equaled or exceeded the highest concentrations observed in primary precipitates (Romaniello et al., 2013).

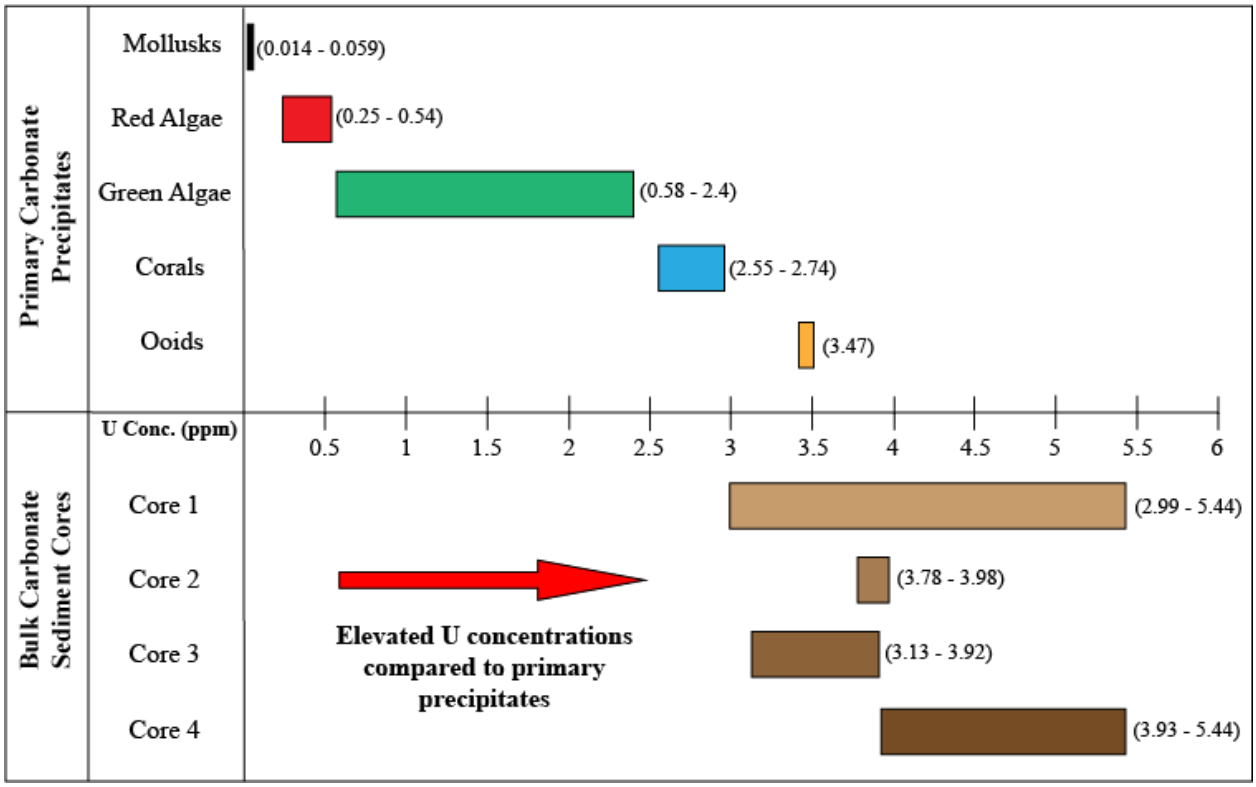

Figure 1. Bahamian U concentrations in primary precipitates and bulk sediment core. Illustrates elevated uranium concentrations compared to primary precipitates. Data is from Romaniello et al., 2013.

Similarly, core $\delta^{238}U$ values were significantly heavier (ranging from -0.06‰ to -0.30‰) than average seawater values (-0.41‰) (Romaniello et al., 2013). This shows significant fractionation of $^{238}U/^{235}U$ with the authors implying a contribution from an authigenic U source (Romaniello et al., 2013). The end result of their study was that a correction factor of 0.2‰ –

0.4‰ must be subtracted from $\delta^{238}U$ values in future paleo-redox proxy studies (Romaniello et al., 2013).

Lab experiments have indicated a role of biotic reduction in ^{238}U-enriched fractionation (Rademacher et al., 2006; Stylo et al., 2015; Chen et al., 2016). Significant fractionation ($\Delta^{238}U$ = 0.86‰) between solid U^{IV} and dissolved U^{VI} shows preferential incorporation of ^{238}U into the reduced species (Stylo et al., 2015). U isotope fractionation ($\Delta^{238}U$ = 0.7‰) has also been observed in the modern Black Sea between organic rich sediment and the deep-water column, implying that U reduction in the sediment is primarily the result of biotic processes (Stylo et al., 2015). Manganese nodules have a fractionation of -0.2‰ in $\delta^{238}U$ toward lighter isotopic compositions, implying that the lighter isotope (^{235}U) is preferentially adsorbed (Brennecka et al., 2010; Weyer et al., 2008; Stirling et al., 2007).

More work is needed in order to accurately describe and quantify the processes driving the $^{238}U/^{235}U$ paleoredox proxy. The various methods described above, which fractionate U isotope from seawater into sediments under anoxic conditions, cause difficulty in accurately using this proxy. This thesis takes an in-depth look on constraining authigenic U in carbonates when applying in the $^{238}U/^{235}U$ carbonate model used by Brennecka et al. (2011), and Romaniello et al. (2013).

1.2 Permian–Triassic

Isotopic research focusing on the Permian–Triassic Boundary (PTB) interval and particularly on the extinction event has provided a higher resolution of global changes (Grice et al., 2005; Brennecka et al., 2011; Nestell et al., 2015; Hongfu et al., 2001; Riccardi et al., 2007; Riccardi et al., 2006; Bowring et al., 1998; Kamo et al., 2003; Clarkson et al., 2015; Kaiho et al., 2012; Algeo et al., 2007; Algeo et al., 2010; Algeo et al., 2011; Son et al., 2007). It is important

to focus research on this interval, because the PTB represents the largest mass extinction event in Earth's history, resulting in the destruction of ~90% of marine species (Erwin, 1994; Stanley, 2007). Currently, proposed kill mechanisms for the end-Permian include, a large bolide impact (Kaiho et al., 2001; Daoyi & Zheng, 1991), large-scale volcanism from the Siberian Traps (Renne & Basu, 1991; Renne et al., 1995; Wignall, 2005), and global oceanic anoxia (Wignall & Hallam, 1992; Wignall & Twitchett, 1996; Erwin, 1994; Isozaki, 1997; Kump et al., 2005; Brennecka et al., 2011; Ehrenberg et al., 2008). The $\delta^{238}U$ proxy can be used to understand and study global anoxia through the PTB interval.

Despite the evidence in support of global oceanic anoxia, there is continued debate regarding the strength and length of anoxia. The "rapid expansion of global anoxia" hypothesis (Kump et al., 2005; Meyer et al., 2008; Riccardi et al., 2007; Brennecka et al., 2011; Elrick et al., 2017) suggests that anoxia abruptly preceded the base of the extinction event horizon. At a carbonate section in Dawen, southern China, the average U isotopic composition of carbonates before the PTB extinction horizon ($\delta^{238}U$ = ~ -0.37‰) is similar to modern seawater values ($\delta^{238}U$ = ~ -0.41‰) (Brennecka et al., 2011). $\delta^{238}U$ values shift abruptly at the extinction horizon towards values averaging -0.65‰ suggesting that the change toward a lighter U isotopic composition is due to the deposition of heavy U preferentially deposited in anoxic facies such as black shales (Brennecka et al., 2011).

Using a constant source (e.g., riverine input), U fluctuations can be estimated through mass balance equations (Brennecka et al., 2011; Montoya-Pino et al., 2010; Weyer et al., 2008). This methodology was applied to carbonate sediments through the PTB interval at the Dawen section in China. This study showed a rapid (sixfold) increase in ocean anoxia and supported rapid anoxia studies (Brennecka et al., 2011; Kump et al., 2005; Meyer et al., 2008; Riccardi et

al., 2007; Elrick et al., 2017), which have challenged previously held views of an extended period of ocean anoxia preceding the end Permian extinction (Wignall & Twichett, 1996; Cao et al., 2009; Isozaki, 1997). New estimations of the U isotope fractionation factor have recently lowered the predicted sixfold increase in ocean anoxia to a ~2.5 to 5 fold increase in anoxia for the PTB (Rolison et al., 2017).

Recent work has shown a global record of oceanic redox variation, lasting ~8 m.y. before the Late Permian mass extinction and a 700 k.y. long interval following the extinction event (Elrick et al., 2017). U isotopic data from Daxiakou, China, show that 70% to 100% of marine U was removed to anoxic sinks resulting in a U concentration similar to the modern ocean (<5%) (Elrick et al., 2017). Samples directly below the extinction horizon at Dawen show high variability ranging from a $\delta^{238}U$ of -0.8‰ to 0.2‰ and these fluctuations could be caused by the addition of heavy ^{238}U by authigenic processes (Brennecka et al., 2011). It is important to understand the nature of authigenic U in order to constrain variability and suggested correction factors used in $\delta^{238}U$ paleo-redox proxies. Past studies using bulk $\delta^{238}U$ values may have overestimated the primary anoxic signal of paleo-ocean conditions. A sequential extraction method was applied to the PTB interval in order to constrain authigenic U, as well as the anoxic conditions that preceded the extinction interval sampled at Lung Cam.

1.3 Sequential Extraction

One aspect of this thesis was to develop and test an extraction method for the evaluation of U distribution in soils and sediments by analyzing various chemical phases of the sediment. Sequential extraction methods have been used in various studies to determine the distribution of heavy metals within sediment phases (e.g., Rao et al., 2007; Surija & Branica, 1995; Rutten,

2001; Mseddi et al., 2010; Ruttenberg, 1992; Jensen et al., 1998; Zimmerman & Weindorf, 2010). A quantitative assessment is crucial in order to separate diagenetic effects on carbonate uranium trends. The sequential extraction targeted the following phases in order; exchangeable ions, carbonates, apatite, oxides, organics and residual matter. Once optimized, this method was used to perform a study on the PTB in Vietnam.

One issue of sequential extractions regards chemical specificity. Chemical speciation in sediments is defined as the process of identification and quantification of the different defined species, forms or phases in which an element occurs or concentrates in the sediment matrix (Rao et al., 2008; Hall et al., 1996; Santamaria-Fernandez, 2004; Tessier et al., 1979). Chemical speciation can be further defined by identifying functional forms, operationally defined fractions, and specific chemical compounds or oxidation states (Quevauviller, 1998; Rao et al., 2008). Functional forms are mobile forms, plant-uptake available species and exchangeable cations (Quevauviller, 1998; Rao et al., 2008). Operationally defined fractions are described by the specific procedure or reagent used to target a phase (Quevauviller, 1998; Rao et al., 2008). Specific chemical compounds or oxidation states define compounds such as ferrous iron (Fe^{2+}) (Quevauviller, 1998; Rao et al., 2008). Using a sequential extraction methodology for this thesis was important in separating out authigenic influences on the carbonate sediment samples used.

2. Materials and Methods

2.1 Geologic Setting

2.1.1 Exuma Islands, TheBahamas

The Bahamas have been extensively used for the study of carbonate sediment deposition and was used here as a modern analog for authigenic U incorporation. Preliminary analysis was conducted on a bulk sediment core (Core 1) provided by Dr. Herrmann, and collected from the southern Exuma Islands (Fig. 2) in The Bahamas (Romaniello et al., 2013).

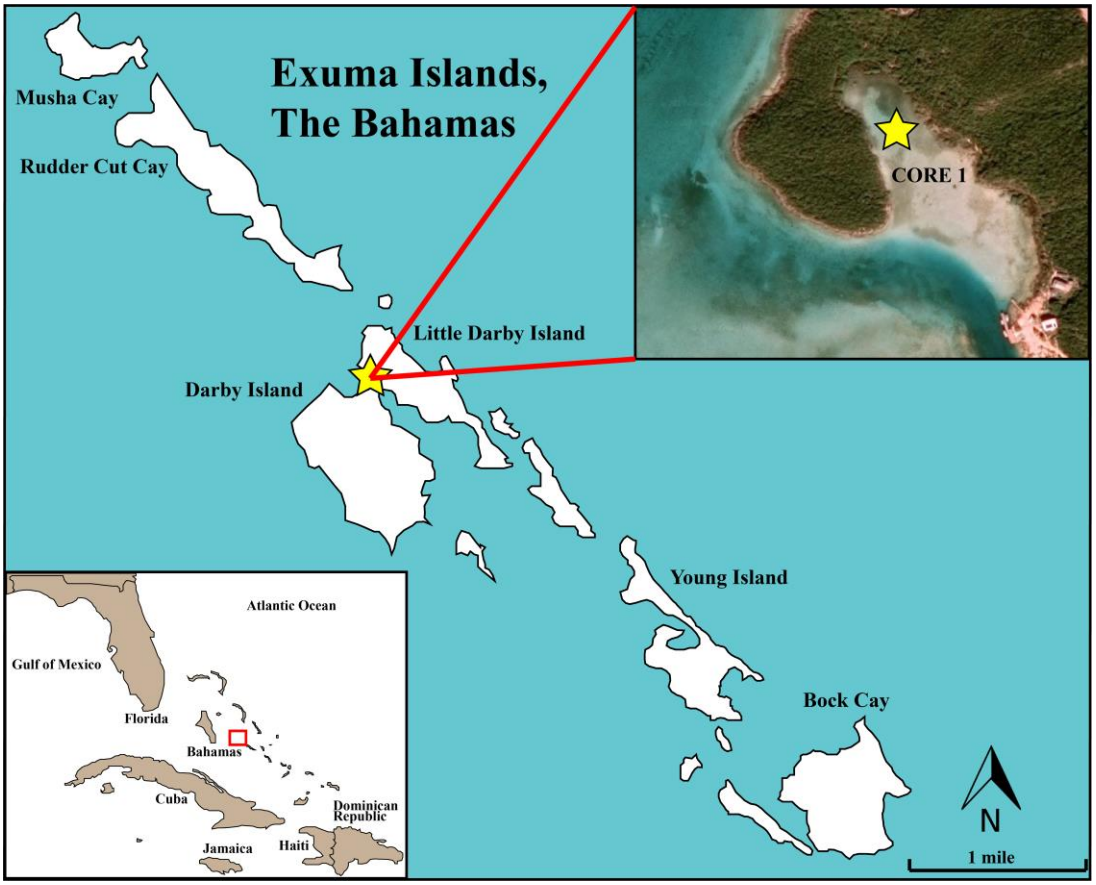

Figure 2. Map of Exuma Islands where bulk sediment Core 1 was taken at Little Darby Island, The Bahamas. Inset maps show aerial photograph where Core 1 was taken (© 2017 Google) and regional location map.

Core 1 is located on the northern end of a narrow channel between the Little Darby and Darby Islands (Romaniello et al., 2013). This core was taken from a small lagoon with an open connection to the ocean, and the area was dominated by calcareous green algae (*Halimeda incrassate*) and dense turtle grass (*Thalassia testudium*) (Romaniello et al., 2013).

2.1.2 Lung Cam, Vietnam

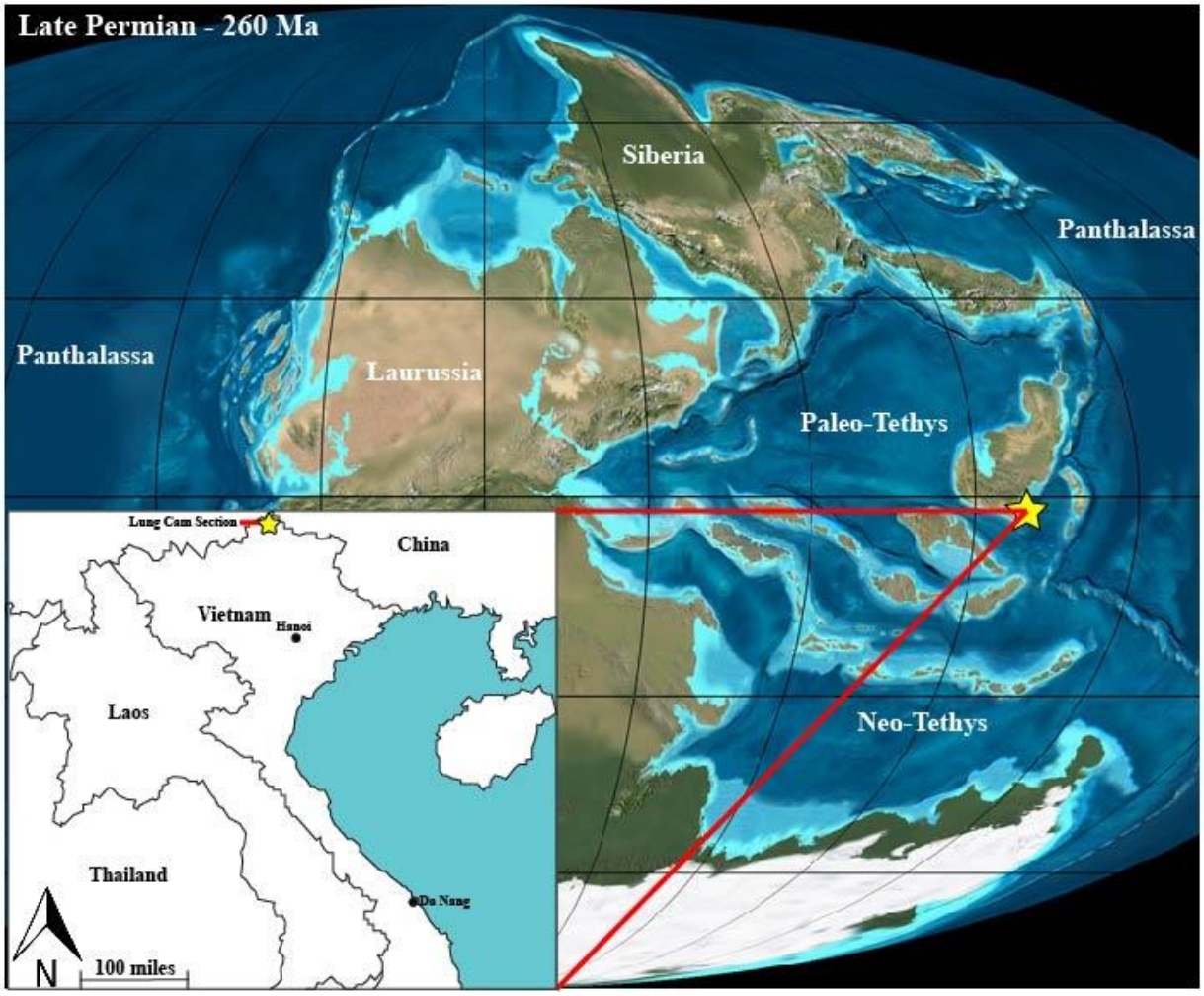

Figure 3. Paleogeographic map of the Late Permian (after Blakey 2003) showing relative position of the Lung Cam section. Inset map shows location of the Lung Cam section in North Vietnam near the border with China.

Samples were taken from the Lung Cam carbonate section located in the Ha Giang Province (Fig. 3) in North Vietnam an area currently being studied by Dr. Ellwood at LSU (Nestell et al., 2015; Wardlaw et al., 2015; Ellwood et al., 2017). Dr. Ellwood provided the samples used for this thesis. Thirty samples from this dataset were selected for sequential extraction and were chosen based on previous U & Mo concentration data provided by Dr. Ellwood. Figure 4 shows the outcrop picture of the Lung Cam section.

Figure 4. Outcrop photo of Lung Cam section. Outcrop is located on the right side of the picture. Photo provided by Dr. Ellwood

This section contains mainly limestones beds, which were selected for sequential extraction in order to identify and constrain authigenic U contribution as it relates to the $\delta^{238}U$ proxy. It is important to clarify that the Lung Cam section has been correlated to the global

stratotype section and point (GSSP) of the PTB at Meishan using graphic correlation methods. (Ellwood et al., 2017)

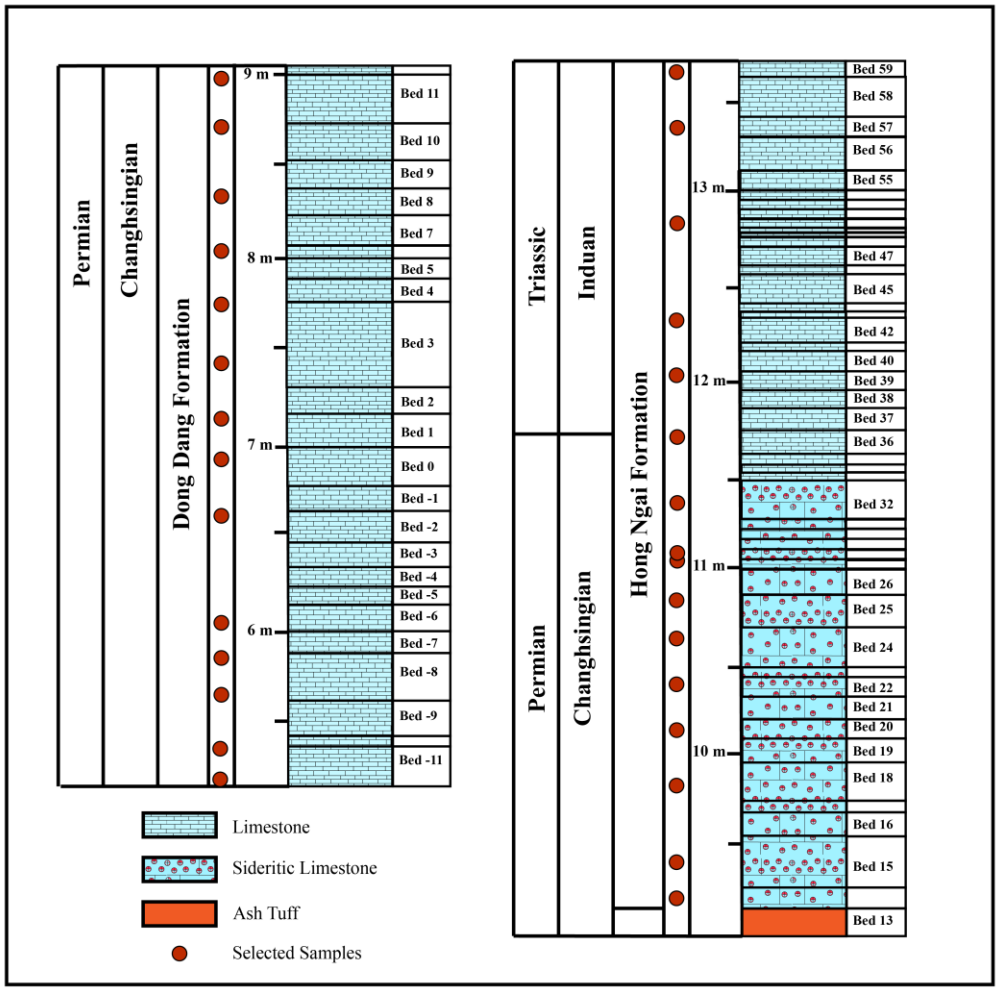

Figure 5. Stratigraphic column of the Lung Cam section showing Permian–Triassic Boundary. Red dots are selected samples for analysis.

The PTB interval for the Lung Cam section (Fig. 5) begins with 1 m of limestone corresponding with Beds 5-11 overlain by Bed 12, which is a very thin (~1cm) microbial limestone layer (Nestell et al., 2015). Bed 13 has been described as a 14 cm-thick ash tuff (Nestell et al., 2015), which is the uppermost bed of the Dong Dang formation (Late Permian) (Son et al., 2007). This unit was correlated to Bed 25 at the GSSP section in Meishan (Nestell et al., 2015; Ellwood et al., 2017). Beds 14-32 are a 2.3-meter thick unit containing siderite or

ankerite limestone (Nestell et al., 2015). Son et al. (2007) had previously described Beds 14-32 as being a dolomitic limestone, however XRD analysis showed no significant dolomite (Nestell et al., 2015).

The GSSP for the PTB is defined by the first appearance datum (FAD) of the conodont *Hindeodus parvus* and is located at the base of Bed 27c, Meishan Section D, Changxing County, Zhejiang Province, China (Hongfu et al., 2001). The paleontologically defined PTB has been constrained using U/Pb zircon dating for an age ranging from <251.4 ± 0.3 Ma to >250.7 ± 0.3 Ma (Bowring et al., 1998). U/Pb zircon dating has also dated the age of the event horizon to 252.6 ± 0.2 Ma (Mundil et al., 2004). At the Lung Cam section the PTB has been identified between Bed 36 and 37 using graphic correlation work (Ellwood et al., 2017) and occurs ~0.8m above the lowest observed occurrence point (LOOP) of *H. parvus* (Wardlow et al., 2015).

2.2 Sequential Extraction Methodology

Several modifications were made to the original Surija and Branica (1995) procedure. First, the initial extraction called for using Ammonium Acetate, but this was replaced by Sodium Bicarbonate. Recent work by Morin et al. (2016) showed that Sodium Bicarbonate was effective at removing Uranium in exchangeable fractions or non-crystalline uranium species (Morin et al., 2016). Second, the apatite extraction is not seen in typical "Tessier sequential extractions". However, due to U incorporation into apatite, it is important to account for possible uranium incorporation into apatite species during diagenesis. For this reason, two phosphate standards and one apatite standard were used to test the apatite extraction phase. Third, sample: solution ratios were reduced to 1:25 for every original fraction besides carbonate. Preliminary runs showed incomplete digestion of carbonate with any sample: solution ratio below 1:100. Fourth, sample

size was reduced to 0.5g to reduce and conserve reagent material, rather than the 1g sample size used by Surija and Branica (1995).

All carbonate samples underwent the modified sequential extraction illustrated in Table 1. During treatment phases, samples were in test tubes under occasional agitation and in certain phases heated on hotplates and buffered to specific pH's. At the end of each respective phase, the supernatant was separated by pipette after 30-minute centrifugation at 4,000 rpms. This was accompanied by two 10 ml washes of deionized water and centrifuged.

Several standards were tested to evaluate the effectiveness of a modified sequential extraction (Table 1) from Surija and Branica (1995). The tested materials were the following: Moroccan Phosphate Rock (BCR-CRM032), Phosphate Rock (NIST SRM 120c), Pure Apatite Standard, Italian marine limestone (IAEA-B7), and Puratronic Carbonate Standard. The extracts were analyzed for U concentrations utilizing Thermo iCAP Q ICP-MS and compared to certified values where available to gauge the effect each reagent had on the particular chemical fraction.

Sequential Extraction Methodology					
Phase		**Reagent**	**Sample:Solution Ratio**	**Applications**	**Time/Heat**
Exchangeable	E1	1 m Sodium Bicarbonate ($NaHCO_3$)	1:25	1X	24 hours at 25° C
Carbonate	E2	1 m Sodium Acetate (CH_3COONa) buffered to pH of 5 with acetic acid ($C_2H_4O_2$)	1:100	1X	24 hours at 25° C
Apatite	E3	1 m Nitric acid (HNO_3)	1:10	1X	1 hour at 25° C
Oxide	E4	1 m Hydroxylamine Hydrochloride in 25% acetic acid ($C_2H_4O_2$)	1:25	1X	6 hours at 95° C
Organic	E5	0.02 molar Nitric Acid (HNO_3) in 30% Hydrogen Peroxide (H_2O_2)	1:25	3X	24 hours at 85° C
Residual	E6	Conc. Nitric Acid (HNO_3)	1:25	3X	24 hours at 95° C
Total Digest	TD	Conc. Nitric Acid (HNO_3)	1:25	3X	24 hours at 95° C

Table 1. Expanded section of the modified sequential extraction procedure illustrating the various extraction reagents and specific preparation for each phase (Surjia & Branica, 1995)

2.3 ICP-MS Methods

Runs were conducted at Louisiana State University (LSU) on a Thermo iCap QC ICP-MS for U concentration data in order to test the effectiveness of the sequential extraction procedure. An external calibration modified from EPA Method 200.8 was used to analyze for U and other trace metals (Appendix A & B). Extracts obtained from the sequential extraction were dried and brought up in 2% nitric acid for stock solution for ICP-MS measurement. Samples were diluted to appropriate dilutions to reduce the estimated total dissolved solid content below 0.2% w/v. All solutions were prepared using ultrapure-deionized water and all reagents used were Trace Metal Grade. Multiple dilutions of a multi-element standard (QCP-QCS-3) were used in order to create an external calibration curve and for quality check. Calcium, Rubidium and Strontium standards were added to the QCP-QCS-3 multi-element standard for quantification purposes. Instrument drift and suppression effects were corrected using an internal standard: IV-ICP-MS-71D (^{6}Li, Sc, In, Tb, Y, Bi). The cones of the ICP-MS were conditioned by aspiring a 300 ppm Ca standard for 30 minutes before each run. Each fraction was run individually to limit the matrix affects due to the different reagents used during the experiment. In order to ensure full U recovery, the summation of U concentrations for all phases of the sequential extraction were compared to the U concentrations of a bulk digest run.

2.4 Pre-collected X-Ray Fluorescence Data (XRF)

The Lung Cam section has pre-collected XRF data that were provided by Dr. Ellwood. This was used to compare values against the summation and total digest of the sequential extraction methodology.

Chapter 3. Results

3.1 Uranium Distribution in Selected Standards by Sequential Extraction

U concentrations (Table 2) and trace metals are shown in Figure 6. The majority of U extracted from the phosphate apatite standards (BCR-CRM032, NIST 120c, Apatite) was in the apatite-associated fraction. However, the Moroccan phosphate (BCR-CRM032) had significant enrichment in the exchangeable phase (~25 %). In contrast, the majority of U extracted for the carbonate extracts was primarily located in the carbonate fraction although significant Uranium contribution (~33%) was seen in the apatite fraction for the IAEA-B7 standard. Successful application of the sequential extraction methodology is seen in the Puratronic standard with 99% of all Ca being removed during the carbonate fraction extraction phase (Fig. 6).

Extraction	BCR-CRM032	IAEA-B7	NIST 120c	Puratronic Carbonate	Pure Apatite
E1	34.73	0.09	6.21	BDL*	5.02
E2	1.81	1.32	4.68	0.003	4.63
E3	70.37	0.74	93.16	0	61.62
E4	19.37	0.01	7.14	0.0004	4.14
E5	4.91	0.00	6.04	0.001	3.96
E6	0.09	0.0004	0.92	0	23.89
SUM	131.29	2.16	118.15	0.052	103.26
TD	135.13	2.02	123.22	0	114.84
Certified Value	125	1.65	114	N/A	N/A

Table 2. Uranium concentrations (PPM) of the selected standards from the sequential extraction methodology. Sum extraction is the summation of extracts E1 through E6. *Below Dectection Limit (BDL)

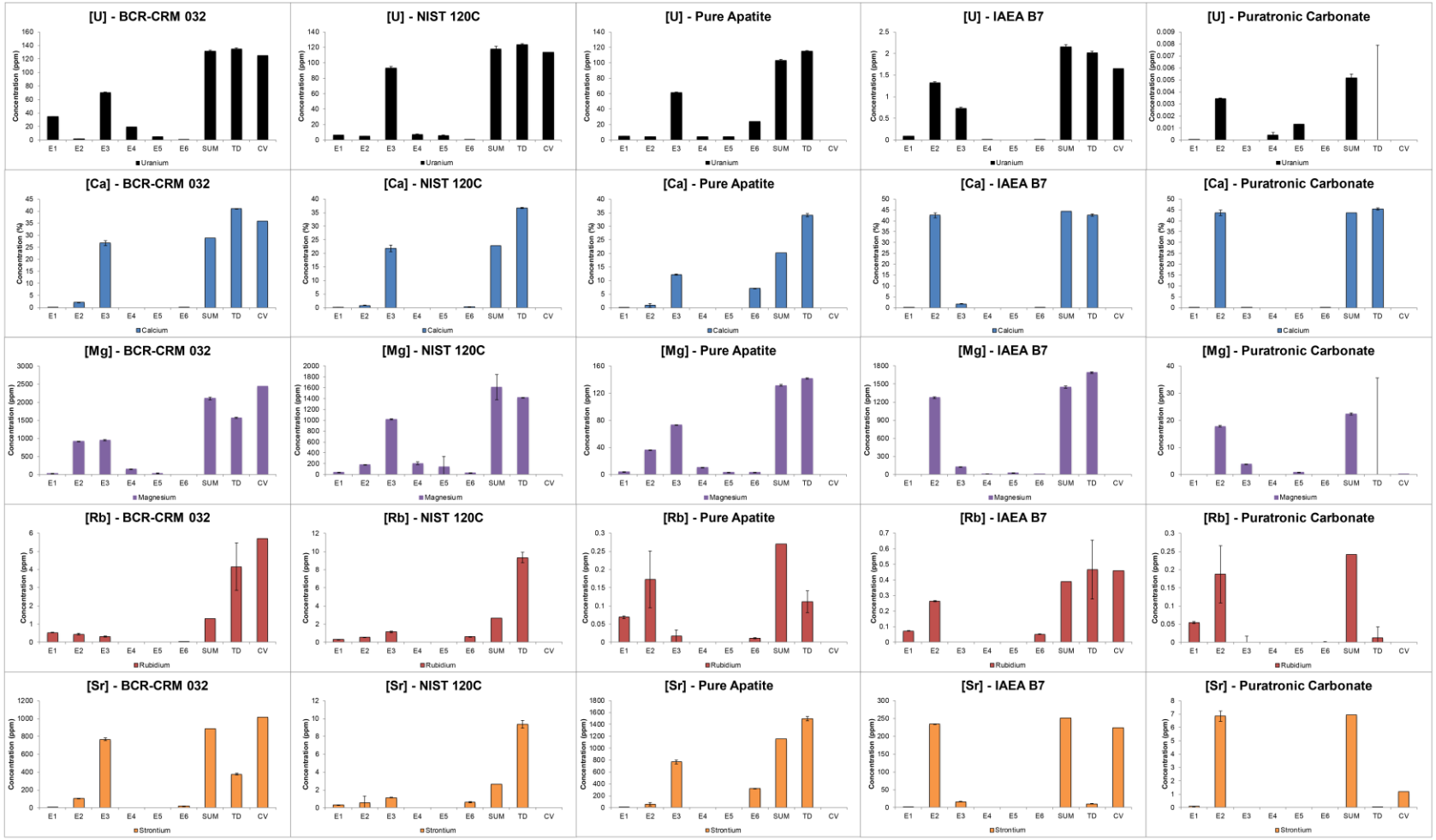

Figure 6. Elemental concentrations (U, Ca, Mg, Rb, Sr) for the chemical fractions targeted with a modified sequential extraction. The tested standards are: (A) Moroccan Phosphate Rock: BCR-CRM 032, (B) Italian marine limestone: IAEA-B7, (C) Phosphate rock: NIST 120c, (D) Puratronic carbonate, (E) Pure apatite. Extraction steps: E1 – Exchangeable metals, E2 – Carbonate, E3 – Apatite, E4 – Oxide, E5 – Organic, E6 – Residual, SUM – Summation of all extraction steps, TD – Total Digest.

3.2 Sequential Extraction in Modern Carbonates

3.2.1 U Extraction of Modern Carbonates

The uranium distribution of the Bahamian extracts for the modified sequential extraction is shown in Figure 7 and Appendix B. The U of the extracts are plotted relative to depth and contrasted with Uranium % relative to the summation of the sequential extraction.

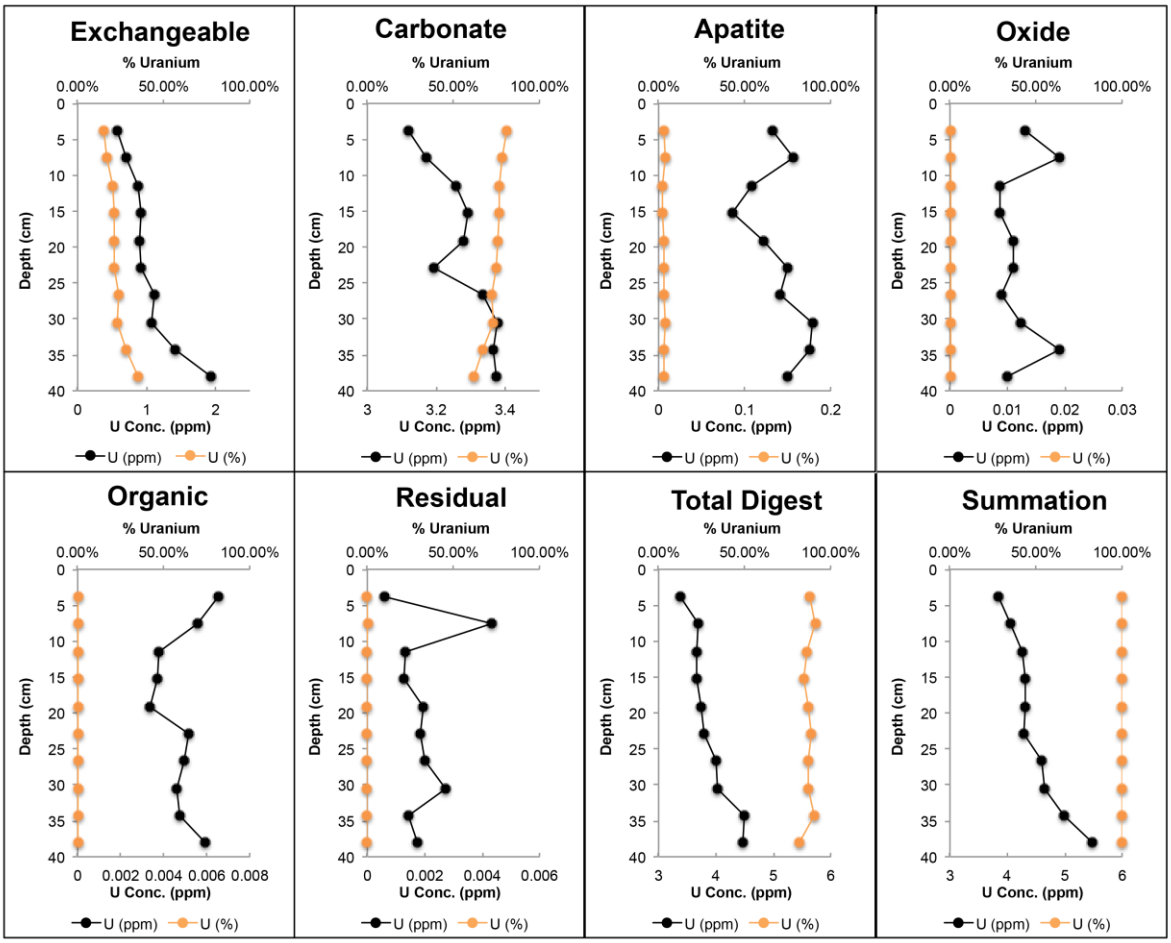

Figure 7. Uranium concentrations vs depth (cm) for each chemical fraction used in the sequential extraction method applied to the Bahamian carbonates. The % Uranium for the E1-E6 fractions are based on the Summation. The % plot for the Summation graph is a comparison to the Total Digest.

The majority of U was found in the carbonate fraction with an average U concentration of 3.27 ppm. U concentration increases downcore in the carbonate fraction (3.12 ppm to 3.37 ppm) and in the exchangeable/non-crystalline uranium species fraction (0.58 ppm to 1.94 ppm). The majority of authigenic U is found in the exchangeable or non-crystalline uranium species fraction (E1) with the rest of the fractions contributing negligible amounts of U.

3.2.2 Elemental Breakdown in Modern Carbonates

The elemental breakdown for each fraction in the sequential extraction used for the Bahamas samples is shown below in Figures 8 - 14. Twelve elements were selected (U, Mo, V, Cr, Mg, Co, Th, Mn, Ni, Cu) to illustrate the respective species or fraction that was targeted. Concentrations for the selected elements and trace metals are given in Appendix B.

In the E1 fraction (Fig. 9); U, Mo, and Co show an increase in concentration with depth. U and Co show ~25% of the total extracted concentration, while 75% of the total Mo is found in the E1 fraction. In contrast, V, Cr, and Mg show a decreasing concentration with depth. The majority of V (~75%) is extracted in the E1 fraction, while 25% of the Mg is extracted. Negligible amounts of Th, Mn, Sr, Rb, Ni, Cu were extracted in the E1 fraction. In terms of Ca, there is negligible contribution suggesting that the Sodium Bicarbonate reagent does not prematurely attack the carbonate fraction.

In the E2 fraction, all elements and trace metals shown in Fig. 10 besides Cu and Th, show an increase in concentration with depth. Thorium is stable around 0.1 – 0.2 ppm while negligible amounts of Cu were extracted in the E2 fraction. The majority of U, Co, Mn, Sr, and Ni seems to be extracted during the carbonate fraction. Th and Rb show 50% of the total respective values removed while Mo, V, and Cr show 5% - 25% of the total summation

accounted for in the E2 fraction. Results suggest that this methodology is successful regarding complete carbonate digestion with 99% of all Ca found within the carbonate fraction in Bahamian samples.

In the E3 fraction (Fig. 11); the majority of elements and trace metals are less than 5% of the total summation. However, the majority of Cu is extracted in the apatite fraction, with over ~50% of the total Cu removed. V, Cr, Rb, and Th values range from ~5% to ~20% of the total concentration.

In the E4 fraction, V, Cr, and Rb values range from 5% to ~25% of the total value (Fig. 12). Small spikes in Th and Cu are observed. All other elements and trace metals extracted were found to have negligible concentrations. In the E5 fraction (Fig. 13): Cu and Cr values were found to be ~50% of the total concentrations. Rb, Mn, and Th averaged around ~25% of the total value, while Mo ranged from ~5% to 15%. All other elements and trace metals were found to have negligible concentrations. In the E6 fraction, only Th is shown to have any appreciable concentration left (~5% to ~25% of the total value) (Fig. 14). All other elements and trace metals were found to have negligible concentrations.

The summation of the sequential extraction is typically higher than the total digest but have similar trends. This is observed for in U, Mo, and Co. Mn, Sr, and Mg (Fig. 15), which have lower values in the summation than the total digest, but continue to show similar trends. For Cr, the total digest and summation match within ~5%. However, Th and Cu have extremely varying values between the summation and total digest (3X). Elemental crossplots are shown in Figures 16-17. Trace metals were chosen based on the various trends observed in the E1 and E2 fraction.

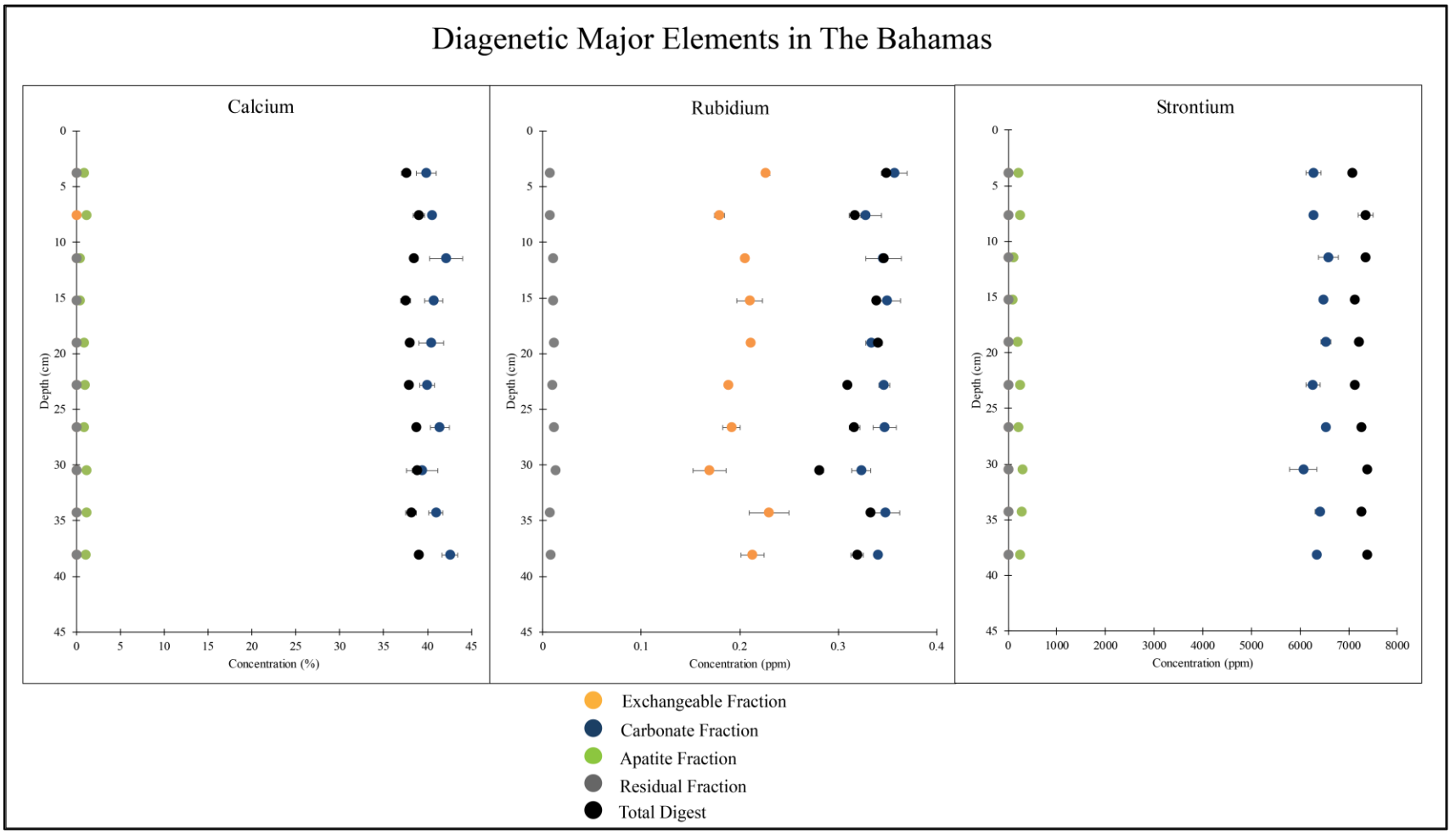

Figure 8. Diagenetic major elements (Ca, Rb, Sr) for Core 1 in The Bahamas. Exchangeable, Carbonate, Apatite, Residual, and Total Digest fraction data is shown.

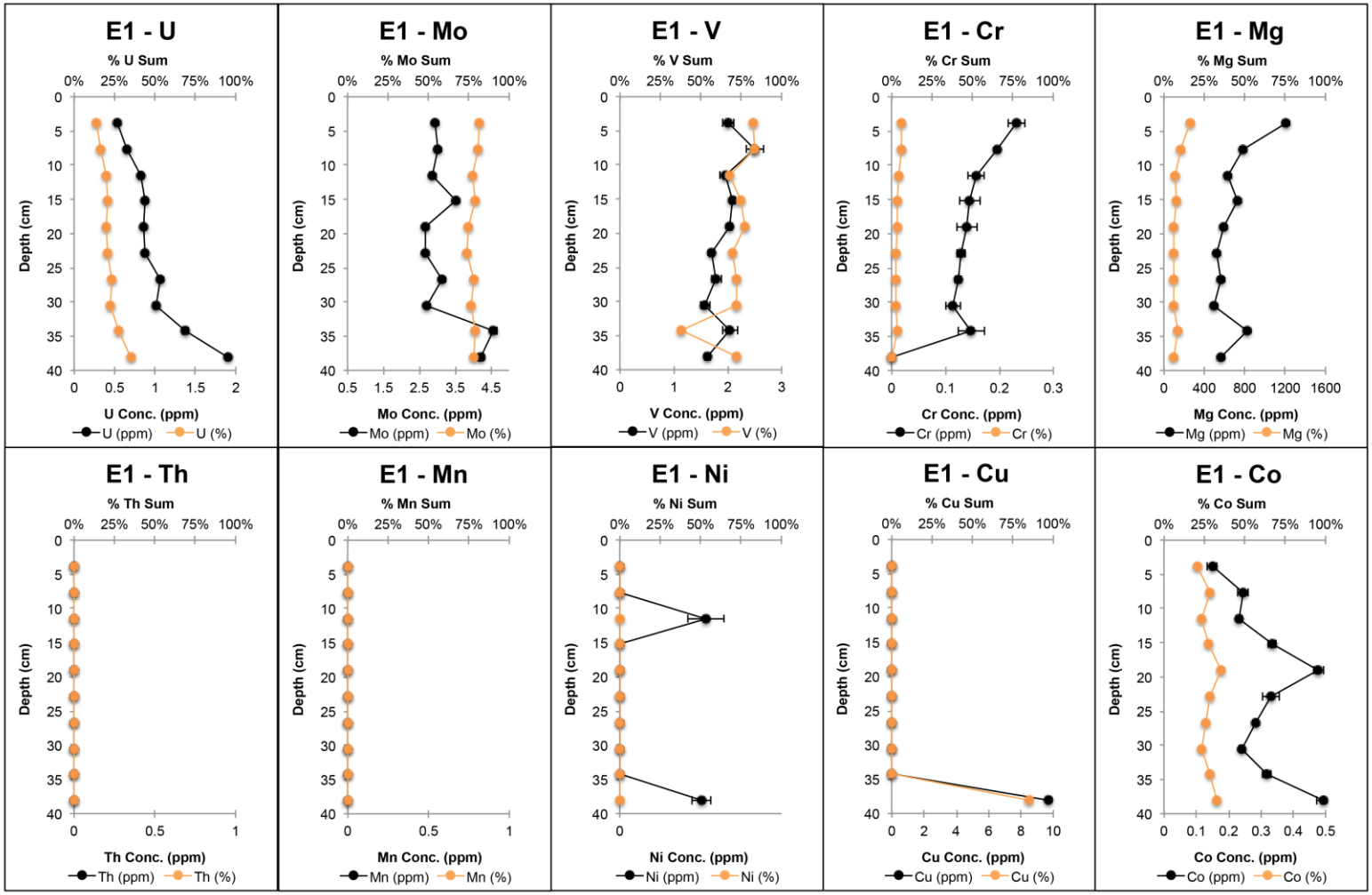

Figure 9. Elemental concentrations for the exchangeable fraction [E1] used in the sequential extraction method applied to Bahamian carbonates. % Sum of each element is based on the percentage of the E1 fraction relative to the total summation of the sequential extraction.

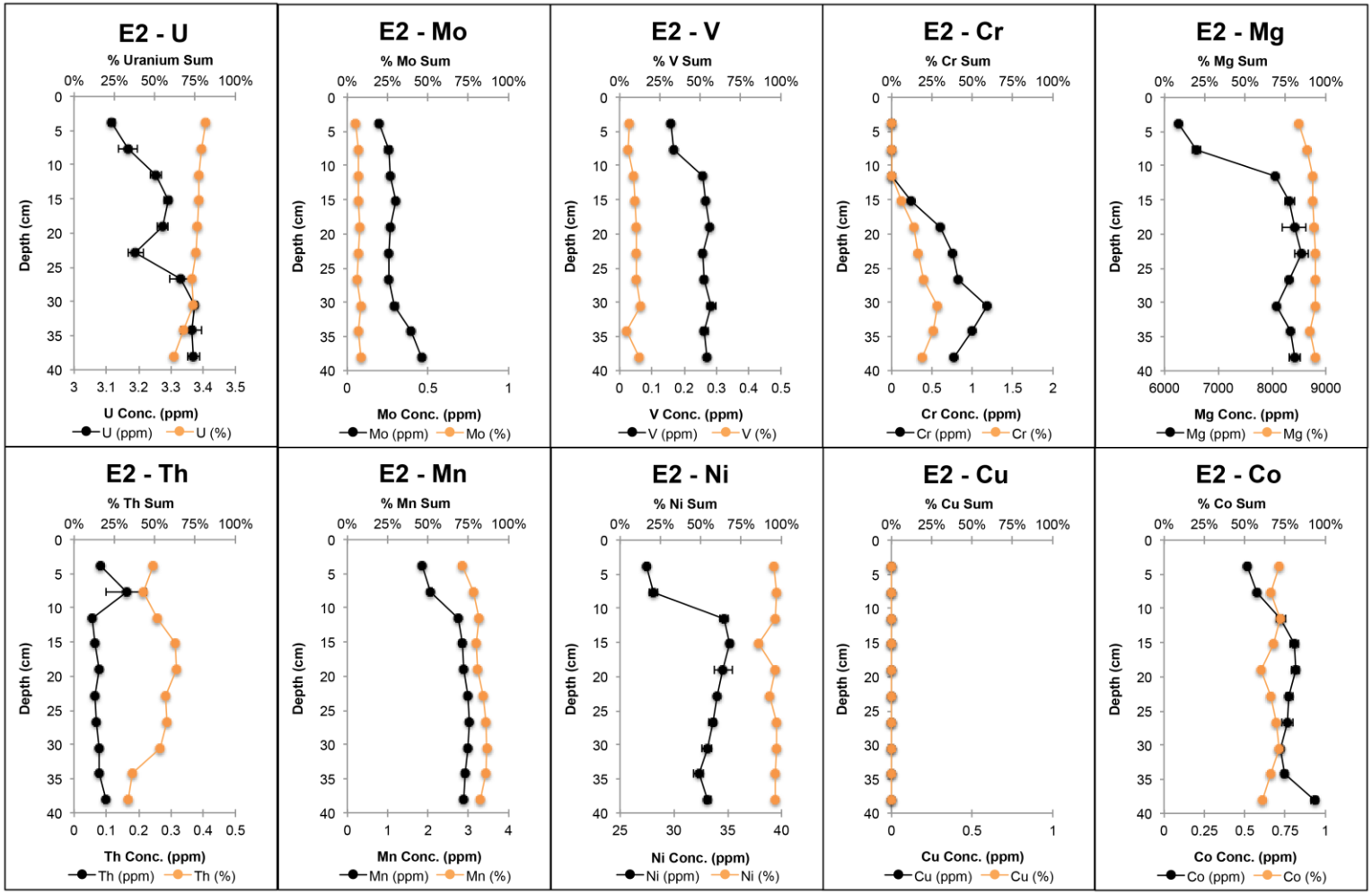

Figure 10: Elemental concentrations for the carbonate fraction [E2] used in the sequential extraction method applied to Bahamian carbonates. % Sum of each element is based on the percentage of the E2 fraction relative to the total summation of the sequential extraction.

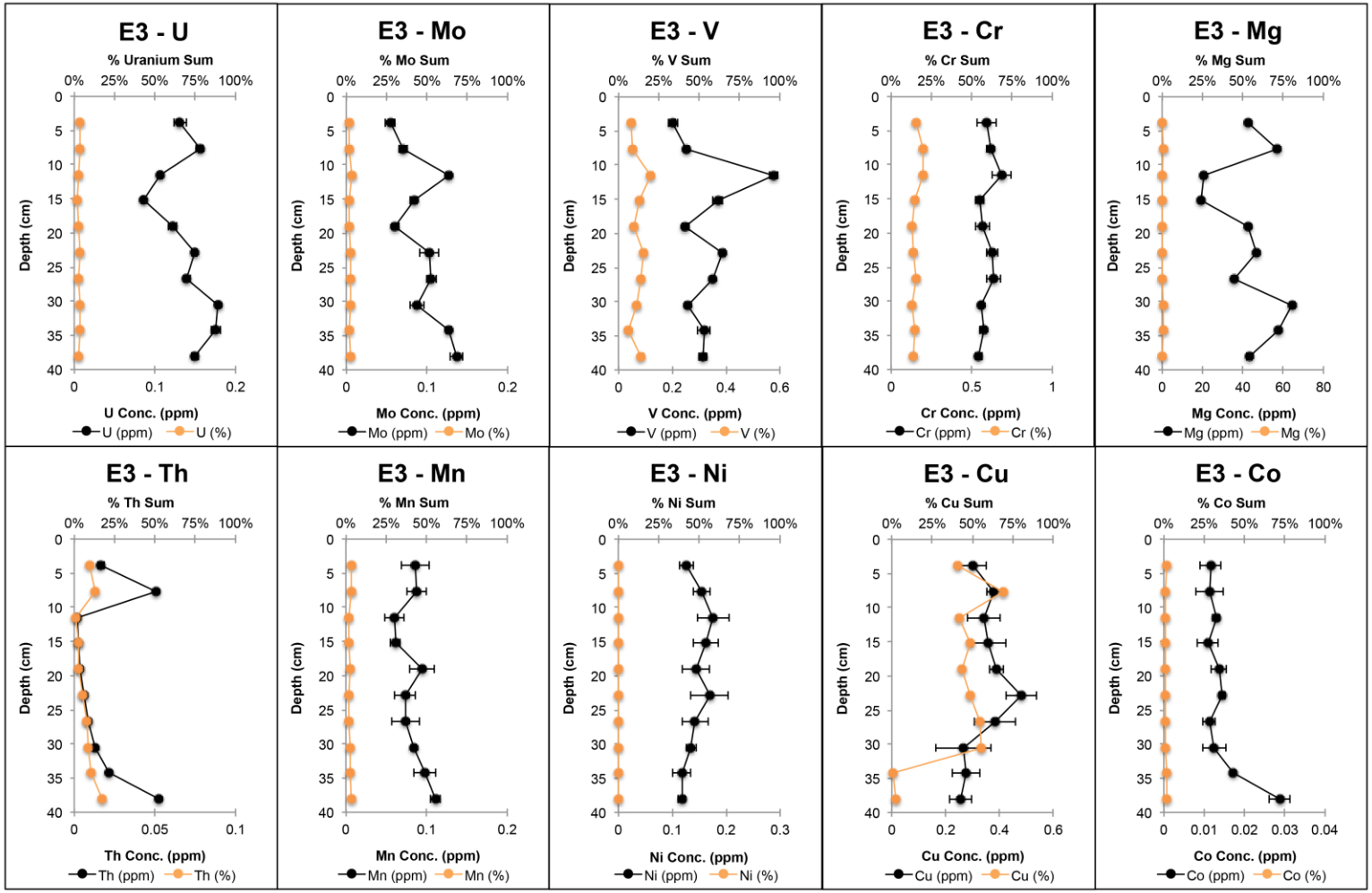

Figure 11: Elemental concentrations for the apatite fraction [E3] used in the sequential extraction method applied to Bahamian carbonates. % Sum of each element is based on the percentage of the E3 fraction relative to the total summation of the sequential extraction.

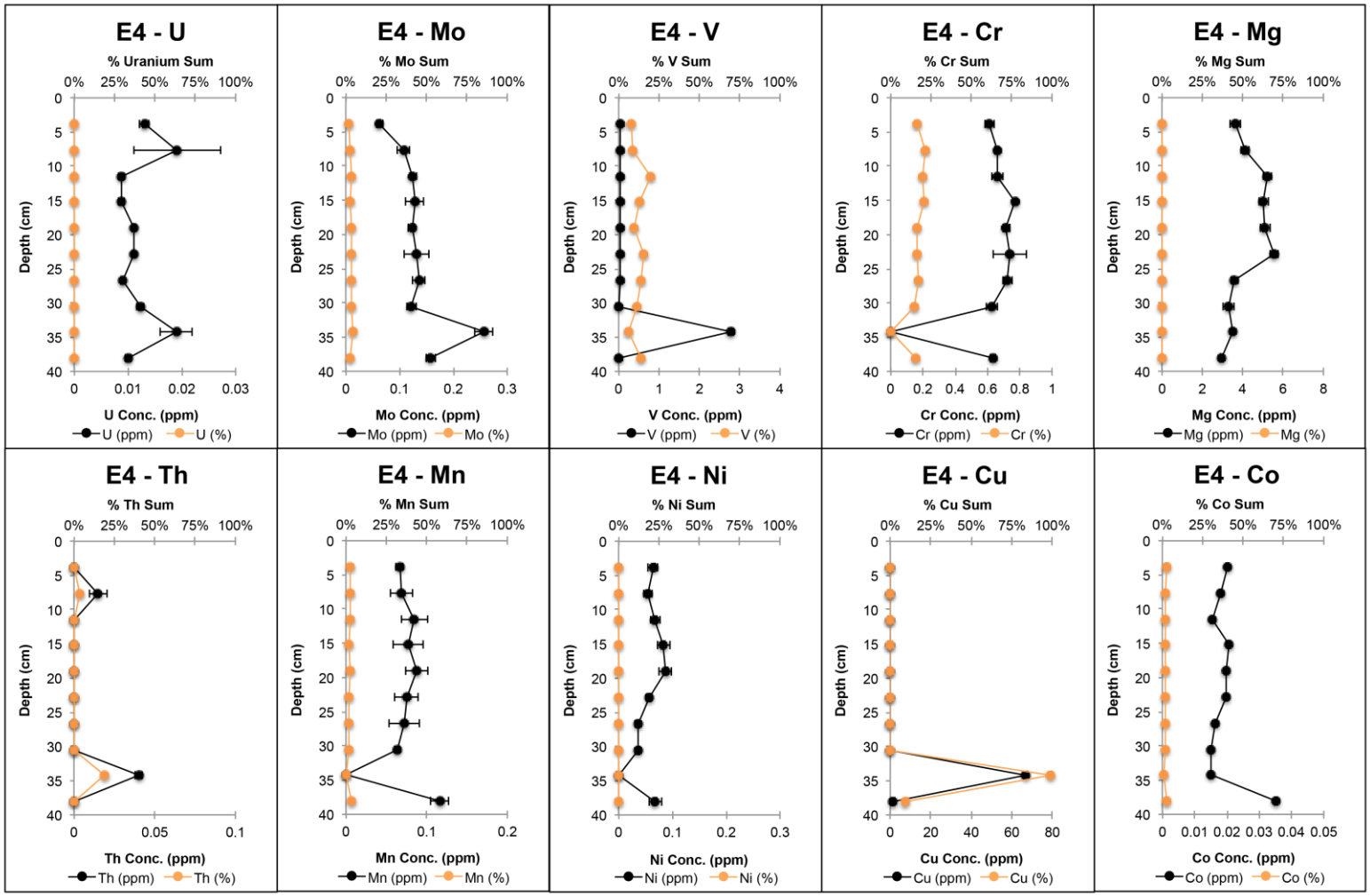

Figure 12: Elemental concentrations for the oxide fraction [E4] used in the sequential extraction method applied to Bahamian carbonates. % Sum of each element is based on the percentage of the E4 fraction relative to the total summation of the sequential extraction.

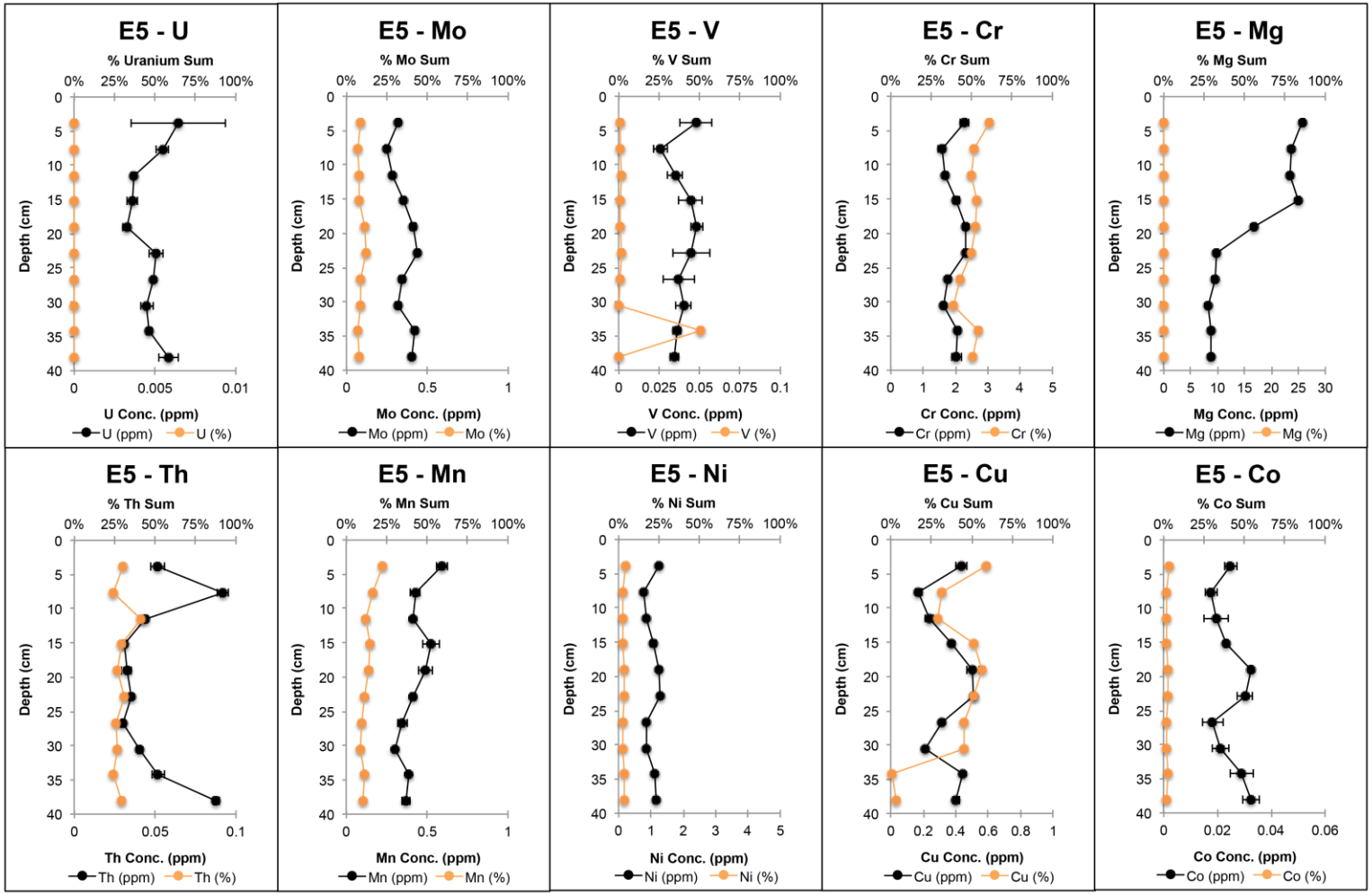

Figure 13: Elemental concentrations for the organic fraction [E5] used in the sequential extraction method applied to Bahamian carbonates. % Sum of each element is based on the percentage of the E5 fraction relative to the total summation of the sequential extraction.

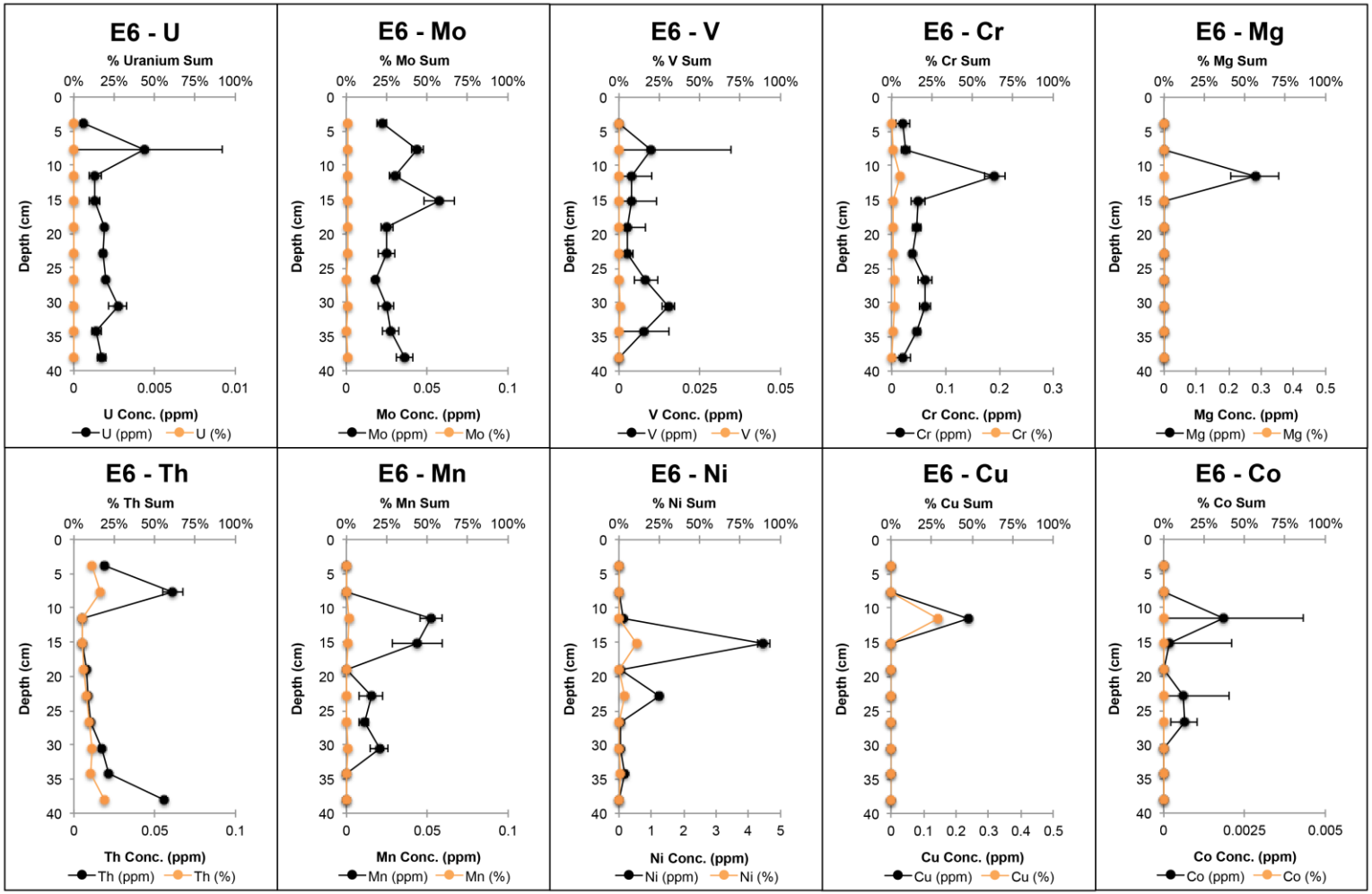

Figure 14: Elemental concentrations for the residual fraction [E6] used in the sequential extraction method applied to Bahamian carbonates. % Sum of each element is based on the percentage of the E6 fraction relative to the total summation of the sequential extraction.

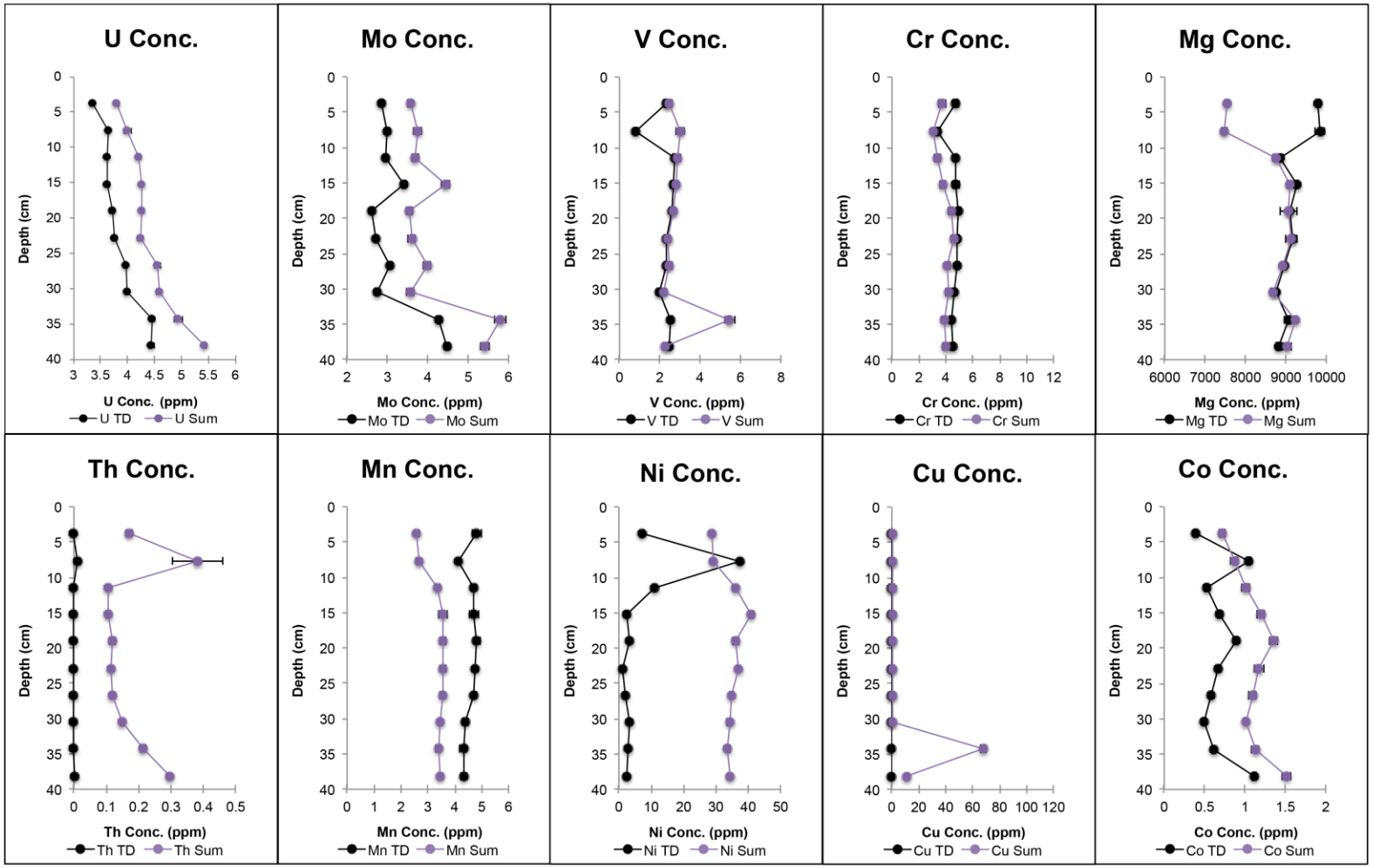

Figure 15: Elemental concentration comparison between the Total Digest and the Summation of the sequential extraction methodology applied to Bahamian carbonates.

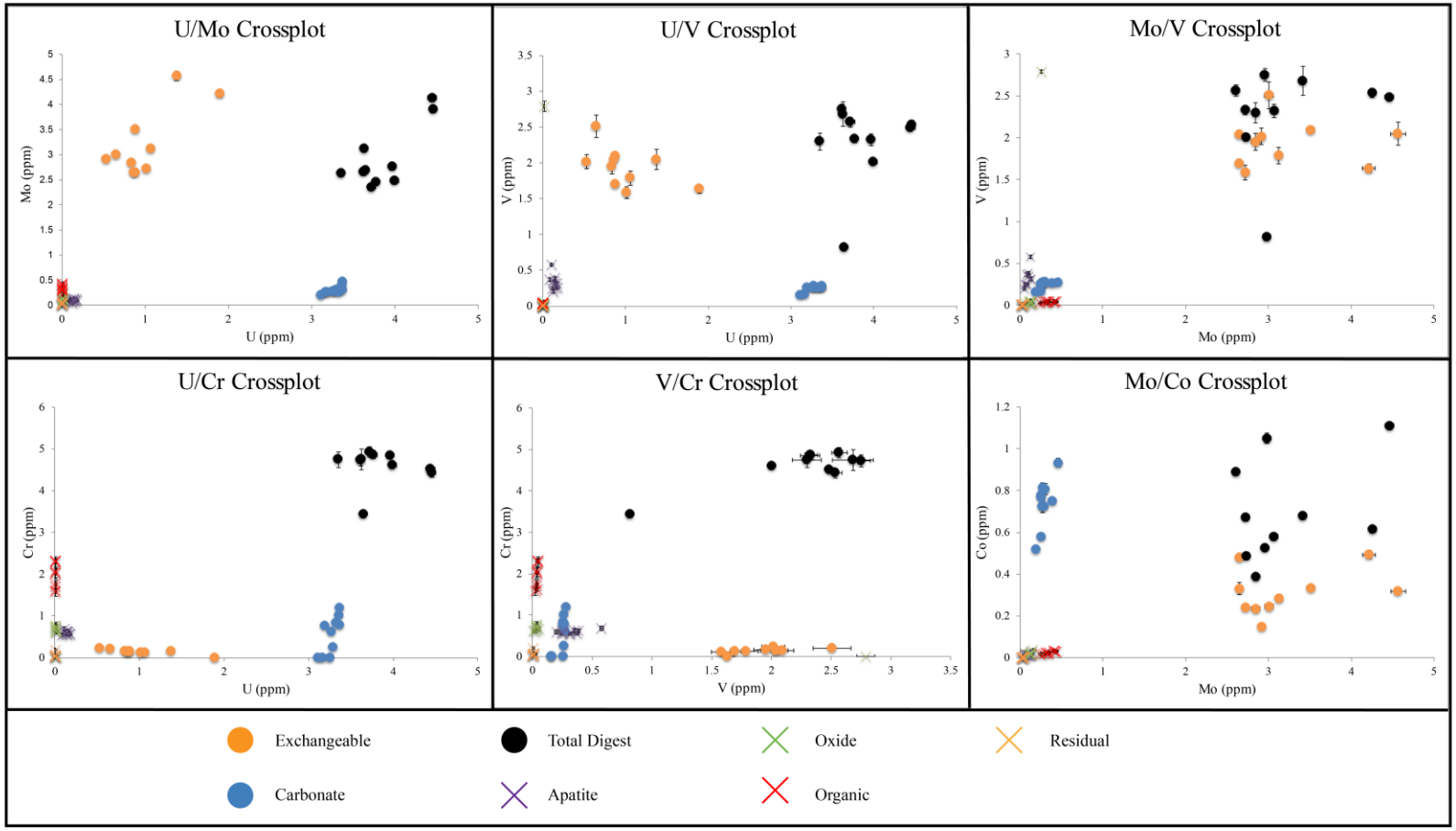

Figure 16: Elemental crossplots of U/Mo, U/V, Mo/V, U/Cr, V/Cr and Mo/Co using the chemical fractions [E1,E2,E3,E4,E5,E6] and Total Digestion concentrations.

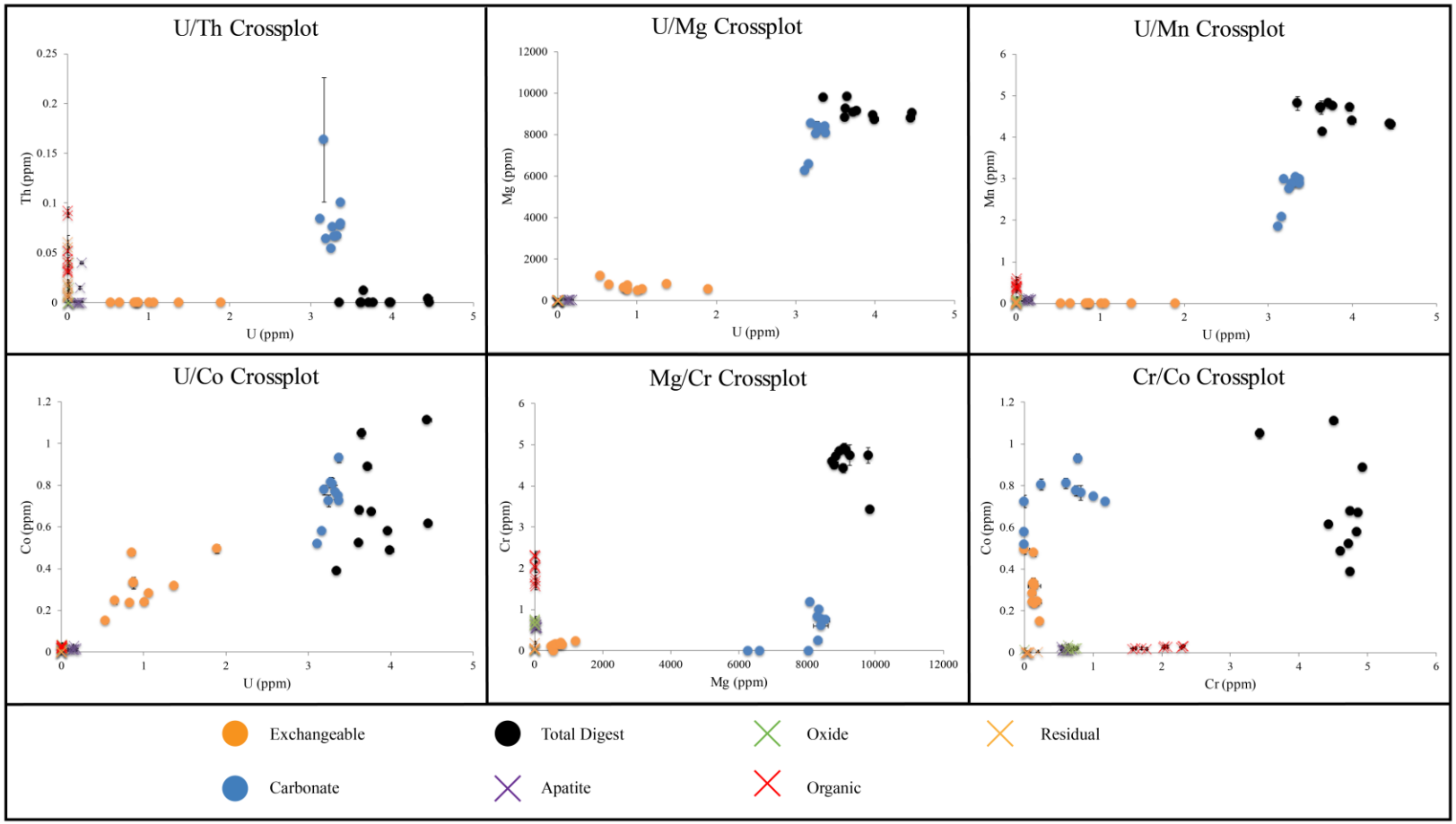

Figure 17: Elemental crossplots of U/Th, U/Mg, U/Mn, U/Co, Mg/Cr and Cr/Co using the chemical fractions [E1,E2,E3,E4,E5,E6] and Total Digestion concentrations.

3.3 Sequential Extraction of Lung Cam Carbonates

3.3.1 U Extraction of Lung Cam Carbonates

The uranium distribution of the extracts for the modified sequential extraction is shown in Figure 18 and Appendix C. U in the Lung Cam extracts is plotted relative to depth and plotted alongside Uranium % relative to the summation of the sequential extraction.

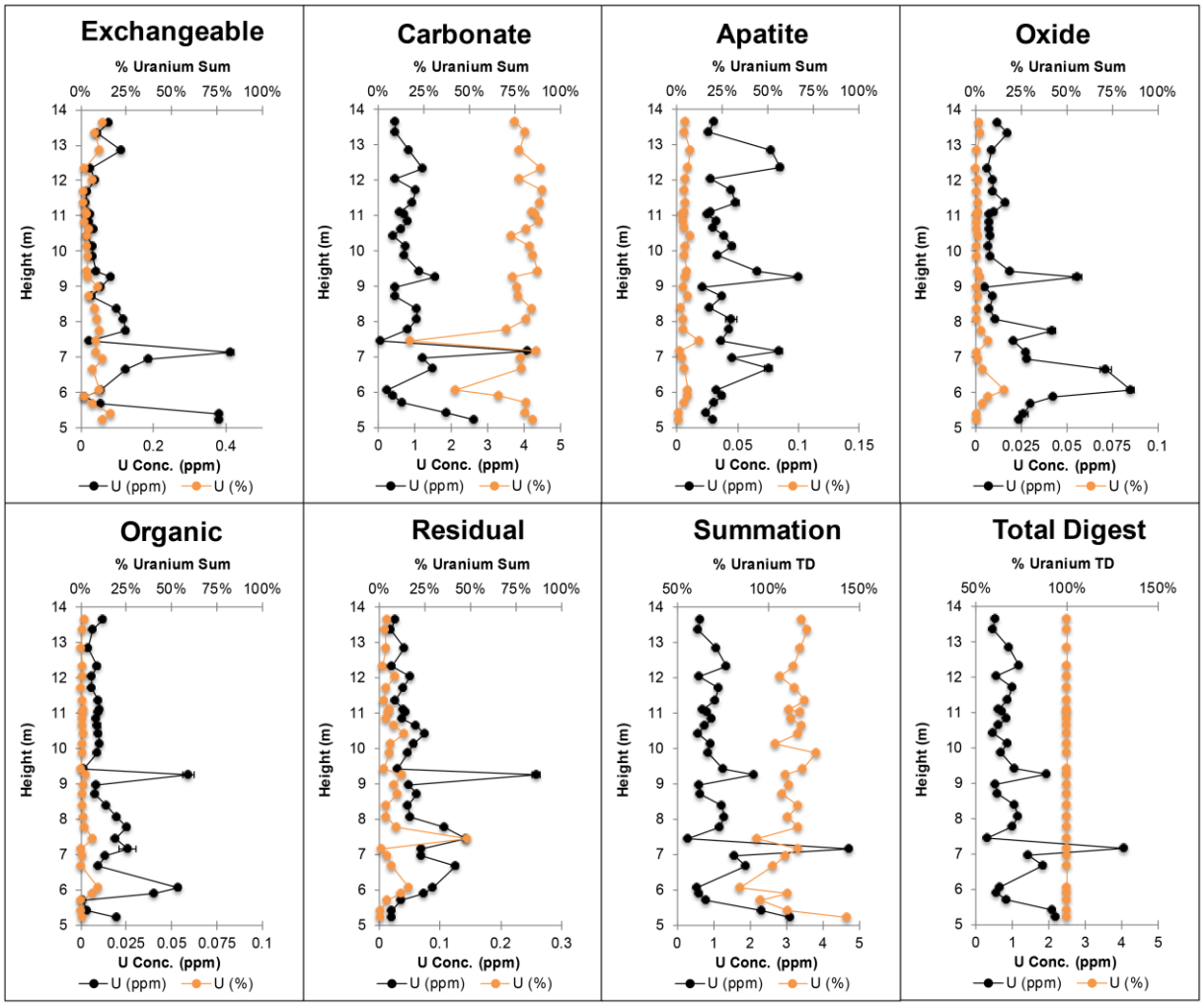

Figure 18: Uranium concentration vs depth (m) for each chemical fraction used in the sequential extraction method applied to the Lung Cam carbonates.

Triassic samples have a relative flat-line trend with U concentrations ranging from 0.4 ppm to 1.5 ppm. This is in contrast to the high variability (0.05 ppm to 4 ppm) seen in the Permian samples. In the Triassic, the majority of authigenic U is seen in the exchangeable (E1) fraction with U contributions, relative to the bulk, ranging from 5% to 18 %. The second highest authigenic U seen in the Triassic samples are in the residual phase with contributions, relative to the bulk, ranging from 2% to 12%. The rest of the fractions for the Triassic samples contribute negligible amounts of U (0% to 5%).

Permian samples have high variability (0.05 to 4 ppm). This high variability is discussed in 4.3.6. Similar to the Triassic, the majority of authigenic U is seen in the exchangeable (E1 fraction). However, in terms of the second highest authigenic U, there is wide variability within each fraction, E3, E4, E5, and E6, all contributing to the bulk, depending on the respective sample.

3.3.2 Elemental Breakdown for Lung Cam Carbonates

In the E1 fraction (Fig. 19); U, Mo, V have values from 3% to 20% of the total value of their respective concentrations. Co has a wide range from 5% to 50% of the total concentration of Co. All other elements and trace metals are negligible.

The E2 fraction (Fig. 20) represents the largest contribution of elements, which is expected due to the Lung Cam samples being carbonate-dominated. This E2 fraction also represents the majority of U values with the samples representing >75% of the total U. Thorium, within the carbonate fraction, represents ~75% of the total Th and remains relatively stable within the section. Magnesium within the lower section of Lung Cam is primarily dominating the carbonate phase, but upsection, Mg concentration increases rapidly representing ~50% of the

total Mg within the carbonate fraction, suggesting a change in lithology. Studies by Nestell et al. (2015) have shown this section to not be dolomitic. Mo, V, Cr, Rb, and Cu have negligible contributions. The E3 fraction (Fig. 21) represents the second largest contribution of elements, suggesting a significant source of apatite. In the E3 fraction, the remaining Mg component is found, suggesting this is a biological carbonate apatite, beginning in Bed 3 and continuing into the Triassic carbonates. Mo, V, Cr, Mg, Co, Th, Mn, Sr, Rb, Cu have values ranging from 2% - 50% of the total value of their respective concentrations.

In the E4 fraction (Fig. 22), V and Cr have values ranging from 5% to 25% of the total value of their respective concentrations. All other elements and trace metals are negligible, suggesting no significant source of oxides. The E5 fraction (Fig. 23) represents the third largest contribution of elements, which shows that the Lung Cam section has some input from both terrestrial and marine organic matter. Mo, V, Cu and Cr have significant concentrations, suggesting they are incorporated into organic material during redox conditions. All other elements and trace metals are negligible. The E6 fraction (Fig. 24) represents detrital resistant minerals such as quartz and clays. A significant portion of U was found in this fraction representing 2% to 20%. V, Cr, Th, and Rb elements have values ranging from 2% to 75% of their respective concentrations. All other metals and trace elements are negligible.

Elemental comparisons between the summation, total digest, and pre-collected XRF data (Fig. 25) shows interesting trends. U, V, and Cr within the uppermost part of the Lung Cam section are relatively similar in concentration. However, there is a stark contrast within the lower portion of the section, with XRF values 2X-3X larger than the total digest and summation values. This is suggested to be due to resistant detrital minerals that were not be fully digested. Th, Mn, Mg, Co, and Cu have similar profiles and concentrations.

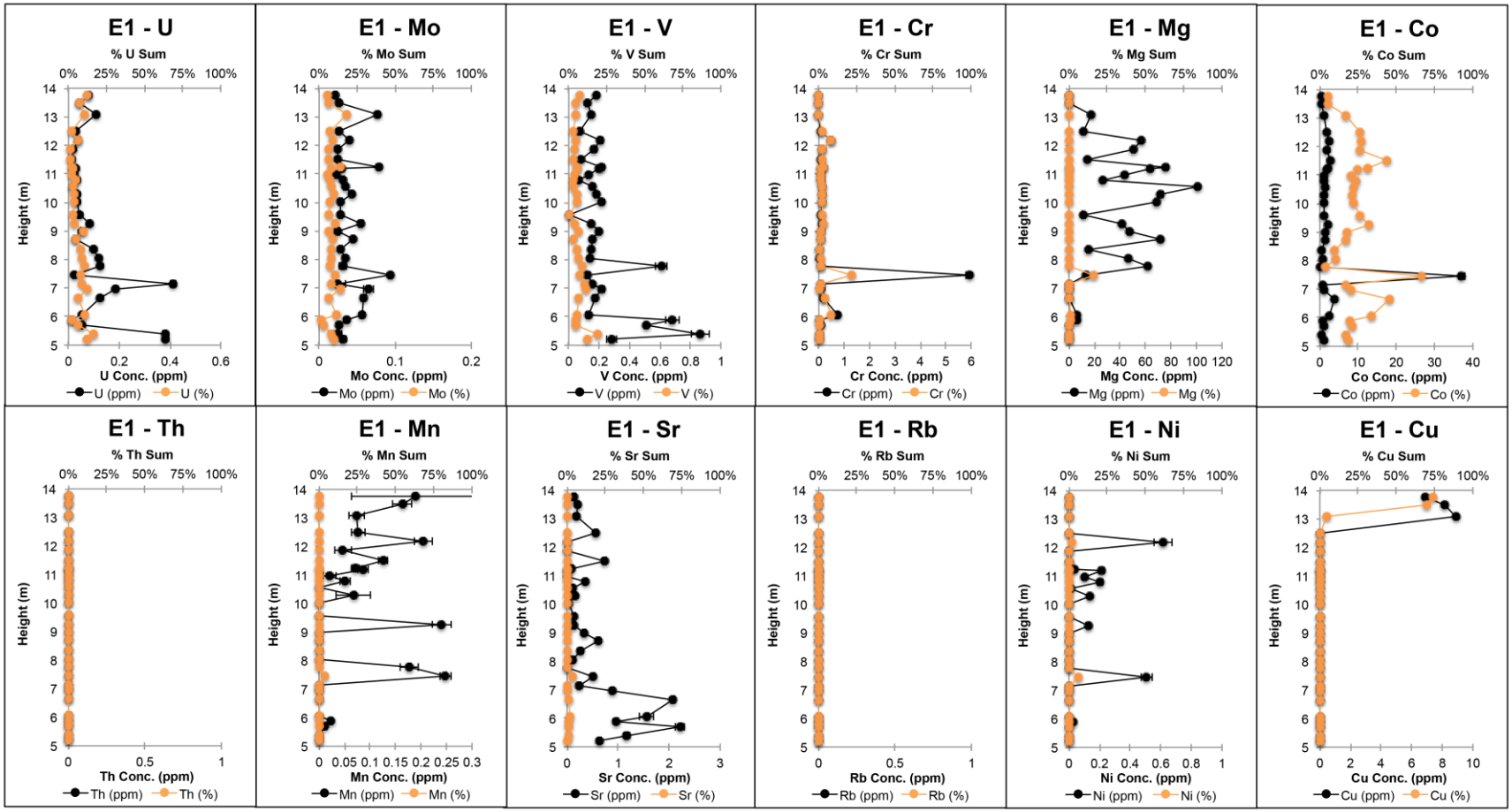

Figure 19: Elemental concentrations for the Exchangeable fraction [E1] used in the sequential extraction method applied to Lung Cam outcrop. % Sum of each element is based on the percentage of the E1 fraction relative to the total summation of the sequential extraction.

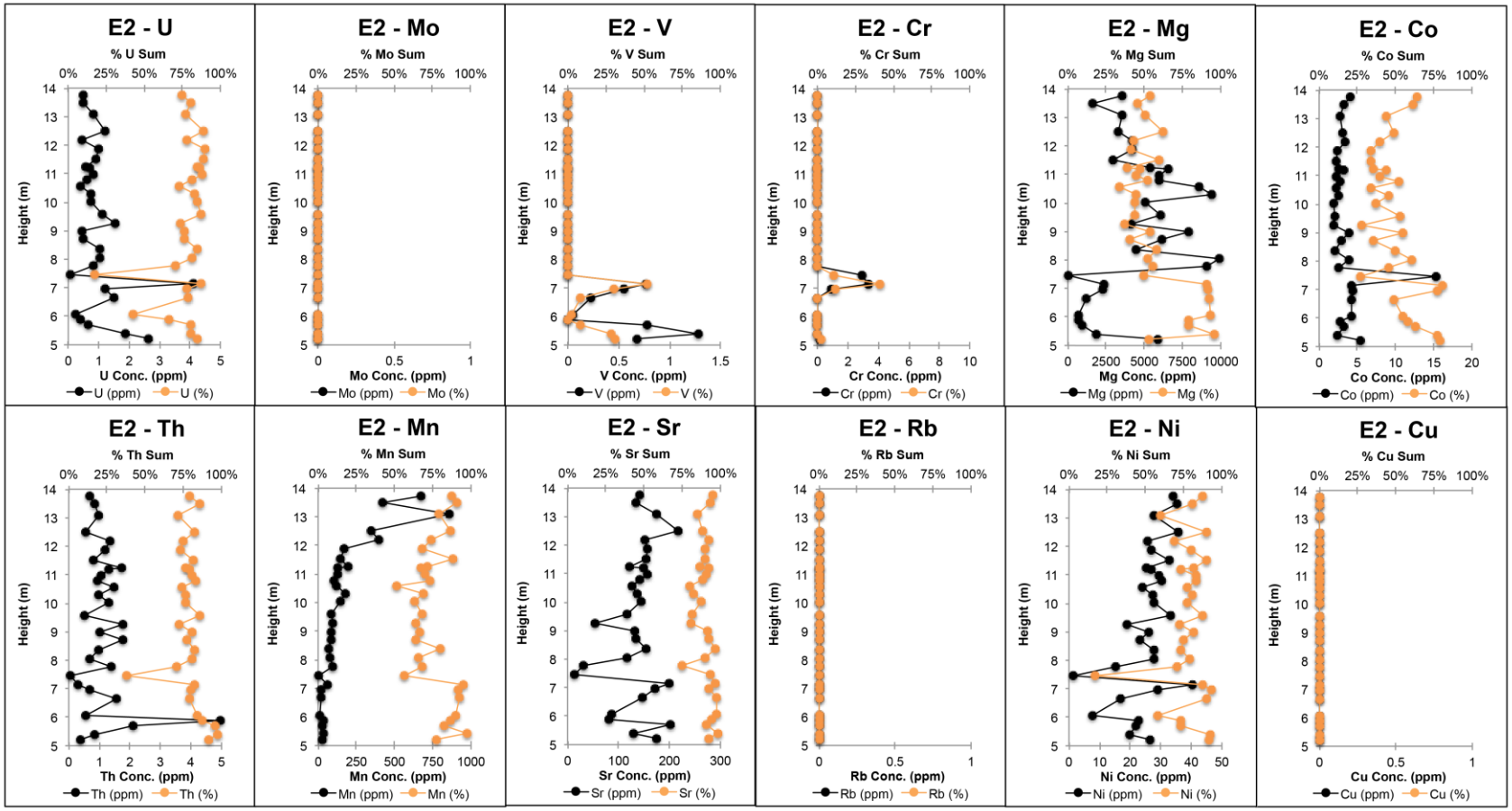

Figure 20: Elemental concentrations for the Carbonate fraction [E2] used in the sequential extraction method applied to Lung Cam outcrop. % Sum of each element is based on the percentage of the E2 fraction relative to the total summation of the sequential extraction.

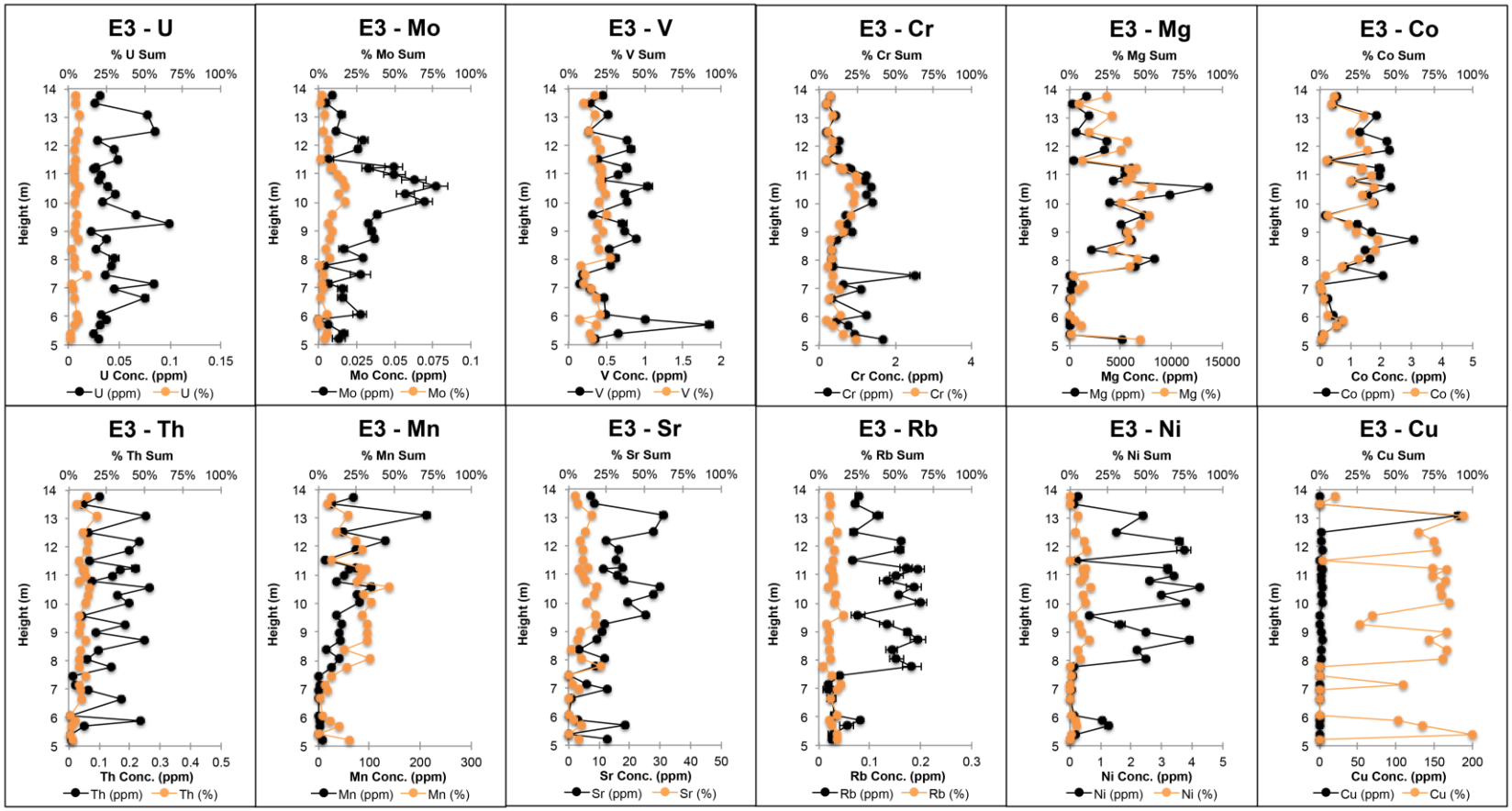

Figure 21: Elemental concentrations for the Apatite fraction [E3] used in the sequential extraction method applied to Lung Cam outcrop. % Sum of each element is based on the percentage of the E3 fraction relative to the total summation of the sequential extraction.

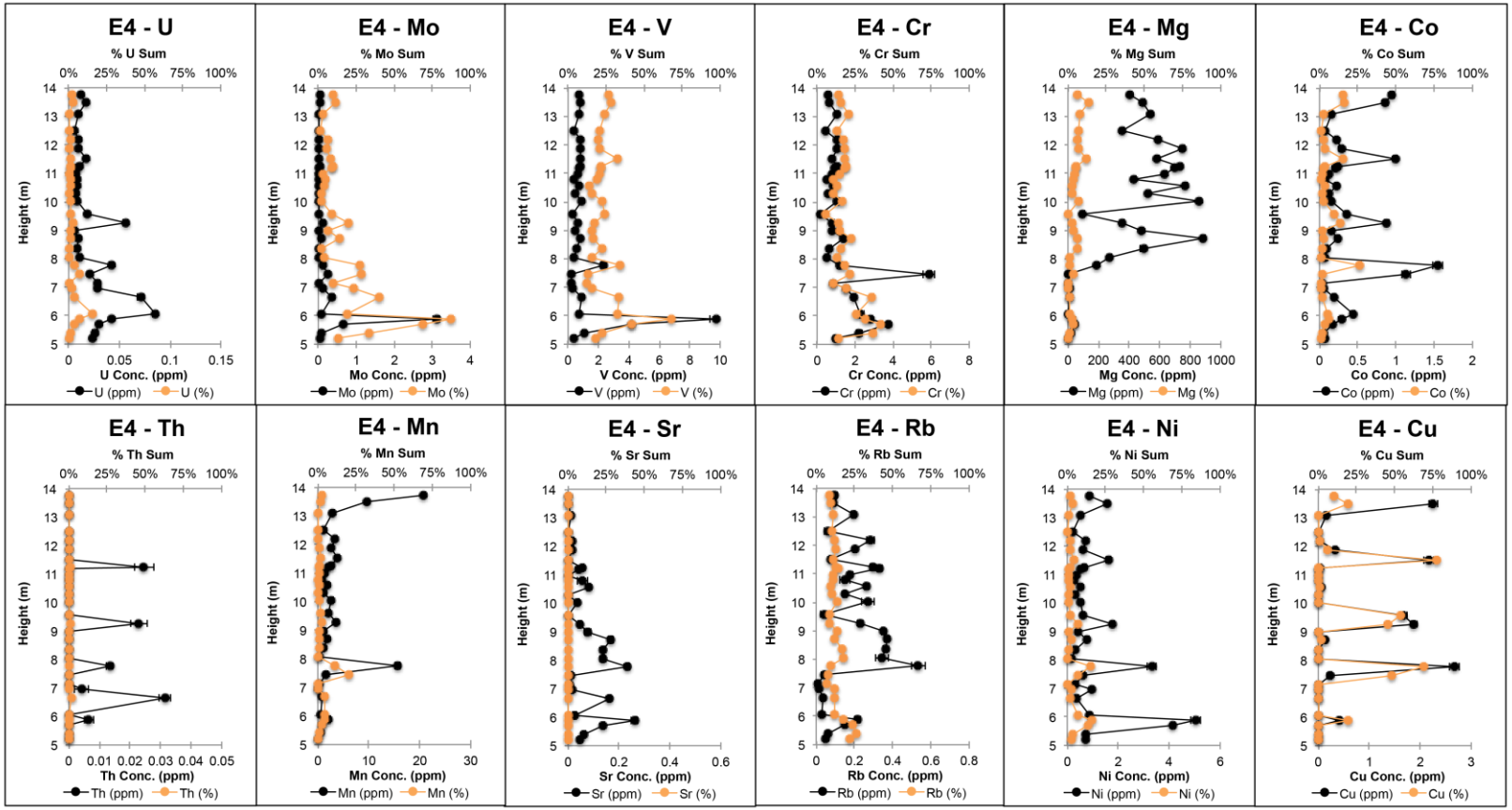

Figure 22: Elemental concentrations for the Oxide fraction [E4] used in the sequential extraction method applied to Lung Cam outcrop. % Sum of each element is based on the percentage of the E4 fraction relative to the total summation of the sequential extraction.

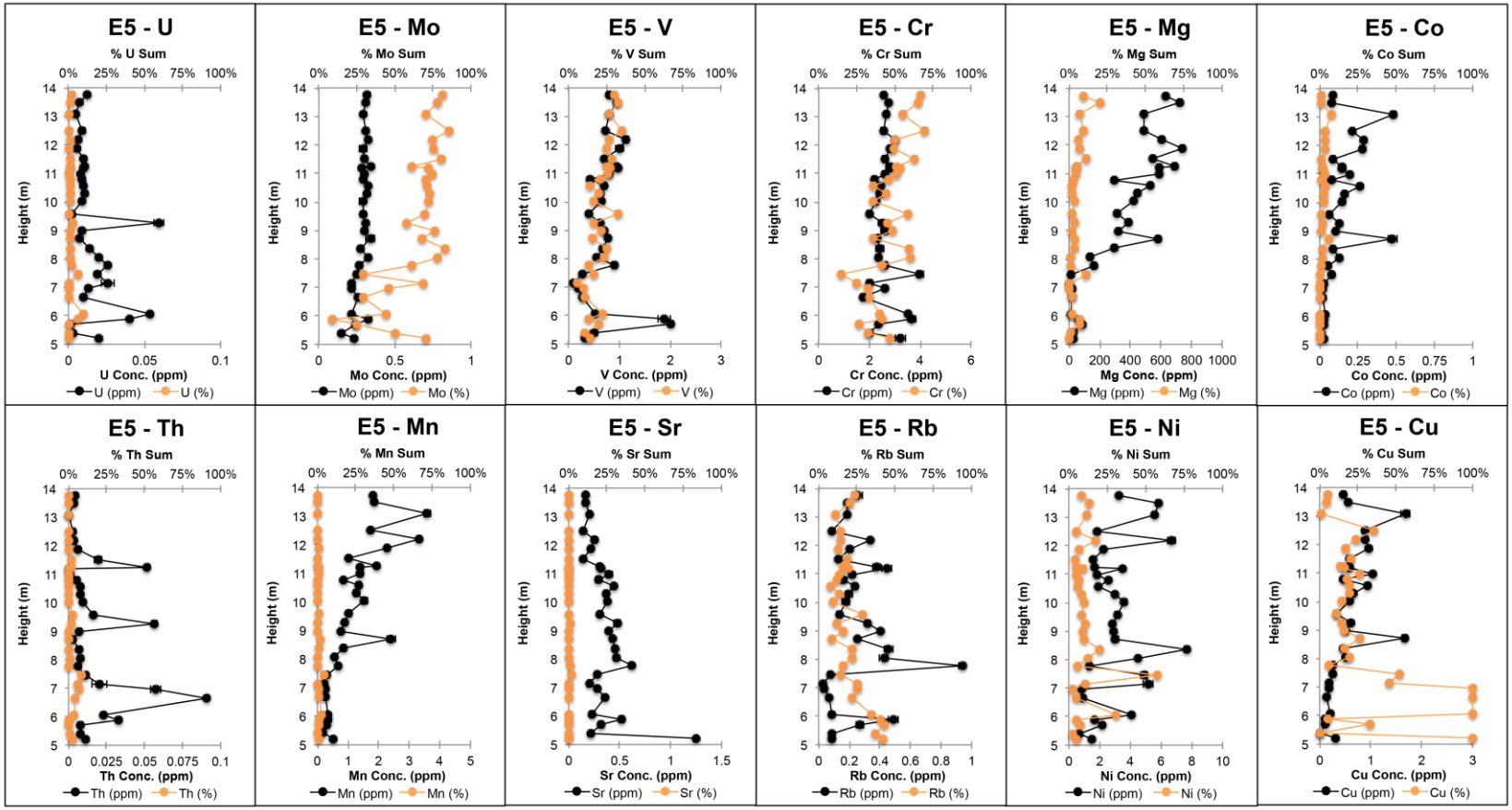

Figure 23: Elemental concentrations for the Organic fraction [E5] used in the sequential extraction method applied to Lung Cam outcrop. % Sum of each element is based on the percentage of the E5 fraction relative to the total summation of the sequential extraction.

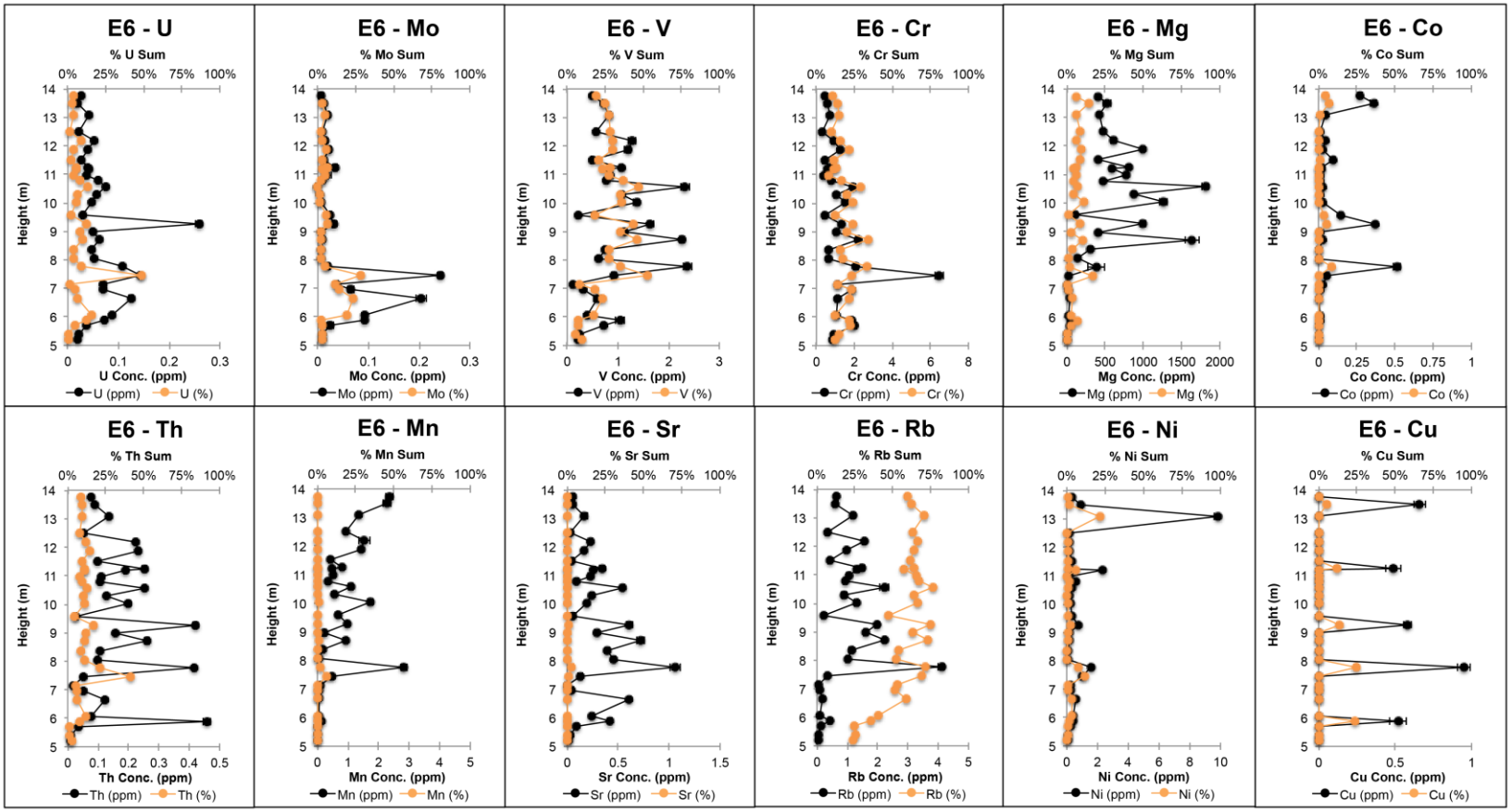

Figure 24: Elemental concentrations for the Residual fraction [E6] used in the sequential extraction method applied to Lung Cam outcrop. % Sum of each element is based on the percentage of the E6 fraction relative to the total summation of the sequential extraction.

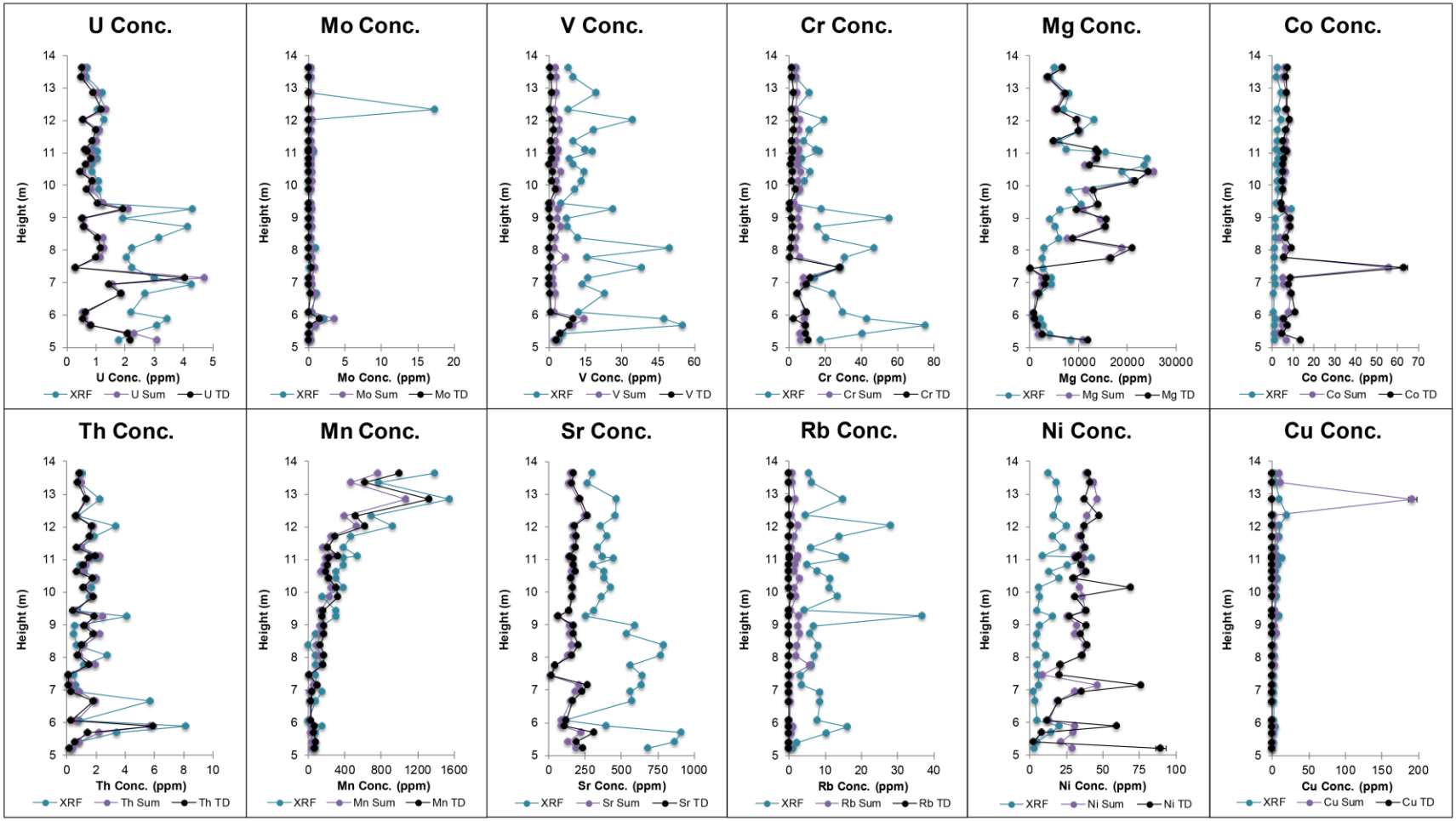

Figure 25: Elemental concentration comparison between the Total Digest, and Summation of the sequential extraction methodology applied to the Lung Cam Section. Pre-collected XRF data from Dr. Ellwood is shown in blue.

Chapter 4. Discussion

4.1 Effectiveness of Sequential Extraction

The exchangeable phase contains weakly surface-bound metals that interact with common ions such as Mg, Ca, K, Na, which are present in the pore space of the sediment during deposition (Zerbe et al., 1999). The use of the exchangeable step in the past has been primarily for preconditioning (e.g. removal of salt) samples to prevent contamination in the following extractions. The two carbonate standards (IAEA B7 and Puratronic Carbonate) in Figure 6 show that the E1 extraction does not affect the carbonate fraction in any significant way (<0.01% Ca). This is important in order to show that any digestion during the exchangeable extraction phase is reflective of the true exchangeable fraction, and does not have a contribution from the carbonate fraction. The standard BCR-CRM 032 (Moroccan phosphate rock) does show some U contribution, approximately 25% of the U summation, but low yields of other elemental concentrations (Mg, SR, Mn, Ni). The low yields of the other phosphate standards, NIST 120c and Pure Apatite, indicate that this U contribution in BCR-CRM 032 could be adsorption of U on the apatite matrix surface rather than early digestion of any carbonate or apatite fraction.

The carbonate fraction was successful in terms of fully dissolving calcium carbonate with 99% of all Ca contribution (Fig. 6). Preliminary runs showed incomplete digestion of carbonate with any sample: solution ratio below 1:100. A 1:100 sample:solution ratio is critical for full digestion of any carbonate material. The digestion of standards, IAEA B7 and Puratronic Carbonate, begin during the E2 phase with the use of sodium acetate. In the apatite/phosphate standards (BCR-CRM032, NIS T120c, and Pure apatite), 1.48 % - 4.48 % of the U contribution

was found in the carbonate fraction showing a small effect of the Sodium Acetate affecting the phosphate and apatite standards.

All three apatite standards show significant U contributions during the apatite extraction phase, particularly with NIST 120c and the pure apatite standard. For the oxide phase, hydrous oxides comprised of Mn and Fe are typically extracted together and are well known sinks for incorporation of heavy metals (Rao et al. 2007). The oxide fraction was expected to be minimal in the majority of standards tested, and all values show low yields. The organic phase is a test for any potential organic matter that is present in the samples due to preferred sequestration of Uranium in organic material (terrestrial and organic marine derived) during anoxic/euxinic conditions (Tribovillard et al., 2011; Weyer et al. 2008). No organic fraction was expected in the standards tested and all values show low yields. The detrital fraction is used to separate sedimentary U from detrital terrigenous phases due to authigenic processes (Andersen et al., 2014; Andersen et al., 2016; Asael et al., 2013). No residual fractions were expected in the standards tested and all values show low yields.

Overall, the uranium summations for the standards tend to be within approximately 89% - 106% of the total digestion. The summations are also within approximately 103% - 130% for the published certified values for the BCR-CRM 032, NIST 120c (Jochum et al. 2005) and published values for IAEA B7 (Tonarini et al. 2003). The relatively close recoveries for the summation/total digestion, negligible contribution of Ca in exchangeable fraction (<0.01%), full digestion of Ca within the carbonate fraction (>99% Ca) show the successful application of the sequential extraction methodology used in this thesis (Fig. 6 & 8).

4.2. Application of SE to The Bahamas samples

4.2.1 Exchangeable (E1) Fraction

In the Bahamas, almost all of the authigenic U present is associated with the exchangeable fraction (77% to 91% of authigenic U). U concentrations in the E1 fraction tend to range between 15% to 35 % of the bulk U concentration found in each sample. U concentrations increase downcore from 0.53 ppm to 1.89 ppm, which mirrors the trend of increasing U concentrations seen in (Fig. 26) both the carbonate fraction (E2) and the total digestion (TD) of Bahamian samples, as well as published values from Romaniello et al. (2013).

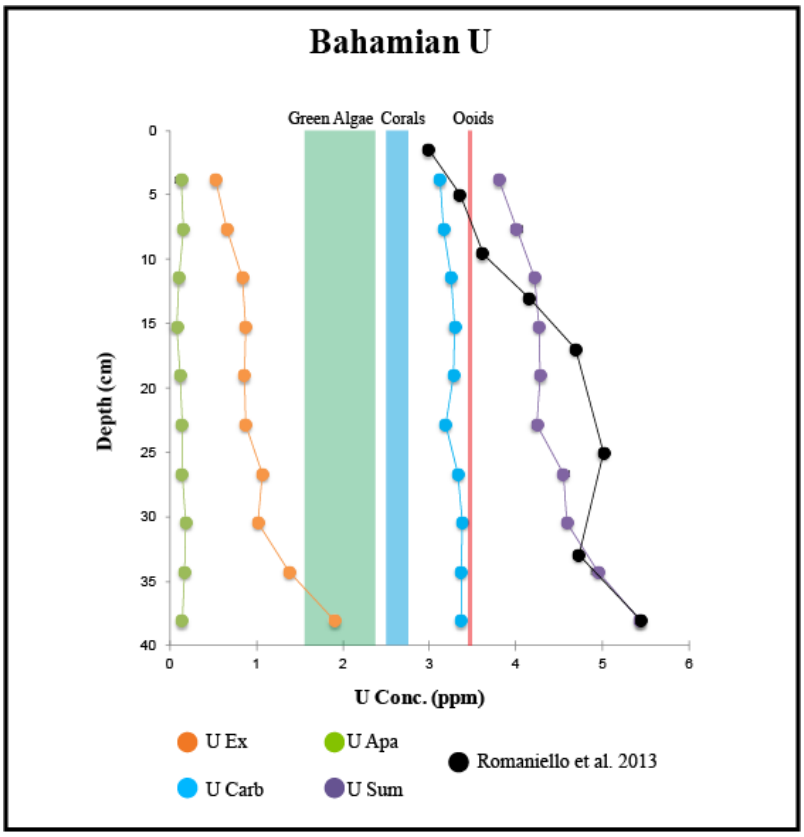

Figure 26. Bahamian U concentrations for the three largest U fractions (exchangeable, carbonate, apatite) seen in Core 1 sediment core. Exchangeable and Apatite fractions represent largest authigenic U contributions to total U concentration. Range of primary precipitates (calcareous green algae, corals, ooids) and previous U concentration data from Romaniello et al. 2013 is shown.

Authigenic accumulation of U can occur in anoxic and reducing conditions with early diagenesis favoring the reduction of U(VI) into a (UIV) species (Anderson et al., 2014; Romaniello et al., 2013; Komlos et al., 2008; Stirling et al., 2015; Hua et al., 2006). This reduction can occur abiotically (Hua et al., 2006; Weyer et al., 2008; Tribovillard et al., 2006), or be biologically-mediated (Lovley et al., 1993; Stylo et al., 2015; Basu et al., 2014; Boyanov et al., 2011; Gu et al., 2003; Rademacher et al., 2006). Authigenic U is most often associated with uraninite and coffinite as these are the primary U(IV) minerals (Cumberland et al., 2016). Dispersed uraninite has been suggested to be the primary source of authigenic U found in the Bahamian sediments (Romaniello et al., 2013) due to the ability to precipitate over a broad range of pH and Eh (Cumberland et al. 2016). Uranium solubility increases as pH increases and UO_2^{+2} to carbonate will dominate speciation when pH is greater than 6 (Krestou & Panias, 2004). Furthermore, U isotope fractionation can significantly affected by pH and can impact estimates of marine anoxia (Chen et al. 2017). For the Bahamian bulk sediment core that was used for this thesis, the range of pH was between 7.1 to 7.3 with no apparent trend downcore (Romaniello et al., 2013). Due to the affinity of UO_2^{+2} to complex with carbonate, it is possible for adsorption onto carbonate mineral surfaces (Kelly et al. 2006).

Furthermore, measurements from Bahamian bulk sediment cores show relatively low pH, high pCO_2, and high H_2S concentrations (Romaniello et al., 2013). These conditions are common during sulfate reduction which has been found to reduce soluble U(VI) into insoluble U(IV) (Lovley et al., 1991; Lovley et al., 1993; Komlos et al., 2008). During these reduction processes, biomineralization can occur, which is the process of metal and inorganic precipitation to form poorly-crystalline or crystalline structures (Cumberland et al., 2016; Stetten et al., 2018). Laboratory and field-based studies have shown the presence of a non-uraninite U(IV) species,

commonly termed monomeric, mononuclear, or molecular U(IV) (Bhattacharyya et al., 2017; Morin et al., 2016; Alessi et al., 2012; Bernier-Latmani et al., 2010; Fletcher et al., 2010; Stylo et al., 2015). Of particular interest is a study done by Morin et al. (2016), which found non-crystalline U(IV) species in lacustrine sediments using Sodium Bicarbonate, which is the reagent that was used for the exchangeable fraction in this thesis.

Several lines of evidence suggest that the authigenic U accumulation could be a non-crystalline mononuclear U(IV) species. First, the use of a weak acid such as Sodium Bicarbonate infers that the U contribution is most likely from a weakly surface-bound species or complex. The suggestion that the exchangeable contribution could be from uraninite does not apply due to evidence that uraninite begins to have solubility in buffered acetic acid solutions (Quejido et al., 2005), such as what was used in the carbonate fraction (Table 1). Second, conditions in the Bahamas are conducive to the production of a non-uraninite species (Alessi et al., 2014; Bhattacharyya et al., 2017; Bernier-Latmani et al., 2010; Boyanov et al., 2011) due to the high rates of respiration and sulfate reduction seen in Bahamian pore waters (Romaniello et al., 2013; Romaniello et al., 2016). This is further supported by the high concentrations of Mo and V seen in the exchangeable fraction which are being driven by the high concentrations of free H_2S released by bacterial sulfate reduction in Bahamian pore waters (Tribovillard et al., 2006; Romaniello et al. 2016). The implications of a biogenically produced non-uraninite species toward the ^{238}U paleo-redox proxy are be further discussed in 4.4

4.2.2 Carbonate (E2) Fraction

U incorporation into carbonate rocks is well known as oxidized (U^{VI}) is incorporated into calcium carbonate structures during carbonate precipitation in concentrations ranging from 0.1

ppm to 10 ppm (Reeder et al., 2001; Kelly et al., 2003; Weyer et al., 2008). Primary precipitates in the Bahamas (corals, ooids, algae, and mollusks) show a wide variability in U concentrations ranging from 0.014 ppm to 3.5 ppm U (Chung and Swart, 1990; Romaniello et al., 2013). The carbonate fraction of the core used in this thesis shows U concentrations increasing downcore with depth (3.12 ppm to 3.37) and averages 62%-82% of the total sum U concentration found. Other redox sensitive metals (Mo, V, Cr, Co) concentrations increase downcore as well supporting highly reducing conditions (Fig. 10). The U concentration seen in the carbonate fraction (Fig. 26) sits in between the highest observed concentrations of primary carbonate precipitates, 3.0 ppm for coral and 3.5 ppm for ooids (Swart, 1990; Romaniello et al., 2013). One of the goals of this thesis was to accurately separate out the carbonate fraction for future studies such as ^{238}U isotope analysis. Initial results suggest that the methodology was successful due to the relatively similar concentrations to primary carbonate precipitates. However, there is a possibility that the slight increase in U concentrations with depth, still seen in the carbonate fraction, could be due to authigenic Uraninite or aragonite cement targeted by the buffered acetic solution, as suggested in 4.2.1.

4.2.3 Apatite (E3) Fraction

Precipitation of phosphate minerals such as hydroxyapatite and carbonate fluorapatite is thermodynamically favored in many carbonate sediment systems (Kitano et al., 1978; Vieillard & Tardy, 1987; McGlathery et al., 1994). Uranium can incorporate into the crystal structure of francolite (carbonate flour-apatite) and can be significantly enriched (50-200 ppm) in U concentration compared to other sediments (Adem & Sadagah, 2013; Altschuler et al., 1957; Zhmodik, 1981; Kolodny et al., 2017; Soudry et al., 2002). Uranium can be present in these phosphate minerals, during mineral formation, rapidly occurring at the sediment-water interface

or early diagenesis with continued growth (Filippelli, 2011). Phosphorites (carbonate-fluor apatite) have an “open” lattice, which favors ionic substitution (e.g., U for Ca) as well as adsorption onto the crystal lattice (Clarke & Altschuler, 1957; Jarvis et al., 1994). Pore water conditions are favorable for sulfate reduction (Romaniello et al., 2013), and sulfate-reducing bacteria have been associated with the precipitation of authigenic apatite (Tribovillard, 2010; Hiatt et al., 2015). No significant U was seen in the Bahamian samples suggesting no significant U-carrying apatite material in samples.

4.2.4 Oxide (E4) Fraction

No significant uranium concentration was seen in the Bahamas samples (Fig. 12). Regardless it is important to consider this oxide phase in the SE methodology, because hydrous oxides, comprised of Mn and Fe, are well known sinks for incorporation of heavy metals (Rao et al., 2007). This phase can have U enrichment due to incorporation of authigenic U into various oxides and sulfate reduction processes (Klinkhammer & Palmer, 1991; McManus et al., 2005; Algeo & Maynard, 2004). These oxides can be present by coprecipitation, adsorption, surface complex formation, ion exchanges, and penetration of crystal lattices (Hall et al., 1996; Rao et al., 2007).

4.2.5 Organic (E5) Fraction

The organic phase was tested for any potential organic matter that is present in the samples due to preferred sequestration of U in organic material (terrestrial and organic marine derived) during anoxic/euxinic conditions (Tribovillard et al., 2011; Weyer et al., 2008). Uranium incorporation into organic matter is complex and is related to redox states as well as to the burial rate of organic matter, which can result in fractionation (McManus et al. 2006).

The location where the core was taken in the Bahamas for this thesis is primarily dominated by dense turtle grass (*Thalassia testudium*) (Romaniello et al., 2013). The potential for U to incorporate into buried organic material from these turtle grasses was tested and found to be negligible with no significant U contribution found (Fig. 13).

4.2.6 Residual (E6) Fraction

The detrital fraction is used to separate sedimentary U in detrital terrigenous phases from authigenic phases (Andersen et al., 2014; Andersen et al., 2016; Asael et al., 2013). U contribution found in the Bahamian samples was negligible (Fig. 14). This result was expected because of limited siliciclastic detritus in the Bahamian sediments due to their being located far from continental land masses (Newell & Rigby, 1957). While the Bahamas has a low detrital influence, there is a detrital influence on the PTB at Lung Cam.

4.3 Application of SE to Lung Cam, Vietnam

4.3.1 Exchangeable (E1) Fraction

U concentrations in the E1 fraction for Lung Cam samples range between 6% to 20%, showing significant authigenic U contribution as well. The largest portion of authigenic U found in this fraction is found during the Permian before beginning of the main extinction. There are two high exchangeable U peaks within the Permian part of the section that coincide with a high carbonate U (Fig. 27). The implications for a high U exchangeable fraction in the Lung Cam samples will be discussed in 4.4.

4.3.2 Carbonate (E2) Fraction

Lung Cam samples show wide variability as expected due to the long time scale (Fig. 27) and lithologies involved with U concentrations ranging from 0.05 ppm to 4.09 ppm. The Lung Cam section is primarily limestone (Son et al., 2015; Nestell et al., 2015). The upper portion of the section has a slight amount of siderite/ankerite mineralization (Beds 14-32) (Nestell et al., 2015) which had previously been misidentified as dolomite (Son et al. 2015). A recent thesis by Lindaman (2015) suggested the inability to digest siderite ($FeCO_3$) using a buffered Sodium Acetate. However, results from this thesis suggest that this could be incorrect because carbonate fraction values from beds 14-32 are approximately 73%-88% of the total SE summation. The remaining majority of U contribution in the Lung Cam samples is found in the exchangeable and residual phases. Lindaman (2015) showed that full digestion of siderite was completed in the organic phase. Values here show minimal U contribution in apatite and organic phase, which suggests that any siderite within this sample set was fully dissolved with the carbonate reagent. It is important to clarify that Lindaman (2015) used a 1:12 sample: solution ratio, which during the development of the methodology used in this thesis suggested that a 1:100 sample: solution ratio was necessary for carbonate digestion. While Lindaman (2015) did use a buffered reagent, it is difficult to ascertain what pH the solution was buffered to, as this would affect the solubility of carbonate digestion as well.

4.3.3 Apatite (E3) Fraction

While there is no significantly high uranium concentration within the apatite fraction, the Uapatite ranges from 1% to 7%, with 73% of all samples (22) having between 4% to 7% of total U%. While no high, large-scale authigenic component is seen (>10%), such as the exchangeable

fraction, there clearly is a case for targeting the apatite fraction in removal of authigenic U for future studies.

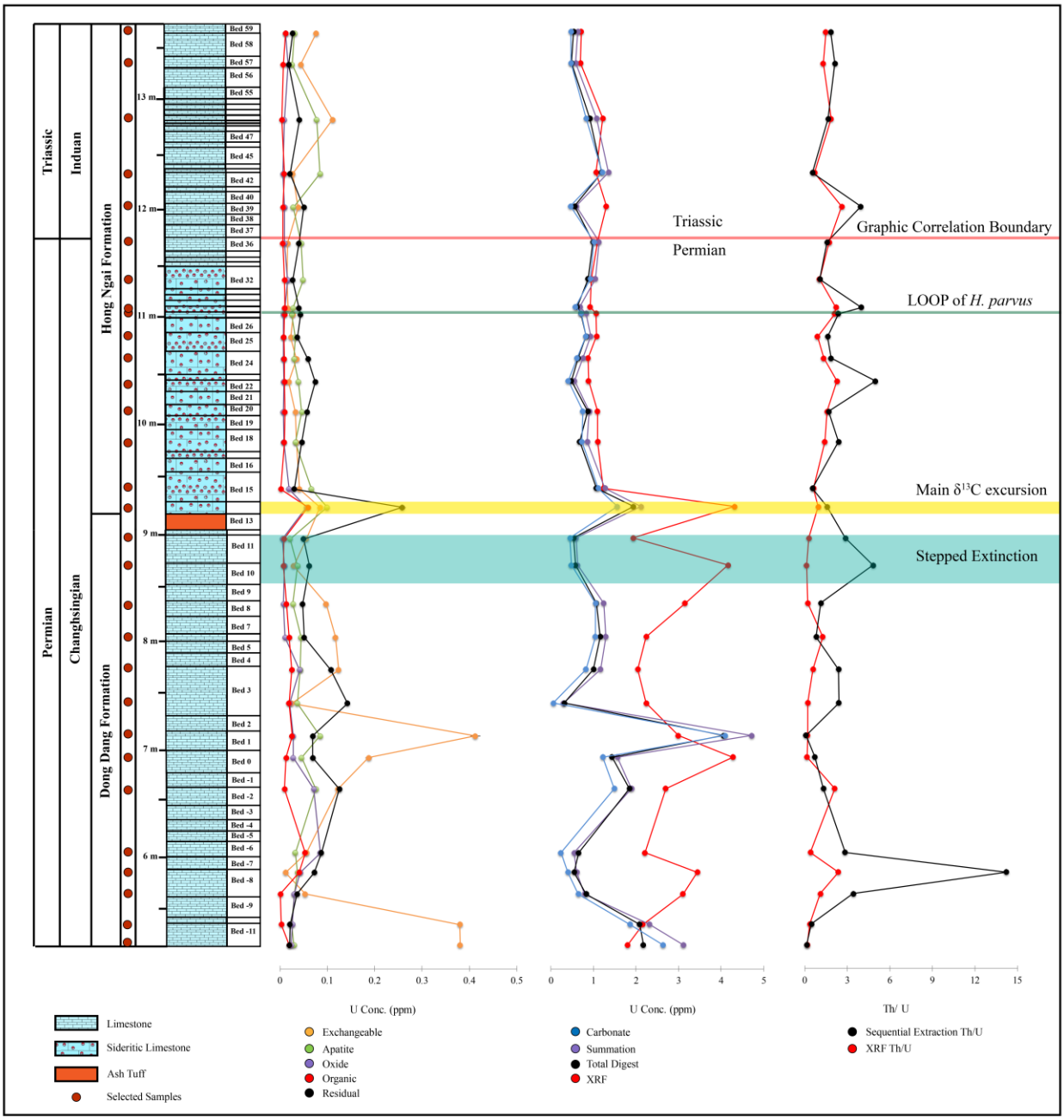

Figure 27: A composite section of Lung Cam showing geochemical profiles for sequential extraction fractions, total digest, XRF, and Th/U ratios. XRF data provided by Dr. Ellwood. Stepped Extinction, $\delta^{13}C$ and graphic correlation boundary is from Nestell et al. 2015 during previous study of Lung Cam Section.

4.3.4 Oxide (E4) Fraction

No significant uranium concentration was seen within the oxide fraction in the Lung Cam samples (Figure 22 and 27). U oxide ranges from 1% to 7% with one outlier peak of 16% for total U. Only 4 samples are between 4% and 7% of total U. However, samples such as LC 19 with a high Uoxide peak, illustrate the importance of applying a sequential extraction technique to carbonate samples. Fe-Mn oxides have a fractionation of -0.2‰ in $\delta^{238}U$ toward lighter isotopic compositions implying that the lighter isotope (^{235}U) is preferentially adsorbed (Weyer et al., 2008; Stylo et al,. 2015). An authigenic contribution of 16% U oxide could potentially alter the $\delta^{238}U$ values relative to ancient seawater conditions.

4.3.5 Organic Fraction

In terms of organics for the Lung Cam section, it is suggested to be a mix of terrestrial and marine organic material. A recent study by Nestell et al. (2015) showed a high terrestrial charcoal influx into the marine environment incorporating carbon into ocean floor sediments by agglutinated foraminifera (Nestell et al., 2015). No significant amount of U was found within the Lung Cam sections suggesting no authigenic U organic component (Fig. 23).

4.3.6 Residual Fraction

For the Lung Cam samples, the E6 fraction represents the second largest U contribution, with samples ranging between 0.018 ppm to 0.25 ppm, representing approximately 1% to 16% of the total U. It is important to note that not all detrital material will be digested due to the difficulty of digesting resistant silica minerals. This is seen in samples LC 5 – LC 85 (Carbon Isotope Excursion, Fig. 27) when comparing the total digest and summation values to XRF

values done by Nestell et al. (2015). The total digest and summation values in the lower Lung Cam section appear to be 2-6X suppressed compared to XRF values. This thesis suggests that a majority of the U XRF component is detrital in nature and unable to be fully digested with the current methodology. The use of a strong oxidizing acid such as HF could potentially digest this detrital portion. While the methodology applied here cannot fully account for the detrital portion, the goal of this thesis was to separate out the U carbonate fraction from all authigenic and detrital U, and therefore, the results reported here accomplishes this goal.

4.4 Implications of the δ^{238}U paleo-redox proxy

The numerous mechanisms involved with U incorporation, make it difficult to identify where the largest authigenic U enrichment is seen in bulk carbonate sediments. One aspect of this thesis is to separate out authigenic U from Bahamian bulk sediments in order to delineate U enrichment during early diagenetic processes. Preliminary results show that the majority of authigenic U is found in the exchangeable fraction (Figure 9). A previous study by Romaniello et al. (2013) has shown that the δ^{238}U of the authigenic component is isotopically heavier than average seawater U (Romaniello et al., 2013).

Using a basic mixing equation, it is possible to estimate the potential authigenic δ^{238}U contribution seen in the exchangeable phase within Bahamian bulk sediment. Based on the data, it is assumed that the apatite (E3), oxide (E4), organic (E5), and residual (E6) fractions contribute negligible authigenic U. Therefore, if the assumption is that the authigenic U is only in the exchangeable phase, then the following mixing equation applies;

$$\delta^{238}U_{bulk} = \delta_{ex}{}^{238}U * (1 - f_{carb}) + \delta_{carb}{}^{238}U * (f_{carb})$$

where,

$$f_{carb} = \frac{carbonate\ ppm}{total\ ppm}$$

and,

$$1 - f_{carb} = \frac{exchangeable\ ppm}{total\ ppm}$$

Using concentration values from bulk sediment core 1 from the Bahamas, as well as $\delta^{238}U$ values from Romaniello et al. (2013) shows an average authigenic U component of up to 1.14‰ (range: 0.83 – 1.54‰) present in the exchangeable fraction (Fig. 28). This result supports and is consistent with previous Bahamian carbonate $\delta^{238}U$ studies that indicate an authigenic U contribution between 0.6 – 1.2‰ (Romanielo et al., 2013), and also within range of other $\delta^{238}U$ studies in various reducing environments (Weyer et al., 2008; Romaniello et al., 2013; Stirling et al., 2007; Rolison et al., 2017).

A correction factor has been suggested by Romaniello et al. (2013) of 0.2‰ – 0.4‰ when applying the $\delta^{238}U$ paleo-redox proxy to carbonates. This was based on the heavy authigenic U component seen in Bahamian sediments. This thesis has illustrated the potential to separate out authigenic and detrital U from carbonate fractions. Future studies using the sequential extraction methodology provided in this thesis could use the separated U_{carb} fraction in Permian $\delta^{238}U$ paleo-redox proxy instead of applying a wide range correction factors to tested samples.

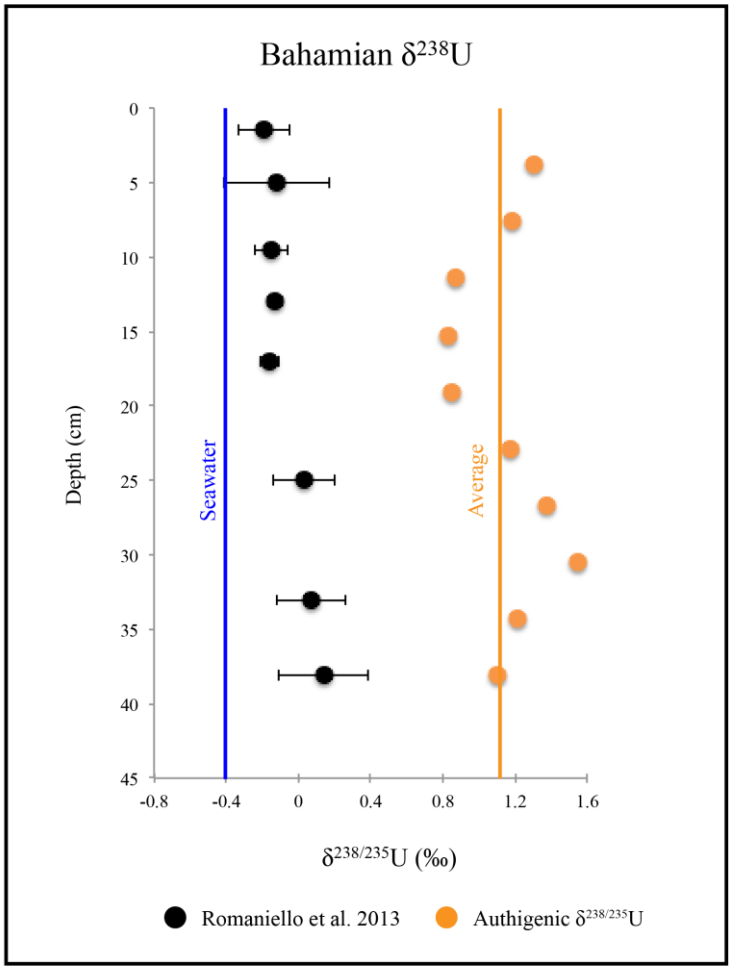

Figure 28: $\delta^{238}U$ values for Bahamian bulk sediment core. Black data points are from Romaniello et al. (2013) and orange data points represent derived potential authigenic $\delta^{238}U$. Vertical blue line represents average U isotope composition of open ocean seawater and vertical orange line represents average authigenic $\delta^{238}U$.

A significant portion of authigenic U is also preserved within Permian–Triassic sediments illustrating preservation of exchangeable enrichment, which was unexpected. It is hypothesized here that the authigenic U found in the exchangeable fraction within Bahamian sediments is primarily a biogenically derived mononuclear U(IV) species. There is uncertainty whether a non-crystalline U(IV) species would be preserved within Permian–Triassic sediments.

Several studies have observed the longevity of non-crystalline U(IV) species with various results. One study suggests that non-crystalline U(IV) is a short-lived species with a rapid transition into Uraninite (Kelly et al., 2009). However, a study by Madden et al. (2012) has shown no evidence of aging or increasing crystallinity for up to four years after which the study ended. More work is needed to identify whether the preserved exchangeable enrichment seen in the Lung Cam samples is a non-crystalline U(IV) species and to incorporate a $\delta^{238}U$ profile for the Lung Cam section.

Chapter 5. Future Direction

While this thesis has shown the ability to separate out various sources of authigenic U from carbonate samples, there are still several questions and concerns that need to be addressed. One concern is that the authigenic U seen in the E1 fraction is due to the fact that U can be remobilized by oxygenation (Gu et al., 2005; Komlos et al., 2008; Komlos et al., 2008; Senko et al., 2002). This possibility could have occurred during the extraction of the core from the sediment or during the chemical reactions occurring during sample analysis potentially coming from a different fraction such as a Fe-Mn oxide. The mobility of U from a different fraction can be addressed in a further study with a comparison between anoxic and oxic sequential extractions on the Bahamian bulk sediment cores. Using a nitrogen filled glove box and all reagents bubbled with nitrogen, to remove oxygen to simulate anoxic conditions, could be a key to resolving this concern.

One question that needs to be addressed is whether the authigenic U accumulation found in the exchangeable fraction is indeed a non-crystalline mononuclear U(IV). One method of testing whether this is true is to apply a KPA technique coupled with ICP-MS (Alessi et al., 2012; Mohsen et al., 1997; Zhou & Gu., 2005). This was used to separate out monomeric U(IV) in a laboratory setting by subtracting the total uranium (ICP-MS) by the soluble U(VI) (KPA technique) (Alessi et al., 2012). Any remaining unextracted material is suggested to be uraninite (Alessi et al., 2012). A KPA/sequential extraction has already been used to identify U species in iron-bearing phyllosilicates (Luan & Burgos, 2012). Bulk extended X-ray absorption fine structure (EXAFS) spectroscopy can also be used to identify and characterize U species (Bhattacharyya et al., 2012). A KPA technique or EXAFS should be adopted in conjunction with

the carbonate sequential extraction used in this thesis to precisely identify the potential U species within the exchangeable fraction in the Bahamian and Lung Cam samples.

Chapter 6. Conclusion

Sequential extraction has been employed in numerous studies to understand the distribution of trace elements within various sediments. This thesis employed a modified sequential extraction technique in order to determine and establish how U varies within chemical fractions in carbonate sediments. This technique is crucial and viable for the separation of authigenic U components that can form during local redox processes.

For Bahamian bulk carbonate sediments, the majority of authigenic U was found within the exchangeable phase with 77%-91% of all authigenic U present. The U concentrations increase downcore from 0.53 ppm to 1.89 ppm and mirror the trend of increasing U seen in previous Bahamian studies. This authigenic U is hypothesized to be a biogenically derived mononuclear U(IV) species. This authigenic U component was found to have a $\delta^{238}U$ of up to 1.14‰ based on the data from this thesis and previous studies.

Future work in necessary to establish whether the authigenic U enrichment seen in Bahamian bulk sediment is in fact a biogenically derived mononuclear U(IV) species. The preservation of Uranium within the exchangeable fraction of Lung Cam carbonates was unexpected and more work is necessary to identify whether a non-crystalline U(IV) species can be preserved during long spatial time-periods. The discovery of an authigenic and heavy $\delta^{238}U$ component that is preserved within the rock record is significant. The use of a sequential extraction methodology as shown can be critical toward the use of $\delta^{238}U$ as a trace metal paleoredox proxies.

References

Abed, A. M., & Sadaqah, R. M. (2013). Enrichment of uranium in the uppermost Al-Hisa Phosphorite Formation, Eshidiyya basin, southern Jordan. *Journal of African Earth Sciences*, *77*:31-40.

Alessi, D. S., Uster, B., Veeramani, H., Suvorova, E. I., Lezama-Pacheco, J. S., Stubbs, J. E., ... & Bernier-Latmani, R. (2012). Quantitative separation of monomeric U (IV) from UO2 in products of U (VI) reduction. *Environmental science & technology*, *46*(11), 6150-6157.

Alessi, D. S., Lezama-Pacheco, J. S., Stubbs, J. E., Janousch, M., Bargar, J. R., Persson, P., & Bernier-Latmani, R. (2014). The product of microbial uranium reduction includes multiple species with U (IV)–phosphate coordination. *Geochimica et Cosmochimica Acta*, *131*, 115-127.

Algeo, T. J., & Maynard, J. B. (2004). Trace-element behavior and redox facies in core shales of Upper Pennsylvanian Kansas-type cyclothems. *Chemical geology*, *206*(3), 289-318.

Algeo, T.J., Hinnov, L., Moser, J., Maynard, J.B., Elswick, E., Kuwahara, K., Sano, H., (2010). Changes in productivity and redox conditions in the Panthalassic Ocean during the latest Permian. *Geology* 38:187-190.

Algeo, Thomas J., Kiyoko Kuwahara, Hiroyoshi Sano, Steven Bates, Timothy Lyons, Erika Elswick, Linda Hinnov, Brooks Ellwood, Jessa Moser, and J. Barry Maynard. (2011). Spatial variation in sediment fluxes, redox conditions, and productivity in the Permian–Triassic Panthalassic Ocean. *Palaeogeography, Palaeoclimatology, Palaeoecology* 308, 65-83.

Altschuler, Z. S., Clarke Jr, R. S., & Young, E. J. (1957). The geochemistry of uranium in apatite and phosphorite. 701.

Andersen, M. B., Romaniello, S., Vance, D., Little, S. H., Herdman, R., & Lyons, T. W. (2014). A modern framework for the interpretation of 238 U/235 U in studies of ancient ocean redox. *Earth and Planetary Science Letters*, *400*, 184-194.

Andersen, M. B., Elliott, T., Freymuth, H., Sims, K. W., Niu, Y., & Kelley, K. A. (2015). The terrestrial uranium isotope cycle. *Nature*, *517*(7534), 356-359.

Andersen, M. B., Vance, D., Morford, J. L., Bura-Nakić, E., Breitenbach, S. F. M., & Och, L. (2016). Closing in on the marine 238 U/235 U budget. *Chemical Geology*, *420*, 11-22.

Anderson, R. F. (1987). Redox behavior of uranium in an anoxic marine basin. *Uranium*, *3*(2-4), 145-164.

Amiel, A. J., Miller, D. S., & Friedman, G. M. (1973). Incorporation of uranium in modern corals. *Sedimentology*, *20*(4), 523-528.

Azmy, K., Kendall, B., Brand, U., Stouge, S., & Gordon, G. W. (2015). Redox conditions across the Cambrian–Ordovician boundary: Elemental and isotopic signatures retained in the GSSP carbonates. *Palaeogeography, Palaeoclimatology, Palaeoecology*, *440*, 440-454.

Banning, A., Rüde, T. R. (2015). Apatite weathering as a geological driver of high uranium concentrations in groundwater. *Applied Geochemistry*, *59*:39-146.

Barnes, C. E., Cochran, J.K. (1990). Uranium removal in oceanic sediments and the oceanic U balance. *Earth and Planetary Science Letters* 97(1):94-101.

Basu, A., Sanford, R.A., Johnson, T.M., Lundstrom, C.C., Loffler, F.E. (2014). Uranium isotopic fractionation factors during U(VI) reduction by bacterial isolates. *Geochimica et a Cosmochimica Acta* 136:100-113.

Bernier-Latmani, R., Veeramani, H., Vecchia, E. D., Junier, P., Lezama-Pacheco, J. S., Suvorova, E. I., ... & Bargar, J. R. (2010). Non-uraninite products of microbial U (VI) reduction. *Environmental science & technology*, *44*(24), 9456-9462.

Bhattacharyya, A., Campbell, K. M., Kelly, S. D., Roebbert, Y., Weyer, S., Bernier-Latmani, R., & Borch, T. (2017). Biogenic non-crystalline U (IV) revealed as major component in uranium ore deposits. *Nature Communications*, *8*.

Bowen, R. (1988). Isotopes in the Earth Sciences. Elsevier Applied Science, London and New York. 115-161.

Bowring, S.A., Erwin, D.H., Jin, Y.G., Martin, M.W., Davidek, K., Wang, W. (1998). U/Pb Zircon Geochronology and Tempo of the End-Permian Mass Extinction. *Science.* 280:1039.

Boyanov, M. I., Fletcher, K. E., Kwon, M. J., Rui, X., O'Loughlin, E. J., Löffler, F. E., & Kemner, K. M. (2011). Solution and microbial controls on the formation of reduced U (IV) species. *Environmental science & technology*, *45*(19), 8336-8344.

Brennecka, G.A., Borg, L.E., Hutcheon, I.D., Sharp, M.A., Anbar, A.D. (2010). Natural variations in uranium isotope ratios of uranium ore concentrates: Understanding the 238U/235U fractionation mechanism. *Earth and Planetary Science Letters.* 291: 228-233

Brennecka, G. A., Herrmann, A. D., Algeo, T. J., & Anbar, A. D. (2011). Rapid expansion of oceanic anoxia immediately before the end-Permian mass extinction. *Proceedings of the National Academy of Sciences.*108(43):17631–17634.

Cao, C., Love, G.D., Hays, L.E., Wang, W., Shen, S., Summons, R.E. (2009). Biogeochemical evidence for euxinic oceans and ecological disturbance presaging the end-Permian mass

extinction event. *Earth Planet SC Lett.* 281:188–201.

Chen, X., Romaniello, S. J., Herrmann, A. D., Wasylenki, L. E., & Anbar, A. D. (2016). Uranium isotope fractionation during coprecipitation with aragonite and calcite. Geochimica et Cosmochimica Acta, 188, 189-207.

Chen, X., Romaniello, S. J., & Anbar, A. D. (2017). Uranium isotope fractionation induced by aqueous speciation: Implications for U isotopes in marine CaCO3 as a paleoredox proxy. Geochimica et Cosmochimica Acta, 215, 162-172.

Chung, G. S., & Swart, P. K. (1990). The concentration of uranium in freshwater vadose and phreatic cements in a Holocene ooid cay: a method of identifying ancient water tables. *Journal of Sedimentary Research*, *60*(5).

Clarkson, M. O., Kasemann, S. A., Wood, R. A., Lenton, T. M., Daines, S. J., Richoz, S., ... & Tipper, E. T. (2015). Ocean acidification and the Permo-Triassic mass extinction. Science, 348(6231), 229-232.

Cumberland, S. A., Douglas, G., Grice, K., & Moreau, J. W. (2016). Uranium mobility in organic matter-rich sediments: A review of geological and geochemical processes. *Earth-Science Reviews*, *159*, 160-185.

Dahl, T.W., Boyle, R.A., Canfield, D.E., Connelly, J.N., Gill, B.C., Lenton, T.M., Bizzarro, M., (2014). Uranium Isotopes distinguish two geochemically distinct stages during the Cambrian SPICE event. *Earth and Planetary Science Letters* 401:313-326.

Dao-yi, X., Zheng, Y. (1993). Carbon isotope and iridium event markers near the Permian/Triassic boundary in the Meishan section, Zhejiang Province, China: *Paleogeography, Paleoclimatology, Paleoecology*. 104:171-176.

Dunk, R. M., Mills, R. A., & Jenkins, W. J. (2002). A reevaluation of the oceanic uranium budget for the Holocene. Chemical Geology, 190(1-4), 45-67.

Ehrenberg, S. N., Svana, T. A., & Swart, P. K. (2008). Uranium depletion across the Permian–Triassic boundary in Middle East carbonates: Signature of oceanic anoxia. *AAPG bulletin*, *92*(6), 691-707.

Ellwood, B. B., Wardlaw, B. R., Nestell, M. K., Nestell, G. P., & Lan, L. T. P. (2017). Identifying globally synchronous Permian–Triassic boundary levels in successions in China and Vietnam using Graphic Correlation. *Palaeogeography, Palaeoclimatology, Palaeoecology*, *485*, 561-571.

Elrick, M., Polyak, V., Algeo, T. J., Romaniello, S., Asmerom, Y., Herrmann, A. D., ... & Chen, Z. Q. (2017). Global-ocean redox variation during the middle-late Permian through Early Triassic based on uranium isotope and Th/U trends of marine carbonates. *Geology*, *45*(2), 163-166.

Erwin, D.H. (1994). The Permo-Triassic Extinction, *Nature*. 367(6460):231-236

Faure, G. 1997. Principles of Isotope Geology Wiley, New York. 2.

Fletcher, K. E., Boyanov, M. I., Thomas, S. H., Wu, Q., Kemner, K. M., & Löffler, F. E. (2010). U (VI) reduction to mononuclear U (IV) by Desulfitobacterium species. *Environmental science & technology*, *44*(12), 4705-4709.

Fujino, O., Umetani, S., Ueno, E., Shigeta, K., & Matsuda, T. (2000). Determination of uranium and thorium in apatite minerals by inductively coupled plasma atomic emission spectrometry with solvent extraction separation into diisobutyl ketone. *Analytica chimica acta*, *420*(1):65-71.

Grice, K., Cao, C., Love, G. D., Böttcher, M. E., Twitchett, R. J., Grosjean, E., ... & Jin, Y. (2005). Photic zone euxinia during the Permian-Triassic superanoxic event. *Science*, *307*(5710), 706-709.

Gu, B., & Chen, J. (2003). Enhanced microbial reduction of Cr (VI) and U (VI) by different natural organic matter fractions. *Geochimica et cosmochimica acta*, *67*(19), 3575-3582.

Gu, B., Yan, H., Zhou, P., Watson, D. B., Park, M., & Istok, J. (2005). Natural humics impact uranium bioreduction and oxidation. *Environmental science & technology*, *39*(14), 5268-5275.

Gvirtzman, G., Friedman, G.M., Miller, D.S. (1973). Control and Distribution of Uranium in coral reefs during diagenesis. *J Sediment Res* 43:985-997.

Hall. G. E. M., Gauthier. G., Pelchat, J. C, Pelchat, P., Vaive, J. E. (1996). Application of a Sequential Extraction Scheme to Ten Geological Certified Reference Materials for the Determination of 20 Elements. *Journal of Analytical Atomic Spectrometry*, 11 (9):787-796.

Hedaya, M. A., Birkenfeld, H. P., & Kathren, R. L. (1997). A sensitive method for the determination of uranium in biological samples utilizing kinetic phosphorescence analysis (KPA). *Journal of pharmaceutical and biomedical analysis*, *15*(8), 1157-1165.

Hiatt, E. E., Pufahl, P. K., Edwards, C. T. (2015). Sedimentary phosphate and associated fossil bacteria in a Paleoproterozoic tidal flat in the 1.85 Ga Michigamme Formation, Michigan, USA. *Sedimentary Geology*, *319*:24-39.

Hongfu, Yin., Zhang, K.X., Tong, J.N., Yang, S.B., Wu, S.B. (2001). The global Stratotype section and point (GSSP) of the Permian–Triassic boundary. *Episodes*. 24(2):102–114

Hua, B., Xu, H., Terry, J., & Deng, B. (2006). Kinetics of uranium (VI) reduction by hydrogen sulfide in anoxic aqueous systems. *Environmental science & technology*, *40*(15), 4666-4671.

Isozaki ,Y. (1997). Permian-Triassic boundary superanoxia and stratified superocean: records from lost deep sea. *Science* 276:235–238.

Jaffey, A. H., Flynn, K. F., Glendenin, L. E., Bentley, W. T., & Essling, A. M. (1971). Precision measurement of half-lives and specific activities of U 235 and U 238. *Physical Review C*, *4*(5), 1889.

Jin, Y.G., Wang, Y., Wang, W., Shang, Q.H., Cao, C.Q. and Erwin, D.H. 2000. Pattern of marine mass extinction near the Permian-Triassic Boundary in South China: *Science.* 289:432-436.

Jochum, K. P., Nohl, U., Herwig, K., Lammel, E., Stoll, B., & Hofmann, A. W. (2005). GeoReM: a new geochemical database for reference materials and isotopic standards. Geostandards and Geoanalytical Research, 29(3), 333-338.

Kamo, S. L., Czamanske, G. K., Amelin, Y., Fedorenko, V. A., Davis, D. W., & Trofimov, V. R. (2003). Rapid eruption of Siberian flood-volcanic rocks and evidence for coincidence with the Permian–Triassic boundary and mass extinction at 251 Ma. *Earth and Planetary Science Letters*, *214*(1), 75-91.

Kaiho, K., Kajiwara, Y., Nakano, T., Miura, Y., Kawahata, H., Tazaki, K., ... & Shi, G. R. (2001). End-Permian catastrophe by a bolide impact: evidence of a gigantic release of sulfur from the mantle. *Geology*, *29*(9), 815-818.

Kaiho, Kunio, Masahiro Oba, Yoshihiko Fukuda, Kosuke Ito, Shun Ariyoshi, Paul Gorjan, Yuqing Riu et al. (2012). Changes in depth-transect redox conditions spanning the end-Permian mass extinction and their impact on the marine extinction: Evidence from biomarkers and sulfur isotopes. *Global and Planetary Change* 94:20-32.

Kelly, S.D., Newville, M.G., Cheng, L., Kemner, K.M., Sutton, S.R., Fenter, P.S., Sturchio, N.C., Spotl, C. 2003. Uranyl incorporation into natural calcite. *Environ. Sci. Technol*. 37:1284-1287

Kelly, S. D., Rasbury, E. T., Chattopadhyay, S., Kropf, A. J., & Kemner, K. M. (2006). Evidence of a stable uranyl site in ancient organic-rich calcite. *Environmental science & technology*, *40*(7), 2262-2268.

Kelly, S. D., Wu, W. M., Yang, F., Criddle, C. S., Marsh, T. L., O'Loughlin, E. J., ... & Kemner, K. M. (2009). Uranium transformations in static microcosms. *Environmental science & technology*, *44*(1), 236-242.

Kitano, Y., Okumura, M., Idogak, M. 1978. Uptake of phosphate ions by calcium carbonate. *Geochem. Jour*. 12: 29-37

Klinkhammer G. P., Palmer M. R. 1991. Uranium in the oceans: where it goes and why. Geochim. *Cosmochim. Acta.* 55:1799–1806.

Kolodny, Y., Torfstein, A., Weiss-Sarusi, K., Zakon, Y., & Halicz, L. (2017). 238 U-235 U-234 U fractionation between tetravalent and hexavalent uranium in seafloor phosphorites. *Chemical Geology*, *451*, 1-8.

Komlos, John, Peacock, A., Kukkadapu, R.K., Jaffe, P.R. (2008). Long-term dynamics of uranium reduction/reoxidation under low sulfate conditions. *Geochimica et Cosmochimica Acta.* 2(15):3603-3615.

Komlos, J., Mishra, B., Lanzirotti, A., Myneni, S. C., & Jaffé, P. R. (2008). Real–time speciation of uranium during active bioremediation and U (IV) reoxidation. *Journal of Environmental Engineering*, *134*(2), 78-86.

Krestou, A., & Panias, D. (2004). Uranium (VI) speciation diagrams in the UO 2 2+/CO 3 2-/H 2 O system at 25° C. *European Journal of Mineral Processing & Environmental Protection*, *4*(2).

Ku, T., Knauss, K.G., Mathieu. G.G. (1997). Uranium in open ocean: concentration and isotopic composition." *Deep Sea Research.* 24(11):1005-1017.

Kump , L.R.; Pavlov, A.; Arthur, M.A. (2005). Massive release of hydrogen sulfide to the surface ocean and atmosphere during intervals of oceanic anoxia. Geology. 33(5):397 400.

Lovley, D. R., Phillips, E. J., Gorby, Y. A., & Landa, E. R. (1991). Microbial reduction of uranium. *Nature*, *350*(6317), 413-416.

Lovley, D. R., Roden, E. E., Phillips, E. J. P., & Woodward, J. C. (1993). Enzymatic iron and uranium reduction by sulfate-reducing bacteria. *Marine Geology*, *113*(1-2), 41-53.

Luan, F., & Burgos, W. D. (2012). Sequential extraction method for determination of Fe (II/III) and U (IV/VI) in suspensions of iron-bearing phyllosilicates and uranium. *Environmental science & technology*, *46*(21), 11995-12002.

McGlathery, K.J., Marino, R., Howarth, R.W. (1994). Variable rates of phosphate uptake by shallow marine carbonate sediments: Mechanisms and ecological significance. *Biochemistry* 25:127-146.

McManus, James, Berelson, W.M., Klinkhammer, G.P., Hammond, D.E., Holm, C. (2005). Authigenic uranium: relationship to oxygen penetration depth and organic carbon rain. *Geochimica et Cosmochimica Acta.* 69(1):95-108.

McManus J, Berelson, W.M., Severmann, S., Poulson, R.L., Hammond, D.E., Klinkhammer, G.P., Holm, C. (2006). Molybdenum and uranium geochemistry in continental margin sediments: paleoproxy potential. *Geochimica et Cosmochimica Acta.* 70:4643–4662.

Meyer, K.M., Kump, L.R., Ridgwell, A. 2008. The biogeochemical controls on photic-zone euxinia during the end-Permian mass extinction. *Geology* 36:747–750.

Montoya-Pino, C., Weyer, S., Anbar, A.D., Pross, J., Oschmann, W., Schootbrugge, B.S.D., Arz, H.W. 2010. Global enhancement of ocean anoxia during Oceanic Anoxic Event 2: a quantitative approach using U isotopes. *Geology.* 38:315–318.

Morin, G., Mangeret, A., Othmane, G., Stetten, L., Seder-Colomina, M., Brest, J., ... & Thouvenot, A. (2016). Mononuclear U (IV) complexes and ningyoite as major uranium species in lake sediments. *Geochemical Perspectives Letter*, *2*, 95-105.

Mundil, R., Ludwig, K.R., Metcalfe, I., Renne, P.R. 2004. Age and timing of the Permian mass extinctions: I/PB Geochronology on closed-system zircons. *Science.* 305:1760-1763.

Murphy, Melissa J. 2014. Fractionation of 238 U/235 U by reduction during low temperature uranium mineralisation processes. *Earth and Planetary Science Letters* 388:306-317.

Nestell, G. P., Nestell, M. K., Ellwood, B. B., Wardlaw, B. R., Basu, A. R., Ghosh, N., ... & Ratcliffe, K. T. 2015. High influx of carbon in walls of agglutinated foraminifers during the Permian–Triassic transition in global oceans. International Geology Review, 57(4), 411-427.

Newell, N. D., & Rigby, J. K. (1957). Geological studies on the Great Bahama Bank. *Special Publication - Society Of Economic Paleontologists And Mineralogists*, *5*(28), 15-72.

Quejido, A. J., Del Villar, L. P., Cozar, J. S., Fernandez-Diaz, M., & Crespo, M. T. (2005). Distribution of trace elements in fracture fillings from the "Mina Fe" uranium deposit (Spain) by sequential leaching: implications for the retention processes. *Applied geochemistry*, *20*(3), 487-506.

Rademacher L. K., Lundstrom, C., Johnson T. M., Sanford R. A., Zhao J., Zhang Z. 2006. Experimentally determined uranium isotope fractionation during reduction of hexavalent U by bacteria and zero valent iron. *Environ. Sci. Technol*. 40:6943–6948.

Rao, C.R.; Sahuquillo, A.; Sanchez, J.F.L., 2008. A review of the Different Methods applied in environmental geochemistry for single and sequential extraction of trace elements in soil and related materials. *Water Air Soil Pollut* 189: 291-333.

Reeder, R. J., Nugent, M., Tait, C. D., Morris, D. E., Heald, S. M., Beck, K. M., ... & Lanzirotti, A. (2001). Coprecipitation of uranium (VI) with calcite: XAFS, micro-XAS, and luminescence characterization. *Geochimica et Cosmochimica Acta*, *65*(20), 3491-3503.

Renne P.R., Basu A.R. 1991. Rapid eruption of the Siberian Traps flood basalts at the Permo Triassic boundary. *Science* 253:176–179.

Renne P.R., Zhang Z., Richardson M.A., Black M.T., Basu A.R. (1995). Synchrony and causal relations between Permian–Triassic boundary crises and Siberian flood volcanism. *Science* 269:1413–1416.

Riccardi, A. L., Arthur, M. A., & Kump, L. R. (2006). Sulfur isotopic evidence for chemocline upward excursions during the end-Permian mass extinction. *Geochimica et Cosmochimica Acta*, *70*(23), 5740-5752.

Riccardi, A., Kump, L.R., Arthur, M.A., D'Hondt, S. (2007). Carbon isotopic evidence for chemocline upward excursions during the end-Permian event. *Palaeogeography, Palaeoclimatology, Palaeoecology.* 248:73–81.

Rolison, J. M., Stirling, C. H., Middag, R., & Rijkenberg, M. J. (2017). Uranium stable isotope fractionation in the Black Sea: Modern calibration of the 238 U/235 U paleo-redox proxy. *Geochimica et Cosmochimica Acta*, *203*, 69-88.

Romaniello, S. J., Herrmann, A. D., & Anbar, A. D. (2013). Uranium concentrations and (super 238) / (super 235) U isotope ratios in modern carbonates from the Bahamas; assessing a novel paleoredox proxy. *Chemical Geology*, 362:305-316.

Santamaría-Fernández, Rebeca (2004). "New Strategies to Determine the Distribution of Trace Elements in Soils and Sediments.". University of Plymouth

Schauble E. A. (2007). Role of nuclear volume in driving equilibrium stable isotope fractionation of mercury, thallium, and other very heavy elements. *Geochimica et Cosmochimica Acta* 71:2170–2189.

Senko, J. M., Istok, J. D., Suflita, J. M., & Krumholz, L. R. (2002). In-situ evidence for uranium immobilization and remobilization. *Environmental science & technology*, *36*(7), 1491-1496.

Senko, J.M., Kelly, S.D., Dohnalkova, A.C., McDonough, J.T., Kemner, K.M., Burgos, W.D. (2007). The effect of U (VI) bioreduction kinetics on subsequent reoxidation of biogenic U (IV). *Geochimica et Cosmochimica Acta.* 71(19):4644-4654.

Son, T. H., Koeberl, C., Ngoc, N. L., & Huyen, D. T. (2007). The Permian-Triassic boundary sections in northern Vietnam (Nhi Tao and Lung Cam sections): Carbon-isotope excursion and elemental variations indicate major anoxic event. *Palaeoworld*, *16*(1), 51-66.

Soudry, D., Ehrlich, S., Yoffe, O., & Nathan, Y. (2002). Uranium oxidation state and related variations in geochemistry of phosphorites from the Negev (southern Israel). *Chemical Geology*, *189*(3), 213-230.

Stanley, S.M. (2007). An analysis of the history of marine animal diversity. *Paleobiology* 33:1–

55.

Starinsky, A., Katz, A., & Kolodny, Y. (1982). The incorporation of uranium into diagenetic phosphorite. *Geochimica et Cosmochimica Acta*, *46*(8), 1365-1374.

Stetten, L., Mangeret, A., Brest, J., Seder-Colomina, M., Le Pape, P., Ikogou, M., ... & Reyss, J. L. (2018). Geochemical control on the reduction of U (VI) to mononuclear U (IV) species in lacustrine sediments. *Geochimica et Cosmochimica Acta*.

Stirling, C. H., Andersen, M. B., Potter, E. K., & Halliday, A. N. (2007). Low-temperature isotopic fractionation of uranium. *Earth and Planetary Science Letters*, *264*(1), 208-225.

Stirling, C. H., Andersen, M. B., Warthmann, R., & Halliday, A. N. (2015). Isotope fractionation of 238 U and 235 U during biologically-mediated uranium reduction. *Geochimica et Cosmochimica Acta*, *163*, 200-218.

Stylo, M., Neubert, N., Wang, Y., Monga, N., Romaniello, S. J., Weyer, S., & Bernier-Latmani, R. (2015). Uranium isotopes fingerprint biotic reduction. *Proceedings of the National Academy of Sciences*, *112*(18), 5619-5624.

Stylo, M., Neubert, N., Roebbert, Y., Weyer, S., & Bernier-Latmani, R. (2015). Mechanism of uranium reduction and immobilization in Desulfovibrio vulgaris biofilms. *Environmental science & technology*, *49*(17), 10553-10561.

Šurija, B., & Branica, M. (1995). Distribution of Cd, Pb, Cu and Zn in carbonate sediments from the Krka river estuary obtained by sequential extraction. *Science of the total environment*, *170*(1-2), 101-118.

Swarzenski, P.W., McKee, B.A.; Skei, J.M.; Todd, J.F. (1999). Uranium biogeochemistry across the redox transition zone of a permanently stratified fjord: Framvaren, Norway." *Marine Chemistry* 67(3):181-198.

Tonarini, S., Pennisi, M., Adorni-Braccesi, A., Dini, A., Ferrara, G., Gonfiantini, R., Wiedenbeck, M., Gröning, M. (2003). Intercomparison of boron isotope and concentration measurements. Part I: selection, preparation and homogeneity tests of the intercomparison materials. Geostandards and Geoanalytical Research, 27(1), 21-39.

Tribovillard, N., Algeo, T. J., Lyons, T., & Riboulleau, A. (2006). Trace metals as paleoredox and paleoproductivity proxies; an update. *Chemical Geology*, 232(1-2):12-32.

Tuovinen, O.H., Hiltunen, P., Vuorinen, A. (1983). Solubilization of Phosphate, Uranium, and Iron from Apatite and Uranium-containing rock samples in synthetic and microbiologically produced acid leach solutions. *Applied Microbiology and Biotechnology*. 17:327-333.

Vieillard, P., Tardy, Y. (1984). Thermochemical properties of phosphates. *Nriagu JO & Moore PB (Eds)*. 171-198.

Wardlaw, B. R., Nestell, M. K., Nestell, G. P., Ellwood, B. B., & Lan, L. T. P. (2015). Conodont biostratigraphy of the Permian–Triassic boundary sequence at Lung Cam, Vietnam. *Micropaleontology*, *61*(4/5), 313-334.

Weyer, S., Anbar, A. D., Gerdes, A., Gordon, G. W., Algeo, T. J., & Boyle, E. A. (2008). Natural fractionation of $^{238}U/^{235}U$. *Geochimica et Cosmochimica Acta*, 72(2):345-359.

Wignall, P.B. (2005). The link between large igneous provinces and mass extinctions. *Elements* 1: 293–297.

Wignall, P.B., Hallam A. (1992). Anoxia as a cause of the Permian/Triassic mass extinction: facies evidence from northern Italy and the western United States. *Palaeogeography,Palaeoclimatology, Palaeoecology* 93:21–46.

Wignall, P.B., Twitchett, R.J. (1996). Ocean anoxia and the end-Permian mass extinction. *Science*. 272:1155–1158.

Yi, Z.Ji, Tan, K.X., Tan, A.L., Yu, Z.X., Wang, S.Q. (2007). Influence of environmental factors on reductive bioprecipitation of uranium by sulfate reducing bacteria." *International Biodeterioration & Biodegradation* 60(4): 258-266.

Zerbe, J., Sobczynski, T., Elbanowska, H., Siepak, J. (1999). Speciation of heavy metals in bottom sediments of lakes. *Polish Journal of Environmental Studies* 8:331-340.

Zimmerman, A.J., Weindorf, D.C. (2010). Heavy metal and trace metal analysis in soil by sequential extraction: a review of procedures. *International Journal of Analytical Chemistry*. vol. 2010, Article ID 387803, 7 pages,. doi:10.1155/2010/387803

Zheng, Y., Anderson, R.F., Green, A.V., Fleisher, M.Q. (2002). Remobilization of authigenic uranium in marine sediments by bioturbation. *Geochimica et Cosmochimica Acta.* 66(10): 1759-1772.

Zhmodik, S.M. (1981). Form of occurrence of Uranium in Apatite in Carbonatites. *Doklady Akademii Nauk SSSR*. 256(3):687-689.

Zhou, P., & Gu, B. (2005). Extraction of oxidized and reduced forms of uranium from contaminated soils: Effects of carbonate concentration and pH. *Environmental science & technology*, *39*(12), 4435-4440.

Appendix A. Detailed Core and Stratigraphy

Bahamas	
Sample Name	Depth (cm)
BC – TF1	38.1
BC – TF2	34.29
BC – TF3	30.48
BC – TF4	26.67
BC – TF5	22.86
BC – TF6	19.05
BC – TF7	15.24
BC – TF8	11.43
BC – TF9	7.62
BC – TF10	3.81

Lung Cam Section		
Sample Name	Height (m)	Bed #
LC -1	5.22	-11
LC – 5	5.41	-11
LC – 11	5.69	-8
LC – 15	5.89	-8
LC – 19	6.07	-6
LC – 31	6.66	-2
LC – 37	6.95	0
LC – 41	7.15	1
LC – 47	7.45	3
LC – 53	7.76	3
LC – 59	8.06	6
LC – 65	8.37	8
LC – 73	8.72	10
LC – 79	8.97	11
LC – 85	9.26	14
LC – 91	9.43	15
LC – 99	9.86	18
LC – 104	10.14	20
LC – 109	10.42	22
LC – 113	10.63	24
LC – 117	10.83	25
LC – 121	11.04	27
LC – 122	11.1	28
LC – 127	11.36	32
LC – 133	11.7	36
LC – 139	12.03	39
LC – 145	12.34	42
LC – 155	12.84	51
LC – 165	13.35	57
LC - 171	13.64	59

Appendix B. Bahamas ICP – MS Data

	25Mg (STD)	43Ca (STD)	44Ca (STD)	51V (KED)	52Cr (KED)	55Mn (KED)	59Co (KED)	60Ni (KED)	63Cu (KED)
	Y (ppm)	%	Y (ppm)	Y (ppm)	Y (ppm)	Y (ppm)	Y (ppm)	Y (ppm)	Y (ppm)
BC-TF1 ex	558.4909	0.007616813	0.002784177	1.6330	X	X	0.4931	0.0505	9.6703
BC-TF2 ex	827.0641	0.019900991	0.010613012	2.0468	0.1481	X	0.3186	X	X
BC-TF3 ex	499.2259	0.013240575	0.002875261	1.5844	0.1147	X	0.2394	X	X
BC-TF4 ex	561.2020	0.008687531	X	1.7910	0.1241	X	0.2825	X	X
BC-TF5 ex	528.9056	0.010310433	0.00116642	1.6979	0.1288	X	0.3306	X	X
BC-TF6 ex	586.1808	0.010175228	0.00180801	2.0387	0.1395	X	0.4780	X	X
BC-TF7 ex	727.3923	0.011540118	0.001505288	2.0950	0.1447	X	0.3342	X	X
BC-TF8 ex	636.4550	0.011266842	0.001673998	1.9538	0.1568	X	0.2335	0.0534	X
BC-TF9 ex	785.6421	0.010583347	0.002840027	2.5076	0.1970	X	0.2445	X	X
BC-TF10 ex	1213.9378	0.007442659	X	2.0161	0.2314	X	0.1487	X	X
BC-TF1 carb	8417.3063	42.54381524	35.99543782	0.2713	0.7776	2.8751	0.9319	33.1467	X
BC-TF2 carb	8342.0843	40.93335692	34.79386536	0.2634	1.0050	2.9042	0.7493	32.3198	X
BC-TF3 carb	8091.0483	39.38201103	33.8076501	0.2841	1.1831	2.9814	0.7253	33.1136	X
BC-TF4 carb	8311.4056	41.40106206	35.68025548	0.2609	0.8205	3.0395	0.7660	33.5935	X
BC-TF5 carb	8546.4729	39.96320967	34.78035089	0.2581	0.7500	2.9806	0.7770	34.0315	X
BC-TF6 carb	8411.6637	40.41061565	34.52507728	0.2778	0.6070	2.8832	0.8125	34.5949	X
BC-TF7 carb	8330.9675	40.69518512	35.23532437	0.2656	0.2446	2.8627	0.8063	35.1765	X
BC-TF8 carb	8054.6549	42.11678995	36.6767998	0.2574	X	2.7591	0.7240	34.6404	X
BC-TF9 carb	6604.5903	40.49192422	33.75734917	0.1668	X	2.0708	0.5777	28.1089	X
BC-TF10 carb	6266.1696	39.81757356	34.52415907	0.1607	X	1.8529	0.5186	27.5041	X

	85Rb (KED)	88Sr (KED)	95Mo (STD)	100Mo (STD)	232Th (STD)	238U (STD)
	Y (ppm)	Y (ppm)	Y (ppm)	Y (ppm)	Y (ppm)	Y (ppm)
BC-TF1 ex	0.21309224	2.72010424	4.1445	4.2158	X	1.8974
BC-TF2 ex	0.22973777	3.12028343	4.4539	4.5682	X	1.3772
BC-TF3 ex	0.16941988	2.90599928	2.6362	2.7214	X	1.0160
BC-TF4 ex	0.19171661	1.75900846	3.0533	3.1253	X	1.0653
BC-TF5 ex	0.1883316	2.6413894	2.6295	2.6500	X	0.8799
BC-TF6 ex	0.21143683	2.90174815	2.6154	2.6512	X	0.8608
BC-TF7 ex	0.21024735	2.73472813	3.4902	3.5126	X	0.8798
BC-TF8 ex	0.20509743	1.47069803	2.8297	2.8473	X	0.8334
BC-TF9 ex	0.17956662	2.78525522	2.9324	3.0096	X	0.6526
BC-TF10 ex	0.22626404	2.60499627	2.9589	2.9186	X	0.5364
BC-TF1 carb	0.34075876	6340.37699	0.3617	0.4606	0.1001	3.3714
BC-TF2 carb	0.3478863	6408.95722	0.2903	0.3929	0.0775	3.3629
BC-TF3 carb	0.32347703	6068.39931	0.2063	0.2969	0.0794	3.3735
BC-TF4 carb	0.34758756	6534.68547	0.2068	0.2585	0.0673	3.3298
BC-TF5 carb	0.34697298	6265.99591	0.1869	0.2569	0.0638	3.1909
BC-TF6 carb	0.33386425	6533.58418	0.2018	0.2704	0.0760	3.2736
BC-TF7 carb	0.34963988	6475.29933	0.2310	0.3025	0.0658	3.2901
BC-TF8 carb	0.34579109	6579.29314	0.2008	0.2688	0.0544	3.2531
BC-TF9 carb	0.32772645	6280.50311	0.1830	0.2581	0.1632	3.1666
BC-TF10 carb	0.35714472	6281.07228	0.1438	0.1948	0.0838	3.1172

	25Mg (STD)	43Ca (KED)	44Ca (KED)	51V (KED)	52Cr (KED)	55Mn (KED)	59Co (KED)	60Ni (KED)	63Cu (KED)
	Y (ppm)	%	Y (ppm)	Y (ppm)	Y (ppm)	Y (ppm)	Y (ppm)	Y (ppm)	Y (ppm)
BC-TF1 apa	43.2719	1.038707466	1.150462771	0.3146	0.5449	0.1110	0.0288	0.1180	0.2546
BC-TF2 apa	57.8561	1.170001533	1.311986753	0.3180	0.5728	0.0977	0.0171	0.1178	0.2765
BC-TF3 apa	64.2499	1.205265385	1.292126572	0.2556	0.5568	0.0839	0.0126	0.1353	0.2656
BC-TF4 apa	35.4910	0.88622646	0.949066083	0.3523	0.6349	0.0742	0.0112	0.1429	0.3822
BC-TF5 apa	46.7949	0.995661754	1.040454145	0.3868	0.6274	0.0733	0.0146	0.1691	0.4807
BC-TF6 apa	42.3595	0.840829893	0.859483526	0.2491	0.5707	0.0944	0.0137	0.1443	0.3888
BC-TF7 apa	19.4636	0.427794778	0.452947592	0.3697	0.5491	0.0614	0.0109	0.1623	0.3586
BC-TF8 apa	20.8055	0.412669544	0.444832042	0.5783	0.6854	0.0598	0.0129	0.1762	0.3415
BC-TF9 apa	56.8922	1.116993201	1.126633851	0.2538	0.6163	0.0878	0.0113	0.1546	0.3804
BC-TF10 apa	42.8724	0.926265809	0.996021032	0.2032	0.5902	0.0866	0.0117	0.1263	0.3001
BC-TF1 ox	2.9667	X	X	0.0118	0.6321	0.1161	0.0352	0.0682	1.0413
BC-TF 2 ox	3.5134	X	X	2.7901	X	X	0.0149	X	67.0031
BC-TF3 ox	3.2975	X	X	0.0096	0.6261	0.0639	0.0150	0.0366	X
BC-TF4 ox	3.6018	X	X	0.0293	0.7246	0.0726	0.0162	0.0358	X
BC-TF5 ox	5.5552	X	X	0.0354	0.7402	0.0753	0.0197	0.0565	X
BC-TF6 ox	5.1143	X	X	0.0358	0.7160	0.0880	0.0197	0.0874	X
BC-TF7 ox	5.0434	X	X	0.0386	0.7699	0.0769	0.0208	0.0840	X
BC-TF8 ox	5.2312	X	X	0.0541	0.6609	0.0847	0.0156	0.0682	X
BC-TF9 ox	4.1237	X	X	0.0378	0.6587	0.0693	0.0182	0.0540	X
BC-TF10 ox	3.6221	X	X	0.0273	0.6122	0.0665	0.0201	0.0638	X

	85Rb (KED)	88Sr (KED)	95Mo (STD)	100Mo (STD)	232Th (STD)	238U (STD)
	Y (ppm)	Y (ppm)	Y (ppm)	Y (ppm)	Y (ppm)	Y (ppm)
BC-TF1 org	X	X	0.4108	0.4033	0.0876	0.0058
BC-TF2 org	X	X	0.4191	0.4256	0.0518	0.0046
BC-TF3 org	X	X	0.3041	0.3186	0.0401	0.0045
BC-TF4 org	X	X	0.3305	0.3437	0.0304	0.0049
BC-TF5 org	X	X	0.4319	0.4405	0.0349	0.0051
BC-TF6 org	X	X	0.3772	0.4133	0.0324	0.0032
BC-TF7 org	X	X	0.3449	0.3545	0.0310	0.0036
BC-TF8 org	X	X	0.2835	0.2875	0.0440	0.0037
BC-TF9 org	X	X	0.2055	0.2461	0.0920	0.0055
BC-TF10 org	X	X	0.3180	0.3170	0.0519	0.0064
BC-TF1 res	0.00836826	0.34611895	0.0334	0.0363	0.0561	0.0017
BC-TF2 res	0.00733356	0.0439855	0.0299	0.0273	0.0215	0.0014
BC-TF3 res	0.0128491	0.01821685	0.0244	0.0247	0.0169	0.0027
BC-TF4 res	0.01171703	0.01356845	0.0203	0.0182	0.0108	0.0020
BC-TF5 res	0.0097746	0.01029592	0.0258	0.0250	0.0085	0.0018
BC-TF6 res	0.01160791	0.01987216	0.0191	0.0250	0.0077	0.0019
BC-TF7 res	0.01050047	0.02517162	0.0503	0.0574	0.0055	0.0013
BC-TF8 res	0.01019117	0.07365928	0.0337	0.0300	0.0056	0.0013
BC-TF9 res	0.00699305	0.00959513	0.0381	0.0442	0.0613	0.0044
BC-TF10 res	0.00733598	0.0097683	0.0223	0.0224	0.0188	0.0006

	25Mg (STD)	43Ca (KED)	44Ca (KED)	51V (KED)	52Cr (KED)	55Mn (KED)	59Co (KED)	60Ni (KED)	63Cu (KED)
	Y (ppm)	X	Y (ppm)	Y (ppm)	Y (ppm)	Y (ppm)	Y (ppm)	Y (ppm)	Y (ppm)
BC-TF1 sum	9030.7531	N/A	N/A	2.2656	4.0123	3.4727	1.5214	34.5634	11.3672
BC-TF2 sum	9239.4107	N/A	N/A	5.4618	3.8547	3.3869	1.1288	33.7444	67.7181
BC-TF3 sum	8666.0364	N/A	N/A	2.1890	4.1628	3.4544	1.0135	34.1880	0.4821
BC-TF4 sum	8921.1322	N/A	N/A	2.4792	4.1451	3.5445	1.0948	34.6585	0.6995
BC-TF5 sum	9137.5248	N/A	N/A	2.4261	4.5866	3.5565	1.1726	36.7901	0.9888
BC-TF6 sum	9062.1458	N/A	N/A	2.6522	4.3984	3.5562	1.3566	36.1032	0.8949
BC-TF7 sum	9107.9188	N/A	N/A	2.8173	3.7820	3.5710	1.1957	40.9834	0.7364
BC-TF8 sum	8740.8280	N/A	N/A	2.8825	3.3937	3.3691	1.0074	35.9292	0.8177
BC-TF9 sum	7475.0353	N/A	N/A	3.0019	3.0699	2.6538	0.8694	29.0806	0.5534
BC-TF10 sum	7552.2312	N/A	N/A	2.4551	3.7381	2.5965	0.7240	28.9745	0.7341
BC-TF1 TD	8816.9418	38.9736644	32.4652939	2.4865	4.5144	4.3300	1.1107	2.5630	X
BC-TF2 TD	9067.7042	38.12657087	31.27472113	2.5339	4.4301	4.3109	0.6140	2.6369	X
BC-TF3 TD	8737.5511	38.84164296	31.10751615	2.0087	4.6018	4.3985	0.4880	3.2109	X
BC-TF4 TD	8957.7791	38.68732962	31.36505544	2.3241	4.8425	4.7182	0.5790	2.1803	X
BC-TF5 TD	9156.8305	37.91602956	30.14155077	2.3312	4.8622	4.7498	0.6725	1.0550	X
BC-TF6 TD	9092.5102	37.95587038	29.6640112	2.5672	4.9241	4.8184	0.8890	3.3008	X
BC-TF7 TD	9261.4217	37.50024107	30.36420569	2.6814	4.7474	4.7200	0.6802	2.6283	X
BC-TF8 TD	8855.1331	38.48455907	31.25125116	2.7524	4.7236	4.7206	0.5237	11.2741	X
BC-TF9 TD	9843.1211	39.0237071	31.40790661	0.8186	3.4318	4.1259	1.0494	37.2778	X
BC-TF10 TD	9795.8522	37.5590137	29.80529694	2.2977	4.7408	4.8203	0.3881	7.1063	X

	85Rb (KED)	88Sr (KED)	95Mo (STD)	100Mo (STD)	232Th (STD)	238U (STD)
	Y (ppm)	Y (ppm)	Y (ppm)	Y (ppm)	Y (ppm)	Y (ppm)
BC-TF1 sum	N/A	N/A	5.2343	5.4105	0.2962	5.4363
BC-TF2 sum	N/A	N/A	5.5610	5.7976	0.2129	4.9408
BC-TF3 sum	N/A	N/A	3.3735	3.5720	0.1493	4.5869
BC-TF4 sum	N/A	N/A	3.8539	3.9877	0.1174	4.5510
BC-TF5 sum	N/A	N/A	3.5063	3.6065	0.1131	4.2376
BC-TF6 sum	N/A	N/A	3.3910	3.5439	0.1198	4.2730
BC-TF7 sum	N/A	N/A	4.3498	4.4390	0.1050	4.2687
BC-TF8 sum	N/A	N/A	3.6021	3.6855	0.1055	4.2075
BC-TF9 sum	N/A	N/A	3.5482	3.7367	0.3821	4.0042
BC-TF10 sum	N/A	N/A	3.5563	3.5698	0.1713	3.8051
BC-TF1 TD	0.31945635	7386.92288	4.1336	4.4655	0.0036	4.4464
BC-TF2 TD	0.33325904	7262.52886	3.9010	4.2574	X	4.4624
BC-TF3 TD	0.28127588	7384.24563	2.4803	2.7335	X	3.9947
BC-TF4 TD	0.31669943	7268.98333	2.7637	3.0703	X	3.9691
BC-TF5 TD	0.30941777	7121.53082	2.4594	2.7217	X	3.7691
BC-TF6 TD	0.34054365	7204.64974	2.3544	2.6102	X	3.7207
BC-TF7 TD	0.33885587	7120.93548	3.1158	3.4161	X	3.6280
BC-TF8 TD	0.3466197	7339.81129	2.6678	2.9595	X	3.6197
BC-TF9 TD	0.31725891	7347.26865	2.7002	2.9854	0.0120	3.6510
BC-TF10 TD	0.34893298	7072.25135	2.6344	2.8497	X	3.3518

Appendix C. Lung Cam ICP – MS Data

	25Mg (STD)	51V (KED)	52Cr (KED)	55Mn (KED)	59Co (KED)	60Ni (KED)	63Cu (KED)	85Rb (KED)	88Sr (KED)	95Mo (STD)	100Mo (STD)	232Th (STD)	238U (STD)
	Y (ppm)	Y (ppm)	Y (ppm)	Y (ppm)	Y (ppm)	Y (ppm)	Y (ppm)	Y (ppm)	Y (ppm)	Y (ppm)	Y (ppm)	Y (ppm)	Y (ppm)
LC 1 ex	X	0.2816	0.0489	X	1.2576	X	X	X	0.6313	0.0309	0.0314	X	0.3806
LC 5 ex	X	0.8654	0.0515	X	0.5330	X	X	X	1.1747	0.0322	0.0244	X	0.3800
LC 11 ex	X	0.5085	0.0747	0.0115	1.0590	0.0008	X	X	2.2089	0.0192	0.0269	X	0.0534
LC 15 ex	6.2992	0.6812	0.0512	0.0227	0.9010	0.0263	X	X	0.9538	0.0491	0.0362	X	0.0120
LC 19 ex	5.9028	0.1290	0.7416	X	2.6176	X	X	X	1.5590	0.0382	0.0569	X	0.0560
LC 31 ex	0.4845	0.1706	0.2037	X	3.9536	X	X	X	2.0815	0.0445	0.0576	X	0.1225
LC 37 ex	X	0.2169	0.0604	X	1.1665	X	X	X	0.8848	0.0457	0.0649	X	0.1873
LC 41 ex	X	0.1595	0.0950	X	0.8870	X	X	X	0.2363	0.0133	0.0243	X	0.4124
LC 47 ex	13.6911	0.1270	5.9479	0.2484	37.0869	0.5087	X	X	0.5006	0.0962	0.0941	X	0.0248
LC 53 ex	62.0972	0.6100	0.0618	0.1773	0.2189	X	X	X	X	0.0261	0.0310	X	0.1239
LC 59 ex	46.6134	0.1358	0.0530	X	0.6858	X	X	X	0.1094	0.0252	0.0340	X	0.1172
LC 65 ex	15.0390	0.1514	0.0366	X	0.3848	X	X	X	0.2614	0.0238	0.0273	X	0.0972
LC 73 ex	71.4905	0.1573	0.0677	X	1.3666	X	X	X	0.6223	0.0156	0.0441	X	0.0288
LC 79 ex	47.6735	0.1980	0.0675	X	1.2911	X	X	X	0.3237	0.0258	0.0254	X	0.0556
LC 85 ex	41.9032	0.1498	0.1531	0.2400	2.1094	0.1247	X	X	0.1340	0.0531	0.0550	X	0.0846
LC 91 ex	10.9331	0.0030	0.0748	X	1.0105	X	X	X	0.1322	0.0230	0.0273	X	0.0414
LC 99 ex	68.8266	0.2151	0.1341	X	1.1068	X	X	X	0.0221	0.0287	0.0282	X	0.0344
LC 104 ex	72.2437	0.1783	0.1246	0.0678	1.2107	0.1333	X	X	0.1572	0.0296	0.0433	X	0.0331
LC 109 ex	101.3188	0.1594	0.1281	X	1.4313	0.0091	X	X	0.1028	0.0338	0.0347	X	0.0186
LC 113 ex	26.3549	0.0665	0.0777	0.0513	1.2501	0.2037	X	X	0.3562	0.0327	0.0309	X	0.0348
LC 117 ex	43.9211	0.1292	0.0869	0.0212	1.1671	0.1030	X	X	X	0.0382	0.0221	X	0.0232
LC 121 ex	63.5250	0.1975	0.0778	0.0864	1.7966	0.2156	X	X	X	0.0234	0.0304	X	0.0278
LC 122 ex	76.0135	0.2118	0.1701	0.0720	2.1925	0.0387	X	X	0.0960	0.0554	0.0784	X	0.0172
LC 127 ex	14.8687	0.0804	0.1023	0.1256	2.8296	X	X	X	0.7314	0.0292	0.0248	X	0.0152
LC 133 ex	50.4183	0.1674	0.1325	0.0472	1.8969	X	X	X	0.0065	0.0239	0.0251	X	0.0166
LC 139 ex	57.1000	0.2107	0.4946	0.2040	2.2946	0.6172	X	X	X	0.0349	0.0400	X	0.0385
LC 145 ex	10.9779	0.0706	0.0879	0.0775	1.6775	X	X	X	0.5593	0.0329	0.0270	X	0.0271
LC-155 ex	17.4460	0.1509	X	0.0744	1.0997	X	8.8755	X	0.1960	0.0454	0.0770	X	0.1108
LC 165 ex	X	0.1244	X	0.1631	0.2947	X	8.1305	X	0.2209	0.0046	0.0265	X	0.0440
LC 171 ex	X	0.1816	X	0.1902	0.3558	X	6.8629	X	0.1222	X	0.0208	X	0.0765

	25Mg (STD)	51V (KED)	52Cr (KED)	55Mn (KED)	59Co (KED)	60Ni (KED)	63Cu (KED)	85Rb (KED)	88Sr (KED)	95Mo (STD)	100Mo (STD)	232Th (STD)	238U (STD)
	Y (ppm)	Y (ppm)	Y (ppm)	Y (ppm)	Y (ppm)	Y (ppm)	Y (ppm)	Y (ppm)	Y (ppm)	Y (ppm)	Y (ppm)	Y (ppm)	Y (ppm)
LC 1 carb	5853.7704	0.6812	0.1559	26.9588	5.3851	26.5296	X	X	173.8309	X	X	0.3704	2.6315
LC 5 carb	1861.3612	1.2805	X	38.8392	2.4134	19.9047	X	X	130.3087	X	X	0.8513	1.8596
LC 11 carb	963.5135	0.7805	X	26.4559	3.1633	21.7563	X	X	201.7572	X	X	2.1023	0.6419
LC 15 carb	701.6683	X	X	38.2338	2.6981	22.6884	X	X	80.8153	X	X	4.9644	0.4007
LC 19 carb	660.4052	0.0461	X	12.7347	4.2404	7.6075	X	X	86.5768	X	X	0.5526	0.2309
LC 31 carb	1184.9180	0.2166	X	16.1553	4.2124	17.0020	X	X	145.7316	X	X	1.5543	1.4912
LC 37 carb	2327.0936	0.5473	0.8969	21.3853	4.4234	29.0592	X	X	171.9320	X	X	0.6906	1.2212
LC 41 carb	2342.6398	0.7604	3.3136	60.2105	4.3190	40.2585	X	X	200.0979	X	X	0.2871	4.0921
LC 47 carb	41.2490	X	2.8881	4.2092	15.3091	1.4319	X	X	13.0007	X	X	0.0479	0.0520
LC 53 carb	9049.8883	X	X	95.0848	2.6536	15.1762	X	X	31.2525	X	X	1.4003	0.8235
LC 59 carb	9932.1739	X	X	81.5413	3.9604	27.8736	X	X	117.1382	X	X	0.6844	1.0429
LC 65 carb	4467.5812	X	X	69.9701	2.0022	27.8292	X	X	153.6572	X	X	0.9800	1.0463
LC 73 carb	6163.3411	X	X	86.1424	2.8441	23.2344	X	X	133.3115	X	X	1.7864	0.4771
LC 79 carb	7903.9058	X	X	87.0393	3.9578	26.2861	X	X	132.5327	X	X	1.0394	0.4504
LC 85 carb	4116.0510	X	X	94.3939	1.8457	18.8278	X	X	53.9285	X	X	1.7616	1.5565
LC 91 carb	6032.2400	X	X	85.7953	2.0345	33.1694	X	X	115.5740	X	X	0.5313	1.1112
LC 99 carb	5095.6668	X	X	146.6280	1.8762	27.7230	X	X	143.2074	X	X	1.3262	0.7239
LC 104 carb	9450.8072	X	X	175.3580	2.5508	27.4215	X	X	137.0907	X	X	0.9758	0.7496
LC 109 carb	8606.5397	X	X	116.0091	2.2149	24.1808	X	X	126.0832	X	X	1.4818	0.4031
LC 113 carb	5947.5319	X	X	105.3937	2.7043	30.3698	X	X	142.6443	X	X	0.9445	0.6137
LC 117 carb	5990.5795	X	X	127.0944	2.2900	29.5659	X	X	156.8761	X	X	1.0708	0.8222
LC 121 carb	6594.7207	X	X	130.0805	3.1905	26.7586	X	X	149.6491	X	X	1.3333	0.7135
LC 122 carb	5360.0432	X	X	198.1326	2.5373	25.0910	X	X	120.6217	X	X	1.7504	0.5760
LC 127 carb	2978.0951	X	X	142.3056	2.2114	32.6329	X	X	153.4993	X	X	0.7944	0.9248
LC 133 carb	4232.3890	X	X	174.3435	2.4082	26.7532	X	X	155.6846	X	X	1.1680	1.0136
LC 139 carb	4243.5387	X	X	395.5037	3.3286	25.7222	X	X	150.4721	X	X	1.3627	0.4611
LC 145 carb	3299.5322	X	X	346.8527	3.1414	35.5950	X	X	217.3483	X	X	0.5417	1.2049
LC 155 carb	3577.3736	X	X	855.8751	2.8004	27.6734	X	X	173.2955	X	X	0.9822	0.8275
LC 165 carb	1642.3192	X	X	424.3254	3.2523	35.4602	X	X	133.3024	X	X	0.8578	0.4708
LC 171 carb	3585.5211	X	X	672.5347	4.0509	34.0502	X	X	142.2632	X	X	0.6823	0.4726

	25Mg (STD)	51V (KED)	52Cr (KED)	55Mn (KED)	59Co (KED)	60Ni (KED)	63Cu (KED)	85Rb (KED)	88Sr (KED)	95Mo (STD)	100Mo (STD)	232Th (STD)	238U (STD)
	Y (ppm)	Y (ppm)	Y (ppm)	Y (ppm)	Y (ppm)	Y (ppm)	Y (ppm)	Y (ppm)	Y (ppm)	Y (ppm)	Y (ppm)	Y (ppm)	Y (ppm)
LC 1 apa	5182.1558	0.3448	1.6584	7.1345	0.0575	0.0053	X	0.0249	12.7638	0.0159	0.0131	0.0105	0.0298
LC 5 apa	14.4433	0.6487	0.9432	0.2357	0.0970	0.1841	0.3398	0.0277	0.2795	0.0172	0.0161	0.0075	0.0245
LC 11 apa	91.0847	1.8465	0.7663	4.4595	0.5791	1.2571	0.2274	0.0551	18.6367	0.0001	0.0067	0.0501	0.0307
LC 15 apa	33.8494	1.0074	0.4456	3.3675	0.7299	1.0728	1.1083	0.0810	3.2134	X	X	0.2345	0.0375
LC 19 apa	3.6472	0.4802	1.2446	0.3662	0.4340	0.1414	X	0.0300	0.0365	0.0238	0.0270	0.0068	0.0321
LC 31 apa	18.3906	0.4634	0.3209	0.1865	0.2608	0.0035	X	0.0252	0.9782	0.0081	0.0153	0.1729	0.0756
LC 37 apa	157.8242	0.2788	1.0814	1.4446	0.0542	0.0696	X	0.0190	12.5724	0.0174	0.0154	0.0659	0.0454
LC 41 apa	240.2592	0.1482	0.6310	2.6394	0.0245	X	0.2093	0.0176	6.1120	0.0066	0.0060	0.0238	0.0844
LC 47 apa	2.3556	0.1856	2.5117	0.6454	2.0578	0.0829	X	0.0420	0.0207	0.0275	0.0272	0.0139	0.0367
LC 53 apa	6491.3163	0.5495	0.3565	25.8236	0.8226	0.1229	X	0.1827	8.7351	0.0025	0.0035	0.1389	0.0427
LC 59 apa	8389.8385	0.6246	0.3252	42.0853	1.6654	2.4826	2.1260	0.1526	11.6736	0.0295	0.0293	0.0617	0.0447
LC 65 apa	2143.1679	0.5318	0.3208	15.0021	1.4798	2.1801	2.2711	0.1439	3.5995	0.0157	0.0162	0.0957	0.0272
LC 73 apa	6029.4999	0.8795	0.4483	42.5170	3.0811	3.9202	4.4903	0.1948	9.4463	0.0335	0.0370	0.2481	0.0372
LC 79 apa	5537.9429	0.7340	0.8488	42.3066	1.7058	2.4773	2.6355	0.1734	11.0786	0.0333	0.0348	0.0907	0.0216
LC 85 apa	5085.8091	0.7075	0.7322	46.8215	1.2261	1.6456	1.0751	0.1337	11.8637	0.0301	0.0323	0.1859	0.0998
LC 91 apa	7290.0833	0.3052	0.6809	36.5359	0.1920	0.6503	1.0605	0.0767	25.1455	0.0339	0.0386	0.0436	0.0664
LC 99 apa	3934.5489	0.7692	1.4135	80.7794	1.7826	3.7748	3.3939	0.2004	19.3756	0.0591	0.0693	0.1986	0.0332
LC 104 apa	9831.9708	0.7387	1.2253	75.7512	1.5579	2.9989	2.6953	0.1574	27.7721	0.0516	0.0572	0.1609	0.0459
LC 109 apa	13637.8033	1.0439	1.3575	105.1480	2.3256	4.2375	3.8080	0.1863	29.9037	0.0681	0.0768	0.2674	0.0392
LC 113 apa	4261.3618	0.4317	1.1849	36.5233	1.0733	2.6330	2.1460	0.1336	18.2207	0.0620	0.0625	0.0782	0.0294
LC 117 apa	5398.6478	0.6501	1.2268	51.3515	1.9436	3.3972	2.9090	0.1527	15.8955	0.0427	0.0496	0.1452	0.0326
LC 121 apa	5414.9560	0.7688	0.8195	60.1136	1.9804	3.2174	3.1236	0.1946	11.4245	0.0317	0.0321	0.1707	0.0250
LC 122 apa	6013.8450	0.7563	0.7547	74.1277	1.9569	3.1987	3.0685	0.1715	17.5767	0.0498	0.0495	0.2193	0.0275
LC 127 apa	410.1880	0.3795	0.2022	14.2342	0.2944	0.2175	0.0473	0.0668	15.4940	0.0067	0.0065	0.0664	0.0488
LC 133 apa	3410.3358	0.8184	0.4778	74.4677	2.2612	3.7228	4.2986	0.1582	16.3104	0.0224	0.0258	0.1967	0.0449
LC 139 apa	3715.8044	0.7732	0.5227	130.9168	2.1799	3.5696	2.8250	0.1618	12.1865	0.0271	0.0293	0.2336	0.0281
LC 145 apa	676.9599	0.2705	0.1912	49.6020	1.3315	1.5255	1.6090	0.0687	27.7285	0.0115	0.0115	0.0628	0.0849
LC 155 apa	1988.3101	0.5224	0.4299	213.2409	1.8475	2.3855	181.3559	0.1164	31.0242	0.0143	0.0151	0.2540	0.0773
LC 165 apa	234.5175	0.2741	0.1832	27.0356	0.4350	0.1314	0.0301	0.0719	8.6330	0.0037	0.0050	0.0496	0.0258
LC 171 apa	1641.6364	0.4542	0.2916	68.4207	0.5750	0.2683	0.9292	0.0776	7.0727	0.0102	0.0092	0.1022	0.0306

	25Mg (STD)	51V (KED)	52Cr (KED)	55Mn (KED)	59Co (KED)	60Ni (KED)	63Cu (KED)	85Rb (KED)	88Sr (KED)	95Mo (STD)	100Mo (STD)	232Th (STD)	238U (STD)
	Y (ppm)	Y (ppm)	Y (ppm)	Y (ppm)	Y (ppm)	Y (ppm)	Y (ppm)	Y (ppm)	Y (ppm)	Y (ppm)	Y (ppm)	Y (ppm)	Y (ppm)
LC 1 ox	6.1253	0.3973	0.9884	0.1846	0.0652	0.7046	X	0.0462	0.0494	0.0454	0.0415	X	0.0240
LC 5 ox	23.2119	1.0433	2.2192	0.5391	0.0626	0.7067	X	0.0617	0.0617	0.1003	0.0983	X	0.0266
LC 11 ox	46.0464	4.1565	3.7252	0.9489	0.1668	4.1510	X	0.1506	0.1395	0.6365	0.6461	X	0.0300
LC 15 ox	27.2364	9.7380	2.7834	2.1191	0.2953	5.0249	0.4223	0.2187	0.2615	3.0413	3.1081	0.0066	0.0426
LC 19 ox	5.4701	0.7515	2.2808	0.6221	0.4398	0.8954	X	0.0296	0.0246	0.0927	0.0942	X	0.0854
LC 31 ox	9.4145	0.8530	1.8996	0.7526	0.1839	0.3899	X	0.0389	0.1633	0.3496	0.3555	0.0314	0.0714
LC 37 ox	9.2629	0.2873	1.5247	0.1289	0.0522	0.9543	X	0.0187	0.0187	0.1056	0.1088	0.0042	0.0282
LC 41 ox	0.0000	0.1832	0.8779	0.2428	0.0432	0.2936	X	0.0079	0.0064	0.0310	0.0313	X	0.0280
LC 47 ox	2.9578	0.2239	5.8798	1.5211	1.1350	0.6221	0.2294	0.0413	0.0127	0.2348	0.2440	X	0.0208
LC 53 ox	187.5677	2.3389	1.1545	15.6167	1.5484	3.3187	2.6651	0.5351	0.2351	0.1066	0.1195	0.0133	0.0419
LC 59 ox	267.8902	0.3567	0.5071	0.4369	0.0716	0.1783	X	0.3467	0.1377	0.0132	0.0174	X	0.0110
LC 65 ox	493.1089	0.5929	0.6432	1.1987	0.0907	0.3043	X	0.3630	0.1389	0.0031	0.0083	X	0.0078
LC 73 ox	882.2143	0.8053	1.4197	1.8215	0.2459	0.7567	0.1323	0.3710	0.1674	0.0756	0.0707	X	0.0098
LC 79 ox	477.6376	0.4966	0.7922	0.9719	0.1496	0.4035	X	0.3505	0.0786	0.0277	0.0270	X	0.0055
LC 85 ox	352.4156	0.6352	0.7686	3.5569	0.8825	1.7973	1.8748	0.2298	0.0462	0.1119	0.1048	0.0229	0.0560
LC 91 ox	93.5356	0.3021	0.1992	2.1525	0.3652	0.6176	1.6712	0.0397	0.0000	0.0387	0.0358	X	0.0189
LC 99 ox	860.8906	0.8626	1.0373	2.5937	0.1559	0.5249	0.0074	0.2716	0.0361	0.0055	0.0092	X	0.0082
LC 104 ox	525.2176	0.4884	0.5512	1.1260	0.1146	0.3179	X	0.1487	0.0026	0.0124	0.0111	X	0.0069
LC 109 ox	762.6347	0.6931	0.8606	1.9116	0.2223	0.5155	0.0508	0.2669	0.0811	0.0193	0.0190	X	0.0083
LC 113 ox	430.1031	0.4079	0.5151	0.9456	0.0728	0.2790	X	0.1507	0.0560	0.0235	0.0195	X	0.0078
LC 117 ox	629.0066	0.6185	0.7494	1.3709	0.1213	0.3789	X	0.1782	0.0000	0.0158	0.0118	X	0.0077
LC 121 ox	695.3259	0.7628	0.9489	2.0779	0.1986	0.5353	0.0144	0.3309	0.0412	0.0298	0.0329	X	0.0077
LC 122 ox	732.4923	0.8162	1.0283	2.5015	0.2322	0.6496	0.0231	0.2977	0.0589	0.0518	0.0556	0.0246	0.0105
LC 127 ox	580.1453	0.7903	0.7731	3.8303	0.9874	1.6167	2.1640	0.0758	0.0000	0.0274	0.0306	X	0.0166
LC 133 ox	751.1319	0.8274	1.0247	2.6397	0.2836	0.6378	0.3286	0.2047	0.0179	0.0259	0.0219	X	0.0099
LC 139 ox	586.4587	0.8254	1.0406	3.2963	0.2289	0.6983	0.0309	0.2864	0.0186	0.0179	0.0263	X	0.0096
LC 145 ox	353.7463	0.4247	0.4724	1.0717	0.0745	0.2428	X	0.0596	0.0000	0.0054	0.0040	X	0.0063
LC 155 ox	535.0681	0.7164	1.0200	2.8745	0.1596	0.5174	0.1716	0.1943	0.0131	0.0102	0.0119	X	0.0092
LC 165 ox	491.5399	0.8259	0.6706	9.7463	0.8592	1.5533	2.2562	0.0915	0.0000	0.0432	0.0457	X	0.0178
LC 171 ox	407.3487	0.6973	0.5486	20.6351	0.9515	0.8488	0.9765	0.0945	0.0000	0.0391	0.0378	X	0.0120

	25Mg (STD)	51V (KED)	52Cr (KED)	55Mn (KED)	59Co (KED)	60Ni (KED)	63Cu (KED)	85Rb (KED)	88Sr (KED)	95Mo (STD)	100Mo (STD)	232Th (STD)	238U (STD)
	Y (ppm)	Y (ppm)	Y (ppm)	Y (ppm)	Y (ppm)	Y (ppm)	Y (ppm)	Y (ppm)	Y (ppm)	Y (ppm)	Y (ppm)	Y (ppm)	Y (ppm)
LC 1 org	27.7081	0.3155	3.2232	0.5253	0.0256	1.5353	0.3070	0.0885	1.2533	0.2424	0.2311	0.0111	0.0195
LC 5 org	28.0489	0.5018	1.9859	0.1759	0.0120	0.6427	X	0.0879	0.2235	0.1345	0.1475	0.0078	0.0033
LC 11 org	88.7423	2.0048	2.3590	0.3029	0.0291	2.2040	0.1117	0.2694	0.3159	0.2190	0.2371	0.0081	0.0010
LC 15 org	60.3511	1.8849	3.6805	0.3401	0.0253	1.6479	0.1204	0.4892	0.5238	0.3360	0.3275	0.0328	0.0404
LC 19 org	14.6557	0.5227	3.5194	0.3649	0.0370	4.0721	0.2020	0.0842	0.2254	0.2272	0.2163	0.0227	0.0535
LC 31 org	20.4537	0.2786	1.7543	0.2675	0.0200	0.9142	0.1431	0.0727	0.3559	0.2491	0.2574	0.0906	0.0097
LC 37 org	17.6663	0.1870	2.5932	0.2660	0.0205	0.8365	0.1793	0.0404	0.2771	0.2145	0.2172	0.0572	0.0133
LC 41 org	4.7923	0.0864	2.0098	0.2222	0.0253	5.1692	0.1728	0.0303	0.2043	0.1962	0.2163	0.0201	0.0258
LC 47 org	9.3536	0.2797	3.9963	0.3253	0.0821	4.8981	0.2491	0.0750	0.2765	0.2456	0.2523	0.0114	0.0192
LC 53 org	166.0835	0.9061	2.5930	0.6744	0.0532	1.3142	0.2510	0.9384	0.6181	0.2625	0.2686	0.0065	0.0255
LC 59 org	140.8276	0.5347	2.3306	0.5567	0.1268	4.5146	0.5092	0.4268	0.4712	0.3246	0.3210	0.0082	0.0195
LC 65 org	292.7442	0.6695	2.4190	0.8634	0.0857	7.6566	0.4515	0.4591	0.4547	0.3006	0.2770	0.0069	0.0139
LC 73 org	581.9607	0.7757	2.3052	2.4191	0.4759	3.0285	1.6707	0.2520	0.4292	0.3287	0.3384	0.0026	0.0075
LC 79 org	324.2140	0.6915	2.6026	0.7892	0.1041	2.9670	0.5195	0.4044	0.3894	0.2902	0.3026	0.0068	0.0085
LC 85 org	390.9280	0.6169	2.4836	0.8857	0.1256	2.8461	0.6169	0.3204	0.4789	0.3057	0.3123	0.0565	0.0594
LC 91 org	314.5094	0.4061	1.9787	1.0395	0.0583	3.1549	0.3463	0.1372	0.3075	0.2771	0.2888	0.0165	0.0019
LC 99 org	422.9635	0.6393	2.2587	1.5295	0.1464	3.6196	0.5785	0.1782	0.3776	0.2798	0.2892	0.0098	0.0091
LC 104 org	445.2978	0.6292	2.3903	1.2684	0.1647	2.9990	0.6610	0.1988	0.3638	0.3027	0.3195	0.0075	0.0104
LC 109 org	533.2780	0.7024	2.4378	1.3561	0.2592	1.9551	0.9468	0.2354	0.4393	0.3117	0.3227	0.0079	0.0095
LC 113 org	295.4535	0.4315	2.1784	0.8564	0.0766	2.5970	0.4667	0.1644	0.2911	0.3037	0.2872	0.0056	0.0092
LC 117 org	588.5907	0.7909	2.5847	1.4116	0.1961	1.8168	1.0270	0.2205	0.3963	0.2951	0.2995	0.0013	0.0082
LC 121 org	585.6999	0.9683	2.7850	1.4124	0.1413	3.4695	0.5985	0.4441	0.3155	0.2766	0.2792	0.0006	0.0099
LC 122 org	690.7653	0.9461	2.7881	1.9210	0.1455	1.6362	0.5737	0.3804	0.3006	0.3106	0.3397	0.0518	0.0104
LC 127 org	551.2166	0.6988	2.6267	1.0247	0.0829	1.5780	0.5780	0.1284	0.1487	0.3024	0.2972	0.0196	0.0098
LC 133 org	741.4305	1.0033	2.8072	2.2788	0.2770	2.2578	0.9577	0.2036	0.2172	0.2867	0.2912	0.0064	0.0057
LC 139 org	609.7807	1.1373	3.0071	3.3066	0.2913	6.6897	0.8985	0.3404	0.2533	0.3174	0.3230	0.0035	0.0062
LC 145 org	491.0603	0.7182	2.5444	1.7455	0.2132	1.8375	0.8890	0.0846	0.1428	0.3197	0.3100	0.0027	0.0091
LC 155 org	489.8178	0.8021	2.6788	3.5878	0.4792	5.5686	1.6837	0.1870	0.2082	0.2879	0.2943	0.0004	0.0043
LC 165 org	724.3716	0.9423	2.7484	1.8576	0.0749	5.8042	0.5518	0.1900	0.1664	0.3104	0.3103	0.0034	0.0069
LC 171 org	631.7064	0.7885	2.5654	1.8300	0.0887	3.2562	0.4734	0.2542	0.1727	0.3057	0.3191	0.0047	0.0122

	25Mg (STD)	51V (KED)	52Cr (KED)	55Mn (KED)	59Co (KED)	60Ni (KED)	63Cu (KED)	85Rb (KED)	88Sr (KED)	95Mo (STD)	100Mo (STD)	232Th (STD)	238U (STD)
	Y (ppm)	Y (ppm)	Y (ppm)	Y (ppm)	Y (ppm)	Y (ppm)	Y (ppm)	Y (ppm)	Y (ppm)	Y (ppm)	Y (ppm)	Y (ppm)	Y (ppm)
LC 1 res	6.8995	0.2116	0.8270	X	X	0.0540	X	0.0497	0.0171	0.0083	0.0094	0.0118	0.0202
LC 5 res	8.4005	0.2522	0.8886	X	0.0008	0.1119	X	0.0595	0.0245	0.0099	0.0089	0.0098	0.0212
LC 11 res	33.9083	0.7117	2.0216	0.0264	0.0050	0.2424	X	0.1523	0.0968	0.0236	0.0251	0.0336	0.0362
LC 15 res	60.8014	1.0397	1.8741	0.1378	0.0108	0.4371	0.5194	0.4302	0.4131	0.0897	0.0925	0.4566	0.0725
LC 19 res	18.2442	0.3962	1.0584	0.0737	0.0085	0.4422	X	0.0976	0.2469	0.0982	0.0919	0.0768	0.0874
LC 31 res	46.0601	0.5987	1.1255	0.0435	0.0059	0.6277	X	0.1972	0.6084	0.2004	0.2038	0.1225	0.1253
LC 37 res	20.9711	0.3303	1.8617	0.0544	0.0125	0.2500	X	0.0820	0.0437	0.0662	0.0651	0.0510	0.0695
LC 41 res	0.0000	0.1185	1.1391	0.0814	0.0293	0.2534	X	0.0632	X	0.0304	0.0369	0.0187	0.0691
LC 47 res	14.0305	0.9226	6.4653	0.4762	0.0523	1.0092	X	0.3476	0.1272	0.2427	0.2410	0.0523	0.1426
LC 53 res	383.7155	2.3750	2.0894	2.8343	0.5126	1.5504	0.9491	4.1007	1.0574	0.0211	0.0194	0.4153	0.1078
LC 59 res	145.1235	0.6212	0.6708	0.0753	0.0011	0.0780	X	1.0041	0.4529	0.0078	0.0077	0.0961	0.0512
LC 65 res	299.9758	0.7452	0.6408	0.1804	0.0070	0.0948	X	1.1265	0.3985	0.0026	0.0061	0.1071	0.0477
LC 73 res	1637.7431	2.2588	2.1901	0.9501	0.0246	0.1899	X	2.2385	0.7239	0.0076	0.0088	0.2602	0.0619
LC 79 res	400.4849	1.1267	1.0722	0.2366	0.0100	0.1662	X	1.6146	0.2883	0.0081	0.0078	0.1567	0.0497
LC 85 res	997.0815	1.6400	1.3287	0.9752	0.3735	0.7671	0.5813	2.0018	0.6103	0.0294	0.0326	0.4211	0.2583
LC 91 res	114.3688	0.2283	0.4210	0.6800	0.1459	0.3009	X	0.2254	0.0490	0.0236	0.0247	0.0270	0.0300
LC 99 res	1262.4281	1.3684	1.5093	1.7305	0.0302	0.2838	X	1.2964	0.1955	0.0064	0.0065	0.2002	0.0463
LC 104 res	869.8124	1.0803	1.0540	0.5767	0.0146	0.1511	X	0.9076	0.2434	0.0078	0.0044	0.1277	0.0571
LC 109 res	1809.7086	2.3190	1.9509	1.1014	0.0317	0.3028	X	2.2237	0.5424	X	X	0.2547	0.0749
LC 113 res	478.4378	0.7825	0.7882	0.3594	0.0111	0.5534	X	0.9386	0.0941	0.0039	0.0079	0.1050	0.0594
LC 117 res	780.6722	0.8389	0.3977	0.4975	0.0125	0.1712	X	1.0442	0.2243	0.0162	0.0177	0.1090	0.0367
LC 121 res	589.0500	0.8353	0.6056	0.4717	0.0186	2.3009	X	1.3137	0.2616	0.0102	0.0120	0.1901	0.0431
LC 122 res	814.7683	1.0715	0.7163	0.7976	0.0230	0.1873	0.4882	1.5001	0.3489	0.0249	0.0333	0.2531	0.0401
LC 127 res	415.8570	0.5051	0.4699	0.4149	0.0981	0.3140	X	0.4249	0.0387	0.0129	0.0104	0.0967	0.0271
LC 133 res	992.8397	1.1951	1.2256	1.4562	0.0239	0.1760	X	0.9976	0.1656	0.0249	0.0221	0.2322	0.0402
LC 139 res	614.2092	1.2795	0.9127	1.5407	0.0410	0.1933	X	1.5639	0.2281	0.0151	0.0143	0.2230	0.0508
LC 145 res	475.2079	0.5760	0.3399	0.9335	0.0122	0.1842	X	0.3696	0.0286	0.0104	0.0088	0.0522	0.0215
LC 155 res	425.8672	0.8352	0.7386	1.3560	0.0480	9.8357	X	1.1868	0.1697	0.0136	0.0204	0.1351	0.0409
LC 165 res	527.4472	0.7282	0.5919	2.2757	0.3621	0.9331	0.6607	0.5854	0.0598	0.0141	0.0110	0.0912	0.0187
LC 171 res	405.1140	0.5076	0.4199	2.3597	0.2738	0.3765	X	0.6335	0.0574	0.0045	0.0062	0.0755	0.0267

	25Mg (STD)	51V (KED)	52Cr (KED)	55Mn (KED)	59Co (KED)	60Ni (KED)	63Cu (KED)	85Rb (KED)	88Sr (KED)	95Mo (STD)	100Mo (STD)	232Th (STD)	238U (STD)
	Y (ppm)	Y (ppm)	Y (ppm)	Y (ppm)	Y (ppm)	Y (ppm)	Y (ppm)	Y (ppm)	Y (ppm)	Y (ppm)	Y (ppm)	Y (ppm)	Y (ppm)
LC 1 sum	11076.6592	2.2319	6.9019	34.8031	6.7910	28.8287	0.3070	0.2093	188.5458	0.3429	0.3265	0.4039	3.1055
LC 5 sum	1935.4658	4.5919	6.0885	39.7899	3.1187	21.5500	0.3398	0.2369	132.0726	0.2940	0.2952	0.8763	2.3151
LC 11 sum	1223.2951	10.0084	8.9468	32.2051	5.0024	29.6116	0.3392	0.6274	223.1549	0.8984	0.9419	2.1941	0.7932
LC 15 sum	890.2058	14.3512	8.8348	44.2211	4.6604	30.8974	2.1704	1.2191	86.1809	3.5162	3.5643	5.6949	0.6057
LC 19 sum	708.3252	2.3257	8.8448	14.1617	7.7773	13.1586	0.2020	0.2414	88.6693	0.4800	0.4864	0.6589	0.5453
LC 31 sum	1279.7213	2.5809	5.3041	17.4054	8.6366	18.9373	0.1431	0.3340	149.9189	0.8516	0.8896	1.9718	1.8957
LC 37 sum	2532.8182	1.8476	8.0184	23.2792	5.7294	31.1697	0.1793	0.1602	185.7287	0.4493	0.4713	0.8689	1.5649
LC 41 sum	2587.6912	1.4562	8.0663	63.3963	5.3285	45.9747	0.3821	0.1190	206.6568	0.2776	0.3148	0.3497	4.7118
LC 47 sum	83.6377	1.7388	27.6891	7.4257	55.7233	8.5530	0.4785	0.5059	13.9385	0.8467	0.8586	0.1255	0.2961
LC 53 sum	16340.6685	6.7795	6.2551	140.2110	5.8092	21.4824	3.8652	5.7569	41.8982	0.4189	0.4420	1.9744	1.1652
LC 59 sum	18922.4671	2.2730	3.8866	124.6955	6.5112	35.1272	2.6352	1.9301	129.9830	0.4004	0.4093	0.8505	1.2866
LC 65 sum	7711.6169	2.6908	4.0603	87.2147	4.0502	38.0649	2.7226	2.0924	158.5102	0.3458	0.3348	1.1897	1.2402
LC 73 sum	15366.2496	4.8766	6.4310	133.8501	8.0383	31.1298	6.2933	3.0563	144.7007	0.4610	0.4989	2.2973	0.6223
LC 79 sum	14691.8586	3.2467	5.3833	131.3436	7.2184	32.3000	3.1550	2.5429	144.6914	0.3852	0.3976	1.2937	0.5915
LC 85 sum	10984.1884	3.7494	5.4661	146.8732	6.5628	26.0085	4.1481	2.6857	67.0617	0.5302	0.5371	2.4480	2.1146
LC 91 sum	13855.6702	1.2447	3.3546	126.2031	3.8064	37.8932	3.0780	0.4790	141.2082	0.3962	0.4152	0.6183	1.2697
LC 99 sum	11645.3245	3.8545	6.3529	233.2612	5.0981	35.9260	3.9798	1.9466	163.2144	0.3795	0.4024	1.7349	0.8550
LC 104 sum	21195.3496	3.1149	5.3453	254.1481	5.6133	34.0216	3.3563	1.4125	165.6297	0.4042	0.4355	1.2718	0.9030
LC 109 sum	25451.2830	4.9178	6.7350	225.5262	6.4850	31.2009	4.8056	2.9122	157.1524	0.4329	0.4532	2.0117	0.5536
LC 113 sum	11439.2430	2.1201	4.7442	144.1297	5.1883	36.6360	2.6128	1.3873	161.6623	0.4260	0.4080	1.1332	0.7544
LC 117 sum	13431.4179	3.0276	5.0455	181.7470	5.7305	35.4331	3.9360	1.5955	173.3923	0.4080	0.4007	1.3264	0.9305
LC 121 sum	13943.2774	3.5328	5.2367	194.2426	7.3260	36.4973	3.7365	2.2833	161.6919	0.3718	0.3866	1.6946	0.8270
LC 122 sum	13687.9276	3.8018	5.4576	277.5524	7.0874	30.8015	4.1536	2.3497	139.0028	0.4926	0.5565	2.2991	0.6817
LC 127 sum	4950.3707	2.4542	4.1740	161.9353	6.5039	36.3591	2.7893	0.6958	169.9120	0.3786	0.3695	0.9771	1.0424
LC 133 sum	10178.5452	4.0116	5.6678	255.2332	7.1509	33.5477	5.5849	1.5640	172.4022	0.3838	0.3861	1.6034	1.1308
LC 139 sum	9826.8917	4.2262	5.9777	534.7682	8.3643	37.4903	3.7545	2.3526	163.1587	0.4123	0.4330	1.8228	0.5942
LC 145 sum	5307.4844	2.0600	3.6359	400.2829	6.4504	39.3850	2.4979	0.5824	245.8076	0.3798	0.3613	0.6595	1.3538
LC 155 sum	7033.8827	3.0269	4.8673	1077.0088	6.4345	45.9807	192.0868	1.6846	204.9068	0.3713	0.4188	1.3718	1.0701
LC 165 sum	3620.1953	2.8949	4.1940	465.4037	5.2782	43.8823	11.6294	0.9388	142.3824	0.3761	0.3985	1.0019	0.5839
LC 171 sum	6671.3266	2.6292	3.8255	765.9704	6.2957	38.8000	9.2419	1.0598	149.6883	0.3595	0.3931	0.8648	0.6306

	25Mg (STD)	51V (KED)	52Cr (KED)	55Mn (KED)	59Co (KED)	60Ni (KED)	63Cu (KED)	85Rb (KED)	88Sr (KED)	95Mo (STD)	100Mo (STD)	232Th (STD)	238U (STD)
	Y (ppm)	Y (ppm)	Y (ppm)	Y (ppm)	Y (ppm)	Y (ppm)	Y (ppm)	Y (ppm)	Y (ppm)	Y (ppm)	Y (ppm)	Y (ppm)	Y (ppm)
LC 1 TD	12008.1612	3.1009	10.5689	69.7802	13.6297	89.6237	X	X	238.0334	X	X	0.1438	2.1710
LC 5 TD	2664.0945	4.4808	9.2379	76.9626	4.6410	2.4668	X	X	188.9119	X	X	0.5602	2.0848
LC 11 TD	1637.9173	8.4428	9.3534	59.0314	7.5688	8.0402	X	X	309.6807	0.0581	0.1151	1.4415	0.8304
LC 15 TD	1065.5140	9.9939	2.4613	69.3613	5.7684	59.3595	X	X	110.1765	1.2466	1.4902	5.8924	0.5462
LC 19 TD	992.3939	0.5437	9.8112	24.0773	11.1586	12.0615	X	X	123.0675	X	X	0.2809	0.6472
LC 31 TD	1792.5191	0.1635	4.5764	26.7971	9.1287	19.6167	X	X	166.7165	0.1454	0.2292	1.8075	1.8440
LC 37 TD	3123.8262	X	9.6445	36.0338	7.8019	35.3584	X	X	228.3462	X	X	0.2965	1.4324
LC 41 TD	3289.2831	0.0794	11.8636	99.8488	8.8556	76.3395	X	X	269.7758	X	X	0.1177	4.0516
LC 47 TD	79.2164	X	28.1579	11.4818	63.1672	19.9379	X	X	17.5086	0.3136	0.3385	0.1376	0.3151
LC 53 TD	16707.3625	0.8062	0.7956	165.3282	5.8810	20.7483	X	X	44.3549	X	X	1.4870	0.9988
LC 59 TD	21104.9885	0.1097	1.3353	168.7083	9.3263	36.2298	X	X	157.5337	X	X	0.7464	1.1611
LC 65 TD	8872.6611	0.5197	1.4892	134.2533	6.4988	39.0308	X	0.2550	203.3310	X	X	1.0302	1.0638
LC 73 TD	15641.2869	1.0869	2.1145	168.6110	8.6538	34.6017	X	0.0087	168.8182	X	X	1.8577	0.5771
LC 79 TD	15774.4332	0.4527	1.8142	166.9792	8.5684	38.6252	X	X	174.6033	X	X	1.1667	0.5312
LC 85 TD	9695.9334	0.0383	0.5558	154.2477	4.6645	27.3752	X	X	60.4499	X	X	1.8868	1.9344
LC 91 TD	14098.9775	X	0.4985	161.8771	4.3055	38.2695	X	X	141.4804	X	X	0.4273	1.0694
LC 99 TD	13098.5227	2.4321	3.5552	322.6611	5.4361	31.0844	X	0.5397	158.3530	X	X	1.8332	0.6750
LC 104 TD	21585.4960	0.9197	1.7561	301.8428	4.8415	69.1406	X	X	164.2373	X	X	1.1296	0.8671
LC 109 TD	24261.0244	1.4819	2.2517	225.8358	5.2839	29.6640	X	X	152.5809	X	X	1.7940	0.4751
LC 113 TD	12424.4687	0.0081	1.2632	191.1586	5.2886	38.4422	X	X	186.3026	X	X	0.7041	0.6374
LC 117 TD	13938.1406	0.8927	1.6832	208.7058	5.6894	35.1926	X	X	174.6675	X	X	1.1057	0.8267
LC 121 TD	13993.4886	1.1236	2.0280	224.7072	7.1585	31.5293	X	0.2344	173.8890	X	X	1.4950	0.7044
LC 122 TD	13641.8373	1.1244	2.3040	328.6946	5.8410	33.3531	X	0.1212	145.9474	X	X	1.9496	0.6114
LC 127 TD	4964.0994	0.6384	1.6283	214.4956	5.0832	38.1421	X	X	185.5195	X	X	0.6516	0.8686
LC 133 TD	10004.7278	1.6887	2.5462	293.3711	6.4255	35.2080	X	X	190.0885	X	X	1.5828	0.9889
LC 139 TD	9669.8669	1.3979	3.0059	626.8809	8.2047	37.3440	X	0.3402	178.4133	X	X	1.7355	0.5576
LC 145 TD	5741.0247	0.4914	1.4073	524.5438	6.9179	47.6910	X	X	268.9619	X	X	0.6204	1.1882
LC 155 TD	7310.9566	0.9313	2.4963	1326.3432	7.0064	37.4467	X	X	217.3622	X	X	1.3122	0.9109
LC 165 TD	3725.1930	0.6459	1.8620	623.8621	6.3759	41.0612	X	X	159.9713	X	X	0.7585	0.4812
LC 171 TD	6733.1216	0.4323	1.7403	1001.1114	7.2243	39.9149	X	X	168.3588	X	X	0.8871	0.5321

Appendix D. Lung Cam XRF Data

	Mn	Mg	Ca	Cr	Cu	Ni	Sr	Th	V	V (2)
	ppm	ppm	ppm	ppm	ppm	ppm	ppm	ppm	ppm	ppm
LC 1	77.446	8443.4	392084.42	19.06	6.44	0.45	753.54	0.39	4.38	4.13
LC 5	77.446	4161.39	384651.54	44.17	5.7	0.54	983.37	0.41	5.66	5.58
LC 11	77.446	2713.95	354920.02	77.09	5.57	11.89	979.18	0.44	51.91	55.34
LC 15	154.892	2291.78	352347.1	45.24	8.9	19.73	425.07	2.29	45.73	47.67
LC 19	0	663.41	43024.94	30.08	2.35	3.09	116.65	0.5	11.96	12.12
LC 31	77.446	1990.23	157591.35	26.54	2.91	1.56	637.42	1.5	23.43	23.04
LC 37	154.892	4523.25	391298.25	12.04	6.36	-1.85	606.9	0.38	14.22	13.65
LC 41	77.446	4462.94	383865.37	14.81	6.3	2.53	625.45	0.08	15.18	15.89
LC 47	77.446	2774.26	382936.26	29.98	5.33	2.43	647.6	-0.52	35.37	38.2
LC 53	77.446	2533.02	379505.7	33.43	6.86	2.04	590.98	0.79	15.51	15.48
LC 59	77.446	3015.5	326332.02	50.52	6.7	9.41	785.26	1.02	47.97	49.8
LC 65	0	6091.31	391512.66	21.58	6.25	-0.39	754.13	0.31	12.25	11.72
LC 73	77.446	5246.97	383579.49	18.77	6.29	-0.27	556.98	0.4	7.61	7.52
LC 79	154.892	4161.39	386080.94	59.72	5.78	0.39	609.29	0.34	7.27	7.23
LC 85	309.784	6272.24	297672.55	19.34	11.79	11.85	265.86	2.34	25.53	26.38
LC 91	309.784	10554.25	373788.1	2.9	6.32	0.52	330.74	0.45	4.9	5.09
LC 99	154.892	8141.85	357850.29	7.38	10.9	1.15	379.52	0.86	11.42	10.64
LC 104	387.23	21048.19	325331.44	7.59	15.27	2.74	422.45	1.49	11.98	13.49
LC 109	309.784	18937.34	312752.72	11.46	8.68	4.63	318.93	1.19	11.51	14.56
LC 113	309.784	23520.9	331978.15	5.06	7.04	1.81	338.95	0.54	9.21	9.88
LC 117	387.23	24063.69	345843.33	7.29	3.79	-0.98	278.79	-1.22	7.7	8.29
LC 121	387.23	15559.98	325688.79	10.7	13.03	-0.94	409.47	-1.9	20.12	17.93
LC 122	542.122	7538.75	328261.71	12.93	22.4	4.41	359.95	3.19	11.21	14.95
LC 127	387.23	6031	369499.9	8.54	6.75	1.24	322.28	-0.58	7.85	9.88
LC 133	464.676	10493.94	330977.57	11.2	8.37	2.46	373.6	1.4	17.47	18.2
LC 139	929.352	13207.89	280662.69	22.29	10.59	5.93	338.65	1.92	36.26	34.4
LC 145	697.014	6935.65	367069.92	5.05	6.57	0.39	442.04	-1.78	7.38	8.11
LC 155	1548.92	8141.85	329976.99	12.85	12.9	6.3	438.28	0.32	19.39	19.47
LC 165	774.46	4101.08	367927.56	5.02	7.78	-0.18	257.6	0.69	8.46	9.79
LC 171	1394.028	5186.66	368713.73	5.2	7.59	1.9	272.64	0.54	6.29	8

	Cr (2)	Co (2)	Ni (2)	Cu (2)	Rb (2)	Sr (2)	Mo (2)	Th (2)	U (2)	(V/Al)/7.7381	V/Al two
	ppm	ppm	ppm	ppm	ppm	ppm	ppm	ppm	ppm	ppm	ppm
LC 1	17.53	1.17	2.98	1.04	1.28	682	0.11	0.32	1.8	2.022	1.906
LC 5	40.34	1.07	4.68	2.13	2.33	871.33	0.27	0.78	2.16	1.556	1.534
LC 11	75.19	1.26	14.22	2.29	10.45	912.85	0.89	3.44	3.1	3.164	3.373
LC 15	43.04	1.62	20.28	4.91	16.26	392.65	2.13	8.17	3.44	2.074	2.162
LC 19	29.81	0.94	4.79	1.8	7.92	107.67	0.24	0.88	2.21	1.862	1.887
LC 31	24.27	0.99	3.58	1.98	8.54	573.43	1.13	5.72	2.7	1.121	1.103
LC 37	9.89	1.53	2.49	2.42	8.49	558.63	0.26	0.72	4.27	3.534	3.392
LC 41	14.18	1.2	6.37	1.78	3.48	639.59	0.23	0.62	2.99	6.328	6.624
LC 47	28.54	1.19	5.28	1.95	3.26	645.75	0.15	0.48	2.24	12.697	13.713
LC 53	30.65	1.37	5.07	1.73	6.16	559.93	0.2	1.21	2.04	2.637	2.632
LC 59	46.95	1.31	11.34	3.09	7.12	769.61	1.06	2.82	2.24	4.428	4.597
LC 65	20.66	1.76	4.28	1.88	8.13	790.57	0.19	0.71	3.15	2.436	2.33
LC 73	16.08	1.52	4.84	2.11	5.73	533.11	0.18	0.5	4.16	2.235	2.209
LC 79	55.3	1.83	6.92	2.53	6.78	591.61	0.21	0.56	1.93	1.879	1.869
LC 85	18.14	9.22	15.8	10.16	36.85	256.27	0.26	4.12	4.31	0.789	0.816
LC 91	2.13	2.14	5.08	3.51	4.27	314.98	0.23	0.76	1.23	0.867	0.901
LC 99	5.9	2.98	6.7	6.26	13.42	366.13	0.08	1.55	1.1	1.025	0.955
LC 104	8.75	2.5	5.9	4.98	11.09	429.16	0.16	1.72	1.09	0.933	1.05
LC 109	11.98	3.39	20.14	7.9	11.39	382.48	0.25	2.01	0.88	0.966	1.222
LC 113	5.27	2.2	13.04	5.26	7.82	379.8	0.21	1.17	0.87	1	1.073
LC 117	7.15	2.93	25.58	8.45	5.1	305.87	0.17	0.96	1.07	1.214	1.306
LC 121	16.73	3.88	42.37	14.15	15.57	443.7	0.74	2.23	1.06	1.275	1.136
LC 122	14.85	2.08	8.89	7.63	14.73	372.55	0.53	2.02	0.92	0.828	1.104
LC 127	8.26	2.62	22.66	4.78	6.02	340.45	0.28	0.99	0.95	0.931	1.171
LC 133	11.44	2.67	15.56	9.67	13.92	399.67	0.15	1.89	1.09	1.022	1.064
LC 139	19.71	4.44	25.17	9.87	28.21	359.73	0.32	3.39	1.3	1.24	1.176
LC 145	3.56	2.54	16.64	20.08	4.46	456.52	17.33	0.74	1.06	1.096	1.205
LC 155	11.18	4.48	19.51	10.03	15.01	467.55	0.21	2.26	1.22	1.099	1.104
LC 165	3.78	2.26	18.21	4.47	6.19	267.91	0.21	0.9	0.69	1.082	1.253
LC 171	4.23	2.35	12.79	3.68	5.57	301.4	0.12	1.05	0.71	0.991	1.261

Appendix E. Standard Data

	25Mg (STD	43Ca (KED	44Ca (KED	51V (KED)	52Cr (KED)	55Mn (KED	59Co (KED	60Ni (KED)
	Y (ppm)	Y (ppm)	Y (ppm)	Y (ppm)	Y (ppm)	Y (ppm)	Y (ppm)	Y (ppm)
Puratronic Carbonate ex	X	6.729922	X	0.075973	X	X	0.003328	X
Pure Apatite ex	4.403068	X	X	0.104273	X	X	0.180636	0.108105
NIST 120C ex	38.37598	0.027216	X	5.647052	X	0.029822	0.199232	0.339003
BCR-CRM 032 ex	40.15257	4.639518	X	4.317988	X	X	0.001947	X
IAEA B7 ex	X	7.79444	X	0.155419	X	X	X	X
Puratronic Carbonate carb	17.84188	X	X	X	X	X	0.947076	51.243097
Pure Apatite carb	36.4753	X	X	0.035373	X	8.238805	0.147598	1.584677
NIST 120C carb	182.2269	X	X	1.694548	0.316538	11.42552	0.767614	4.2767741
BCR-CRM 032 carb	926.7903	X	X	X	0.499833	X	0.106817	4.7345975
IAEA B7 carb	1273.764	X	X	1.160115	X	15.3352	0.811698	41.721767
Puratronic Carbonate apa	3.797658	X	X	X	0.050172	0.037554	X	X
Pure Apatite apa	73.32764	60504.18	X	0.968368	X	4.763013	X	X
NIST 120C apa	1018.637	45016.61	X	14.45251	9.124415	25.98176	0.231406	0.4062389
BCR-CRM 032 apa	950.8646	64603.23	X	37.84615	49.87111	4.914618	0.12148	3.0289845
IAEA B7 apa	130.24	6455.545	X	0.600856	0.313952	1.789889	0.01212	0.0096705
Puratronic Carbonate ox	X	30.90633	X	2.784815	X	X	0.000821	X
Pure Apatite ox	10.58555	1676.015	4470.111	0.516791	X	3.546305	0.004197	0.092957
NIST 120C ox	206.9283	1591.059	4234.759	6.018181	6.143081	9.227497	0.311815	1.6614993
BCR-CRM 032 ox	151.9646	517.0299	1362.04	20.59188	39.26906	0.562842	0.029558	4.6234156
IAEA B7 ox	13.6941	X	X	0.550628	0.294122	0.067509	0.027489	0.107979

	63Cu (KED	85Rb (KED	88Sr (KED)	95Mo (STD	100Mo (ST	232Th (STI	238U (STD)
	Y (ppm)	Y (ppm)	Y (ppm)	Y (ppm)	Y (ppm)	Y (ppm)	Y (ppm)
Puratronic Carbonate ex	5.432604	X	X	X	0.001862	X	1.6225E-05
Pure Apatite ex	5.687796	X	2.313992	0.185135	0.20314	8.728766	5.02762669
NIST 120C ex	7.267418	0.39955	X	0.428781	0.447357	X	6.21284194
BCR-CRM 032 ex	5.256676	0.576519	X	X	0.016374	X	34.7345341
IAEA B7 ex	6.561488	0.319137	0.081664	X	X	X	0.08946064
Puratronic Carbonate carb	X	X	4.299755	0.097294	0.072161	0.153037	0.00343381
Pure Apatite carb	X	X	35.05056	0.014665	0.013108	0.058207	4.63025064
NIST 120C carb	X	0.137823	29.69754	0.130277	0.137108	0.005382	4.68020157
BCR-CRM 032 carb	X	0.096415	85.80072	X	X	0.000269	1.81256459
IAEA B7 carb	X	X	128.3173	X	X	0.177638	1.32373268
Puratronic Carbonate apa	X	X	0.252444	0.006781	0.009929	0.036977	X
Pure Apatite apa	X	X	15.0756	X	X	55.96303	61.6246922
NIST 120C apa	X	0.057254	35.32589	0.197162	0.272987	5.494371	93.1696667
BCR-CRM 032 apa	4.481568	0.063935	123.1596	0.157713	0.210083	0.026926	70.3713871
IAEA B7 apa	X	0.022021	11.5998	X	0.000607	0.039322	0.73504309
Puratronic Carbonate ox	59.48906	0.312435	X	0.031937	0.039198	0.00893	0.00039699
Pure Apatite ox	X	X	18.52205	0.031538	0.053273	13.33629	4.13627201
NIST 120C ox	0.121319	0.698294	33.50607	0.374566	0.426836	0.323873	7.13616172
BCR-CRM 032 ox	0.463471	0.176435	2.110298	0.196341	0.251014	0.282091	19.3670722
IAEA B7 ox	0.090886	0.081259	X	X	0.003421	X	0.00946231

	25Mg (STD	43Ca (KED	44Ca (KED	51V (KED)	52Cr (KED)	55Mn (KED	59Co (KED	60Ni (KED)
	Y (ppm)	Y (ppm)	Y (ppm)	Y (ppm)	Y (ppm)	Y (ppm)	Y (ppm)	Y (ppm)
Puratronic Carbonate org	0.777814	X	106.1718	0.002035	1.408951	0.20216	0.016444	1.8224533
Pure Apatite org	3.643899	2836.543	X	0.353473	0.647703	2.285773	0.032527	1.3735765
NIST 120C org	140.5577	3786.143	X	3.7769	4.776866	6.181562	1.02109	7.0496833
BCR-CRM 032 org	38.28641	789.0614	X	3.623477	8.670301	X	X	X
IAEA B7 org	25.38802	X	112.2685	0.821181	1.982666	0.311597	0.059241	1.1930984
Puratronic Carbonate res	X	X	X	X	0.020499	X	0.003483	0.0078891
Pure Apatite res	3.229714	8776.562	18483.01	0.56473	X	2.652721	X	X
NIST 120C res	27.73428	263.5953	550.9673	1.411316	1.422382	3.664919	0.173808	1.2956748
BCR-CRM 032 res	X	X	X	2.585586	2.759748	0.050133	X	1.5692985
IAEA B7 res	4.566755	X	X	0.245313	0.308325	X	0.007143	0.0345085
Puratronic Carbonate TD	X	1735940	X	X	0.210159	0.981275	1.237737	58.605274
Pure Apatite TD	141.6207	776049.9	X	X	X	3.310316	0.015848	1.2236813
NIST 120C TD	1417.793	587901.2	X	13.79427	7.328197	25.62698	0.652153	7.2704913
BCR-CRM 032 TD	1574.924	593996.5	X	18.10395	26.53566	1.195881	0.093551	6.2011306
IAEA B7 TD	1690.584	1725263	X	1.774217	2.109935	20.86165	1.37274	254.47826

	63Cu (KED	85Rb (KED	88Sr (KED)	95Mo (STD	100Mo (ST	232Th (STD	238U (STD)
	Y (ppm)	Y (ppm)	Y (ppm)	Y (ppm)	Y (ppm)	Y (ppm)	Y (ppm)
Puratronic Carbonate org	0.161411	0.000509	0.102345	0.198235	0.202215	0.048771	0.00133595
Apatite org	X	X	12.29442	X	X	14.64384	3.96170931
NIST 120C org	0.727025	0.509131	18.54894	0.440437	0.566248	0.130858	6.0365674
MPR org	X	0.026488	0.305007	X	X	0.195375	4.90962049
IAEB7 org	0.352465	0.116648	0.088103	0.259335	0.25878	0.004085	X
Puratronic Carbonate res	X	X	X	0.023162	0.022369	0.031143	X
Apatite res	X	X	2.513077	X	X	31.81537	23.8893665
NIST 120C res	X	0.2954	4.383257	0.092405	0.115887	1.177059	0.91963621
MPR res	X	0.002351	X	0.057343	0.07578	1.374883	0.09858262
IAEB7 res	X	0.047359	X	0.009698	0.010214	0.012491	0.00037127
Puratronic Carbonate TD	X	X	4.18455	X	X	X	X
Apatite TD	X	X	12.04587	X	X	907.038	114.84734
NIST 120C TD	X	X	42.73917	0.219752	0.357601	8.383532	123.221126
MPR TD	X	X	28.6401	X	X	2.427629	135.130676
IAEB7 TD	X	X	123.6795	X	X	0.05961	2.01832886

Appendix F. Reagents and Procedural Blank Data

	25Mg (STD)	43Ca (KED)	44Ca (KED)	51V (KED)	52Cr (KED)	55Mn (KED)	59Co (KED)	60Ni (KED)
	Y (ppm)	Y (ppm)	Y (ppm)	Y (ppm)	Y (ppm)	Y (ppm)	Y (ppm)	Y (ppm)
Exchangeable Reagent	0.894979633	0.860398734	0	0.007858444	0	0	0.000410275	0.002233159
Carbonate Reagent	0.059852375	0.103109387	0.012130894	0.000567125	0.052456541	0.002515887	0.00060922	0.000193035
Apa Reagent	0	0	2.584777745	0	0.000132686	0	0	0
Oxide Reagent	0	0	0	0.004856493	0.000729217	0	2.3285E-05	0.002946966
Org Reagent	0.008737919	0	2.040515383	0.000234122	0.033189148	0.005212202	0.00031339	0.020690042
Conc. Nitric	0	0	0	0	0	0	0	0.000505073
Procedural Blank ex	23.80235935	26.75564503	0	0.247552179	0	0	0.0101506	0
Prod Blank carb	4.86290677	16.72568509	3.094358338	0.040360657	5.054713328	0.127526881	0.058012565	0
Procedural Blank apa	3.712593361	0	34.47637031	0.000951756	0.055817768	0.042740771	0	0
Procedural Blank ox	0	0	0	0.098228619	0.020937861	0	0.002780868	0.0584481
Procedural Blank org	0.884252907	0	165.3323036	0.008651894	2.246305818	0.34906474	0.018279708	2.703187278
Procedural Blank res	0	0	0	0	0.027841643	0	0	0.01299552
Procedural Blank TD	0	0	81.67049912	0	0.459759185	0.079241101	0.007897556	0.027424456

	63Cu (KED)	85Rb (KED)	88Sr (KED)	95Mo (STD)	100Mo (STD)	232Th (STD)	238U (STD)
	Y (ppm)	Y (ppm)	Y (ppm)	Y (ppm)	Y (ppm)	Y (ppm)	Y (ppm)
Exchangeable Reagent	3.070801512	0.040035056	0.02327152	0.009577111	0.00911556	0.003761878	0.00166691
Carbonate Reagent	2.062271949	0.002343235	0.004740577	0.001441302	0.001525682	9.21511E-06	3.46737E-05
Apa Reagent	0	0	0	0	0.000104767	5.63911E-05	2.36704E-05
Oxide Reagent	0	0	0.005992022	5.20494E-05	0	0	0
Org Reagent	0.00725052	6.794E-05	0.000147481	0.004538965	0.004361848	0	3.46724E-06
Conc. Nitric	0	0	0	0	6.69605E-07	2.41647E-05	0
Procedural Blank ex	87.60986988	1.200733208	0.663662854	0.228876294	0.226303634	0.098370544	0.042168474
Prod Blank carb	189.5622481	0.148680421	0.444377632	0.163225901	0.159460442	0.002089226	0.003195953
Procedural Blank apa	0	0	0.299483786	0	0.001634936	0.011595262	0.000975441
Procedural Blank ox	0	0	0.067771618	0	0	0	0
Procedural Blank org	0.376503054	0.001129239	0.078066488	0.301528554	0.320760589	0.013382078	0
Procedural Blank res	0	0	0	0.008962169	0.009592835	0.017638754	0
Procedural Blank TD	0.008012849	0	0.036122219	0.076738256	0.077825508	0.044387858	0.00189568

Vita

Christopher Wray is from Houston, Texas. He discovered his passion in geology early in his life through instruction and family gatherings from his grandfather, Cloyd, who was a geologist. These early experiences culminated into a passion, which has continued to this day.

With the love and support of his parents, Ron and Maria, and wife Lauren, Chris applied to and enrolled in the LSU Graduate School. His current advisor, Dr. Achim Herrmann, suggested studying uranium isotopes in carbonates focused on the Permian-Triassic Boundary. With much assistance and patience from all parties involved, Chris successfully defended this thesis on January 24, 2018. Special thanks goes to his wife, Lauren Frech; son, Dylan; and daughter Chloe who without their support this thesis would not have been possible.